INFORMATION TO USERS

This manuscript has been reproduced from the microfilm master. UMI films the text directly from the original or copy submitted. Thus, some thesis and dissertation copies are in typewriter face, while others may be from any type of computer printer.

The quality of this reproduction is dependent upon the quality of the copy submitted. Broken or indistinct print, colored or poor quality illustrations and photographs, print bleedthrough, substandard margins, and improper alignment can adversely affect reproduction.

In the unlikely event that the author did not send UMI a complete manuscript and there are missing pages, these will be noted. Also, if unauthorized copyright material had to be removed, a note will indicate the deletion.

Oversize materials (e.g., maps, drawings, charts) are reproduced by sectioning the original, beginning at the upper left-hand corner and continuing from left to right in equal sections with small overlaps. Each original is also photographed in one exposure and is included in reduced form at the back of the book.

Photographs included in the original manuscript have been reproduced xerographically in this copy. Higher quality 6" x 9" black and white photographic prints are available for any photographs or illustrations appearing in this copy for an additional charge. Contact UMI directly to order.

UMI

A Bell & Howell Information Company
300 North Zeeb Road, Ann Arbor MI 48106-1346 USA
313/761-4700 800/521-0600

Modeling of Nonlinear Active and Passive Devices in Three-Dimensional TLM Networks

by
Lucia Cascio
"Laurea" degree, University of Ancona, Italy, 1993

A Dissertation Submitted in Partial Fulfillment of the Requirements for the Degree of

Doctor of Philosophy

in the Department of Electrical & Computer Engineering

We accept this thesis as conforming to the required standard

Dr. W. J. R. Hoefer, Supervisor
Professor, Department of Electrical and Computer Engineering

Dr. J. Bornemann, Departmental Member
Professor, Department of Electrical and Computer Engineering

Dr. M. A. Stuchly, Departmental Member
Professor, Department of Electrical and Computer Engineering

Dr. H. Muller, Outside Member
Professor, Department of Computer Science

Dr. Yi-Chi Shih, External Examiner
President, MMCOMM Inc., Torrance, CA

Supervisor: Dr. W. J. R. Hoefer

ABSTRACT

The increase in clock rate and integration density in modern IC technology leads to complex interactions among different parts of the circuit. These interactions are poorly represented with traditional lumped circuit design methodologies. Traditional CAD tools, such as SPICE, provide very accurate models for a large variety of active devices, but their description of the passive part of the circuit is progressively becoming insufficient, as the frequencies of the signals increase. Problems such as dispersion, crosstalk and package effects require a full electromagnetic approach in order to predict their impact on the final response of the circuit. On the other hand, the application of a full-wave numerical method for the analysis of a complete device containing nonlinear elements is not sustainable with the present computer capabilities. The spatial and time discretization steps required to accurately model the nonlinear part of the device are much smaller than those necessary to describe the distributed part of the circuit.

In the present thesis, the possibility of modeling nonlinear devices with the three-dimensional TLM method has been explored; a new procedure has been successfully developed and implemented, linking the equivalent circuit representation of the nonlinear device to the transmission line model of the electromagnetic fields in the TLM network. No restrictions are applied on the size of the device, which can thus occupy more than a TLM cell. In order to model devices embedded in heterogenous media, a modification of the TLM node and relative scattering matrix has also been proposed. In view of linking the TLM field solver with a lumped element circuit CAD tool, the modified TLM scattering algorithm has remained independent of the specific device connected to the mesh.

The general methodology shown in this thesis appears to be a promising approach to solve a large variety of electromagnetic problems containing nonlinear elements.

Examiners:

Dr. W. J. R. Hoefer, Supervisor
Professor, Department of Electrical and Computer Engineering

Dr. J. Bornemann, Departmental Member
Professor, Department of Electrical and Computer Engineering

Dr. M. A. Stuchly, Departmental Member
Professor, Department of Electrical and Computer Engineering

Dr. H. Muller, Outside Member
Professor, Department of Computer Science

Dr. Yi-Chi Shi, External Examiner
President, MMCOMM Inc., Torrance, CA

Acknowledgments

I would like to thank the many persons who accompanied me and shared with me this experience.

First, I wish to express my gratitude to my supervisor, Prof. Wolfgang J. R. Hoefer. Thank you for your support through these years, for encouraging me during the difficult times, and for sharing with me the exciting times. Your teachings and style will be an example for me for many years to come.

I wish to thank my former supervisor, Prof. Tullio Rozzi, University of Ancona, Italy, for introducing me to the invisible and fascinating world of electromagnetism.

Thanks to the many, past and present members of the NSERC Chair research group: Dr. Eswarappa Channabasappa, Sherri Cole, Dr. Leonardo De Menezes, Dr. Christof Fuchs, Masafumi Fujii, Dr. Jonathan Herring, Dr. Mario Righi, Christa Rossner, Dr. Poman So, Giampaolo Tardioli and Dr. Qi Zhang. I wish to thank all of you for the inspiring discussions, helpful ideas and suggestions, the continuous encouragement and the relaxing coffee breaks we shared together. I would also like to thank Dr. Kevin Cattell, for his precious collaboration in linking SPICE and the TLM electromagnetic simulator.

The financial support provided by Natural Sciences and Engineering Research Council of Canada, the Science Council of British Columbia, MPR Teltech Inc. of Burnaby, B.C., and the University of Victoria, is gratefully acknowledged.

Very special thanks to the many friends who made my stay in Victoria unforgettable: Mary, Ali, Leonardo and Jon (again), Elena, Dilian and Claudio. Most of all, I wish to thank my "Canadian family": Mario, Cinzia, Gaia and Elena.

My last, heartfelt acknowledgments are to my family in Italy, for understanding and encouraging me to pursue my dreams, and to my husband Giampaolo for accompanying me through the journey of life.

Dedication

To my spouse, Giampaolo

Table of Contents

Acknowledgments iv

Dedication v

Table of Contents vi

List of Figures viii

List of Symbols xiii

Introduction 1

1.1 Field modeling tools 1
1.2 Background and motivation 3
1.3 Original contributions 6
1.4 Overview of the present Thesis 7

2 The Transmission Line Matrix Method 9

2.1 Introduction 9
2.2 The two-dimensional TLM shunt node 12
2.3 The three-dimensional TLM symmetrical condensed node (SCN) . . . 16
2.4 Errors in TLM 21
2.5 Conclusions 24

3 Modeling of Nonlinear Devices 25

3.1 Introduction 25
3.2 P-N junction diode 26
3.3 Bipolar junction transistor (BJT) 30
3.4 Conclusions 33

4 Embedding of Lumped Equivalent Circuits in Three-Dimensional TLM Networks 35

4.1 Introduction 35
4.2 Modeling of one-port equivalent circuits with the 2D TLM shunt

node 36
4.3 Modeling of one-port equivalent circuits with the 3D TLM symmetrical condensed node 40
4.3.1 Device volume equal to a single TLM cell 40
4.3.2 Device volume occupying more than one TLM cell in the three directions 42
4.4 Modeling of one-port lumped devices in heterogenous media using the stub-loaded TLM node 47
4.5 Modeling of two-port lumped devices in 3D-TLM networks 51
4.6 Evaluation of the capacitive effect produced by the device stubs . . . 53
4.7 Conclusions 56

5 Validation of the Device Stub Approach for One- and Two-port Lumped Devices **57**

5.1 Introduction 57
5.2 Modeling of lumped resistive sources in 3D-TLM 58
5.3 Derivation of the recursive formulation for linear, first-order lumped circuits (RC and RL). 62
5.3.1 Validation of the RC and RL equations 65
5.4 Inclusion of one-port nonlinear active and passive devices in the TLM network: p-n junction diode and Gunn diode 69
5.4.1 Validation results for the Gunn diode model 75
5.4.2 Validation of the p-n junction diode model. 81
5.5 Modeling of two-port nonlinear devices in the TLM network: the bipolar junction n-p-n transistor 83
5.5.1 Validation results. 86
5.6 Connection of lumped devices to stub-loaded TLM symmetrical condensed nodes. 89
5.7 A three-dimensional example 91
5.8 Conclusions 94

6 Conclusions and Future Work **96**

6.1 Introduction 96
6.2 The connection with SPICE 97
6.3 Future work 102
6.4 Overall conclusions 103

1 Bibliography **104**

List of Figures

Figure 2.1	Schematic description of the TLM algorithm in two dimensions: (a) impulse excitation, (b) scattering at the node, (c) propagation	10
Figure 2.2	2D-TLM Shunt Node. a) Representation of the node as intersection of transmission lines. b) Lumped element equivalent circuit.	12
Figure 2.3	Elementary Symmetrical Condensed Node (SCN)	17
Figure 2.4	Scattering matrix for the stub-loaded SCN.	20
Figure 3.1	The p-n junction diode and its one-dimensional physical model	27
Figure 3.2	Abrupt p-n junction diode in thermal equilibrium: space charge distribution	27
Figure 3.3	Equivalent large signal model of the p-n junction diode	29
Figure 3.4	The n-p-n bipolar junction transistor and its physical one-dimensional model	30
Figure 3.5	Ebers-Moll static model for an ideal n-p-n bipolar junction transistor	31
Figure 3.6	Rearrangement of the bipolar junction transistor in a common-emitter configuration	32
Figure 4.1	Lumped element connected to a 2D-TLM mesh (shunt node): a) lumped element directly connected to the TLM node; b) lumped element directly connected to a TLM link line; c) lumped element connected to the TLM node by a stub	37
Figure 4.2	Lumped element circuit connected to a 2D-TLM shunt node	38
Figure 4.3	Connection between a TLM SCN and a one-port device: only the voltages along the y-direction are affected by the presence of the lumped circuit.	41
Figure 4.4	Equivalent TLM model of a lumped device occupying more than one cell in the plane perpendicular to the direction of the feeding	

voltage (xz-plane, in this example) 42

Figure 4.5 Equivalent TLM model of a lumped device occupying more than one cell in the direction of the feeding voltage (y-direction, in this example) 44

Figure 4.6 Schematic connection of the active device to the three-dimensional TLM mesh: the active region is modeled as a single element in the direction of the voltage 45

Figure 4.7 Scattering matrix for the stub-loaded SCN equipped with device stubs in the three directions. With this matrix, both heterogeneous material properties and lumped circuits can be included in the TLM simulation. 50

Figure 4.8 The connection of a two-port lumped device to a 3D TLM network. The device is described by a generic 2x2 Y matrix and is connected to two clusters of TLM nodes by means of device stubs. The link lines, which are normally connected in the z-direction during the propagation process, are terminated by open circuits (top view). 52

Figure 4.9 a) Connection of a lumped device to the TLM node by means of a stub. b) The stub is modeled by an equivalent lumped capacitance C_s. 54

Figure 5.1 Connection of a lumped voltage source across M device stubs in the direction the feeding voltage 59

Figure 5.2 Connection of a lumped current source to a TLM network; the source is assumed to occupy M cells in the direction the feeding voltage 60

Figure 5.3 a) Lumped element representation of a capacitor connected to a resistive RF voltage source and b) its three-dimensional representation in a TLM network: the capacitor has been modeled with a parallel plate waveguide and the lumped voltage source has been distributed over the capacitor cross-section. 61

Figure 5.4 Validation of the lumped voltage source model $v_s(t)$: the transient behavior of the voltage produced across the distributed capacitor (Figure 5.3.b) is in very good agreement with the predicted response evaluated for the lumped circuit model of Figure 5.3.a. 62

Figure 5.5 Connection of a sample lumped RC network to a 3D-TLM mesh 63

Figure 5.6	Connection of a sample lumped RL network to a 3D-TLM mesh	64
Figure 5.7	Geometry of the transmission line low-pass filter: a) cross-section of the transmission line. b) position of the capacitor in the direction of propagation	65
Figure 5.8	S-parameters for the low-pass filter illustrated in Figure 5.7. Comparison between the analytical solution (solid line) and the computed results for the three-dimensional TLM model (dashed line)	66
Figure 5.9	Determination of the capacitive effect introduced by the device stubs. A cluster of device stubs has been left open-circuited, thus producing a low-pass effect in the transmission line. In the plots, the solid line is to the analytical solution of the problem in Figure 5.7 with $C=C_s$, while the dashed line is to the TLM simulation.	67
Figure 5.10	S-parameters of the high-pass filter consisting of a lumped inductor placed between the two conductors of the transmission line in Figure 5.7.	68
Figure 5.11	Relative error introduced in the scattering parameters of Figure 5.10 due to the parasitic capacitance introduced by the device stub.	68
Figure 5.12	Connection of a Gunn diode equivalent circuit to a 3D-TLM mesh	71
Figure 5.13	Typical current and differential conductance characteristics for the Gunn diode model, as described in eq. (5.15) (G_{max}=0.01 S, v_m=1V)	71
Figure 5.14	I-V characteristic of a Gunn diode having non-zero operating point	72
Figure 5.15	Equivalent large signal model of the p-n junction diode embedded in a TLM network	74
Figure 5.16	Transmission line oscillator with DC biasing circuit	76
Figure 5.17	Equivalent DC circuit of the stripline oscillator, and determination of the internal resistance value	77
Figure 5.18	Equivalent one-dimensional SPICE model of the three-dimensional TLM circuit in Figure 5.17. The thick lines represent two sections of transmission line. Note the addition of the parasitic capacitances C_s, shunt connected to all the lumped devices.	78

Figure 5.19 Transient behavior of the TLM and SPICE models for the transmission line oscillator. a) Transient response of the voltage $v_2(t)$ for the TLM model, the SPICE circuit including the parasitic capacitances, and the SPICE equivalent circuit without the stub capacitive effect (C_s=0). b) Deviation $v_2(t)|_{TLM}$-$v_2(t)|_{SPICE}$. for the SPICE model containing C_s 79

Figure 5.20 Fourier transform of the time-domain responses shown in Figure 5.19 80

Figure 5.21 Detail of the comparison between the TLM simulation with the backward approximation of the nonlinear conductance, the TLM simulation with numerical resolution of the nonlinear equation, and the SPICE response. 81

Figure 5.22 Evaluation of the dynamic behavior of a p-n junction diode. a) Voltage across the diode, b) current flowing into the device. 82

Figure 5.23 Evaluation of the capacitive effect introduced by the device stubs for the p-n junction diode example. Solid line: deviation $i(t)|_{TLM}$-$i(t)|_{SPICE\ with\ Cs=0}$.
Dashed line: deviation $i(t)|_{TLM}$-$i(t)|_{SPICE\ with\ Cs}$. 83

Figure 5.24 Connection of the bipolar transistor equivalent circuit to a the TLM mesh by means of two sets of device stubs. The biasing circuit is also included in the lumped model. 84

Figure 5.25 Three-dimensional representation of a common-emitter amplifier in a TLM network: the base-emitter and collector-emitter regions have been distributed over two adjacent cross sections of the transmission line. The transistor biasing circuit has also been included in the model. 87

Figure 5.26 Transient response for the common-emitter amplifier of Figure 5.25. The transistor has been modeled as an ideal npn junction. The solid line corresponds to the SPICE model with the inclusion of parasitic capacitances C_s connected to the sources and the transistor base-emitter section. 88

Figure 5.27 Dynamic behavior of the common-emitter amplifier with the inclusion of the nonlinear junction and diffusion capacitances. Comparison between the TLM and SPICE simulations. 89

Figure 5.28 Evaluation of the dynamic behavior of a p-n junction diode. a) cur-

rent flowing into the diode, and b) Deviation $i(t)|_{TLM}$-$i(t)|_{SPICE}$. 90

Figure 5.29 Geometry of the capacitively coupled bandpass filter (dimensions in mm) 91

Figure 5.30 Detail of the graded mesh used for the modeling of the microstrip circuit. (Dimensions in mm) 92

Figure 5.31 Time domain waveforms at the input and output ports of the band-pass filter. 93

Figure 5.32 Comparison between the computed and measured [21] S-parameters for the structure in Figure 5.29 94

Figure 6.1 SPICE layout for the determination of the new incident voltage to be inserted in the TLM simulation. The time evolution of the source $2 \cdot V^r(t)$ is updated at each iteration after the TLM scattering process. 99

Figure 6.2 Schematic representation of the link between the TLM algorithm and the SPICE simulator. The process occurs during a TLM time-step 100

Figure 6.3 Example of calculation of the new incident voltage V^i for the TLM time step k=1, using a SPICE simulation. The voltage source $2 \cdot V^r$ is set to 2 volts when t=0. After half a time-step, the total voltage across the device corresponds to V^i+V^r 101

List of Symbols

The following symbols are used throughout this thesis:

c	speed of light
f	frequency
t	time
v_{line}	impulse velocity in the link lines
ε	absolute permittivity
ε_0	permittivity of free space
ε_r	relative permittivity
μ	absolute permeability
C	capacitance
G	conductance
L	inductance
R	resistance
Y	admittance
$\hat{Y}$	normalized admittance
$\hat{Z}$	normalized impedance
Z_{l0}	link line characteristic impedance
$v(t)$	time-domain voltage
$i(t)$	time-domain current
I	current
V	voltage
E	electric field component
H	magnetic field component
$\mathbf{E}$	electric field vector
$\mathbf{H}$	magnetic field vector
$[M]$	mapping matrix
$[P]$	propagation matrix
$[S]$	scattering matrix
$[V]$	array of TLM voltages
Δt	temporal discretization step
Δt_{line}	temporal discretization step
Δl	spatial discretization step
Δx	node spacing in x-direction
Δy	node spacing in y-direction
Δz	node spacing in z-direction
Γ	link line reflection coefficient
T	link line transmission coefficient
f_s	mesh sampling frequency
ω	angular frequency
I_s	diode saturation current

q	electronic charge
k	Boltzmann's constant
T	temperature in Kelvin
C_j	junction capacitance
C_d	diffusion capacitance
τ	charge transit time
ϕ_0	built-in voltage
α	common base transistor gain
β	common emitter transistor gain
N	number of nodes in device area
M	number of nodes in device height

Prefixes

A subscript prefix is used to denote the time step (iteration) number

Suffixes

The following superscript suffixes are used:

i	pulse incident upon a node
r	pulse reflected from a node

The following subscript suffixes are used:

1,..., 21	pulse on link line or on stub
s	stub parameter (as distinct from a link line parameter)
m	node index in a cluster of TLM cells
d	diode parameter
b	transistor base parameter
e	transistor emitter parameter
c	transistor collector parameter
F	forward gain
R	reverse gain

Common abbreviations

TLM	Transmission Line Matrix
FD	Finite Difference
FDTD	Finite Difference in the Time Domain
TEM	Transverse Electromagnetic
TE	Transverse Electric
TM	Transverse Magnetic
SCN	Symmetrical Condensed Node
2D	Two-dimensional
3D	Three-dimensional

Chapter 1

Introduction

1.1 Field modeling tools

The modeling of electromagnetic (EM) fields has become an important topic of research for such diverse areas as microwave and RF engineering, antenna design, bio-electromagnetics, electromagnetic compatibility and interference, etc. The underlying need in all these areas is the need to characterize, control or eliminate the effects of EM fields. For this to become possible, the governing equations describing the EM fields, that is Maxwell's equations, must be solved with a certain degree of accuracy at any point inside the space of interest. In some special cases Maxwell's equations can be solved completely analytically, to yield to the exact solution of the problem; in general, however, the problems are so complex that a combination of analytical and numerical methods must be applied to approximate the solution within the desired accuracy.

Analytical techniques can constitute a useful tool when the important EM interactions in the problem can be anticipated. Unfortunately, nowadays very few - if any - problems are left that can be solved with these methods alone.

The advent of high-speed digital computers has allowed the efficient application of numerical techniques for the resolution of Maxwell's equations, thus opening new possibilities for the modeling of practical, complex EM problems. Although these methods offer an approximate solution to the problem under study, they usually constitute the only tool to predict with acceptable accuracy the EM field behavior [1-4].

Some of these methods, such as the method of moments, the mode matching method or the spectral domain method, rely on a certain amount of analytical pre-processing and are generally based on an integral formulation of Maxwell's equations. Other

techniques, such as the finite difference methods, the finite element method and the transmission line matrix method are usually based on the differential version of Maxwell's equations and on the discretization of the computational domain, and require less pre-processing [1].

The extensive research conducted in these years has shown that any one of these methods is not capable of solving every possible electromagnetic problem; in general, each particular application will be best approached with one of the techniques available. In recent years, hybrid techniques, based on the subdivision of a complex problem into parts which are then solved with the most suitable methodology, have also received growing attention. The underlying purpose of hybrid approaches is to exploit the advantages of each method in performing its most suitable task. Of course, particular care must be taken when combining two different methods, as stability issues may arise [5].

When selecting the most appropriate technique for the solution of an electromagnetic problem, several aspects must be taken into account. Firstly, the dimensions and geometry of the structure must be considered. Relatively simple geometries and open boundary problems are usually more efficiently handled with an integral formulation approach; vice versa, complex geometries, heterogenous media and closed boundary problems are generally best approached with a differential formulation.

The second aspect to consider is whether a time domain or frequency domain method is preferable. For example, in the analysis of digital circuits the shape of the impulse, the coupling between adjacent lines, the transient effects in the circuit are very important; a time domain approach is capable of providing information about all these phenomena. A time domain method is also useful when nonlinear components are present. When the characterization of a device is needed in a restricted frequency range, for example in the case of high-Q resonant circuits, a frequency domain approach provides a more efficient way to obtain the solution within a desired degree of accuracy.

With respect to these considerations, the transmission line matrix method is classified as a space and time discrete method based on the differential formulation of Maxwell's equations [1]. The main advantages of a time domain method such as TLM are:

- Generality in the geometries and material properties to be modeled. They can be introduced in the numerical simulation without changing the basic algorithm.
- Possibility to analyze transient phenomena.

- Possibility to obtain wide-band frequency information from a single time domain simulation.
- Possibility to model nonlinear phenomena and time-varying material properties (due for example to thermal effects)
- Formulation of the differential operators in terms of an equivalent circuit, thus allowing the use of circuit theory in many steps of the procedure.
- Ease of modularization and parallelization of the algorithm, thus allowing parallel and distributed processing of the simulation.
- Possibility to visualize and animate the EM fields as they propagate in the structure, particularly useful for design and educational purposes.

Because of these advantages, the TLM method has been used to develop general purpose field solvers (Microstripes™, MEFiSTo [6]), capable of solving a large variety of electromagnetic problems. More research is currently under way to increase the efficiency and the range of applications of the method. Improvements in the modeling of matched boundaries, simulation of nonlinear effects, development of special cells to reduce the computational effort, introduction of the thermal behavior are some of the aspects currently under investigation.

The objective of this thesis is to develop and implement a new procedure to model nonlinear active and passive devices by means of the TLM method.

1.2 Background and motivation

The increase in clock rate and integration density in modern IC technology leads to complex interactions among different parts of the circuit. These interactions are poorly represented with traditional lumped circuit design methodologies. Traditional CAD tools, such as SPICE [7], provide very accurate models for a large variety of active devices, but their description of the passive part of the circuit is progressively becoming insufficient, as the frequencies of the signals increase. Problems such as dispersion, crosstalk and package effects require a full electromagnetic approach in order to predict their impact on the final response of the circuit [8]. On the other hand, the application of a full-wave numerical method for the analysis of a complete device containing nonlinear elements is not sustainable with the present computer capabilities. The spatial and time discretization steps required to accurately model the nonlinear part of the device are much smaller than

those necessary to describe the distributed part of the circuit [9].

In many electromagnetic modeling situations, an attractive and efficient solution consists in the division of the problem under study into subvolumes (hybrid problems), some of which are best treated with a distributed electromagnetic model, while other components are more easily described by a lumped circuit representation. Examples of this kind of components are sources of various kinds, non-linear passive and active devices. In such cases it is worthwhile limiting the field description to areas in which this is necessary, and to use a simpler circuit description elsewhere. Among all the present numerical techniques, the time-domain modeling of nonlinear circuits is particularly advantageous, since it provides a natural representation of the nonlinear behavior and of the transient phenomena.

In recent years, two numerical methods have proved to be very efficient and accurate in solving electromagnetic problems in the time-domain: the Transmission Line Matrix method (TLM) [10] and the Finite Difference Time Domain method (FDTD) [11]. The extension of these two techniques to include lumped elements in distributed systems was needed to tackle more complex electromagnetic problems.

The TLM method is particularly suitable for interfacing lumped circuits to distributed structures; in fact, the electromagnetic fields are directly related to the voltages and currents propagating in the TLM transmission line network, and it is straightforward to interpret the connection between the distributed electromagnetic problem and the lumped devices in terms of circuit theory. Moreover, unlike FDTD, the TLM method is very stable at low frequencies, particularly in the presence of one-way absorbing boundary conditions [12]. Finally, another disadvantage of FDTD with respect to TLM is that the electric and magnetic fields are not defined in the same point in space and time; for this reason, in the modeling of lumped devices placed across multiple cells, the FDTD algorithm requires a suitable time averaging procedure even if the device does not contain elements with memory, otherwise instabilities may be encountered [13].

The concept of incorporating nonlinear devices into a TLM mesh was originally demonstrated in [14] where stubs were used to connect active elements to other parts of the circuit. Successively, in [15-16], the active nonlinear subregions were connected to the two-dimensional TLM (2D-TLM) nodes via stubs. The stub reflection coefficient was updated according to the explicit integration of the nonlinear differential equation. Other

contributions to the two-dimensional case focused on the introduction of lumped sources in the TLM network [17].

In the case of three-dimensional problems, Herring and Hoefer [18] have recently demonstrated the possibility of including lumped voltage sources in the three-dimensional TLM (3D-TLM) method, while in [19] the TLM and FDTD techniques have been combined to solve semiconductor problems including both lumped elements and nonlinear devices; the first approach to include active elements into a 3D-TLM network [20] was actually based on a specially developed "half-node" and was thus limited to the study of planar circuits; yet, this method presented the attractive feature that the nonlinear device and the TLM mesh were decoupled, providing flexibility in the integration time-step of the active element model. More recently, a technique to embed linear passive elements in three-dimensional TLM networks has been presented in [21]. In this contribution, the device was directly connected to the TLM link-lines.

A parallel development involved the introduction of lumped elements, including active devices, in FDTD. For the two-dimensional case, the extension of the FDTD method to study hybrid problems was first presented in [22], where sources and passive elements, linear and nonlinear, were incorporated in the FDTD mesh. This technique has then been extended to simulate also active nonlinear devices [23].

Three-dimensional problems have successively been examined: in [24] the above-mentioned procedure ([23]) has been extended to the 3D-FDTD method; more recently, in [26], this technique has been applied to study HF circuits containing non ideal pn-junction diodes and transistors. Successively, the method has been modified [26] and a variable time-step adjusting with the stiffness of the nonlinear differential equations has been introduced. Finally, Taflove et al. [27-28] have presented a general approach for connecting lumped circuits, modeled with SPICE, to a 3D-FDTD cell. In this contribution, based on a circuit interpretation of Ampere's law, an additional lumped capacitance is shunt connected to the lumped circuit and the FDTD cell. This last procedure is very attractive since it relies on very accurate SPICE models of the lumped circuits, rather than on user-developed, approximate models. Moreover, to include different elements, it is only necessary to modify the SPICE file, without altering the generalized FDTD algorithm. The efficient integration techniques developed for SPICE are also directly available without the necessity of user implemented integration schemes.

The objective of this thesis is to develop a general methodology to link the 3D-TLM network (constituted by symmetrical condensed nodes) and lumped equivalent circuits of nonlinear devices.

1.3 Original contributions

The above research objective has been met through the following original contributions to the TLM method:

- *Development of a procedure to link lumped circuits to a 3D-TLM symmetrical condensed node.*

  Similarly to the approach followed in [15] for the modeling of nonlinear devices in 2D-TLM, the procedure proposed in this thesis consists in linking the nonlinear elements, described by lumped equivalent circuits, and the nodes of the 3D-TLM mesh by means of transmission lines of length $\Delta l/2$. These lines will be called "device stubs" in the course of this thesis. While the main interest in this work is toward the modeling of nonlinear devices, the approach can also be used as an alternative to those proposed in [17] and [18], to include lumped sources into the TLM network.

- *Generalization of the method to model lumped circuits extending over more than a single TLM cell.*

  Particular care must be taken in the modeling of devices occupying more than one TLM cell, especially when the device extends over two or more nodes in the direction of the feeding voltage. In this case, when active nonlinear devices are concerned, the entire active region must be modeled as a single element: this will prevent the generation of instabilities in the network. The solution here proposed consists of a series connection of the device stubs which are interfaced with the device.

- *Conception and implementation of a new node accomodating material property stubs as well as device stubs.*

  In order to generalize the novel technique to model lumped circuits embedded in heterogeneous media, a modification of the scattering matrix governing the TLM algorithm is proposed. In this way, different material properties as well as the connection with the lumped circuit can be accommodated in the same TLM cell. The

modified scheme can also be useful to model the package effect of the device in the EM field evolution.

- *Generalization of the procedure to model two-port devices.*

  Finally, the method is extended to model two-port devices. This feature is useful in the characterization of EM problems containing transistors.

1.4 Overview of the present Thesis

The content of this thesis is organized into six Chapters, which are described below:

Chapter 1 contains this introduction and outline.

Chapter 2 contains a review of the TLM method. First, the two-dimensional TLM network is presented and the relationship between the 2D-TLM algorithm and the discretization of Maxwell's equations is discussed. Successively, the characteristics of the three-dimensional symmetrical condensed node are examined; the modeling of problems containing inhomogenous media is also addressed. Finally, a brief review of the typical causes of error affecting a numerical TLM simulation is offered.

In Chapter 3 a brief overview of the models available in the literature to describe nonlinear semiconductor devices is presented. In particular, the equivalent one-dimensional circuits of the pn-junction diode and the npn bipolar junction transistor are described. These models are then linked to the TLM network to model nonlinear circuits.

Chapter 4 presents a novel method to interface the 3D TLM network and a lumped element circuit modeling a nonlinear device. The link between the distributed mesh and the circuit is provided by device stubs. The procedure does not impose restrictions regarding the number of cells occupied by device. The inclusion of both one-port devices and two-port devices is considered, and the case of devices embedded in heterogeneous media and graded meshes is also examined. Finally, the capacitive effect introduced by the device stubs is also determined.

In Chapter 5 the general procedure previously described is specialized for each of the lumped circuits introduced in the TLM mesh. A number of canonical one-dimensional examples is used to validate the device stub approach proposed in this thesis. The results of the TLM simulations are compared with the theoretical behavior when this is easy to

determine, or with SPICE analyses. Finally, a fully 3D example is presented. In this case, the modeling results are compared to measurements available in the literature.

Chapter 6 contains the overall conclusion of the thesis and a discussion of the future research directions opened up by this thesis.

Chapter 2

The Transmission Line Matrix Method

2.1 Introduction

In this Chapter a review of the Transmission Line Matrix (TLM) method will be given.

The TLM method is a differential time-domain numerical modelling technique [10], suitable for solving general electromagnetic problems; they may involve nonlinear, heterogenous, anisotropic, time-dependent material properties and arbitrary geometries.

While other numerical techniques such as finite difference (FD) and finite element (FE) methods provide a mathematical discretization approach to the solution of Maxwell's equations, the TLM method consists in a physical discretization approach [1]. In fact, the TLM method is founded on the analogy between electrical circuits and the propagation of electromagnetic fields.

To model an electromagnetic problem with the TLM technique, the continuous field region of interest is replaced by a network of transmission-line elements; the point at which the transmission-line elements intersect is referred to as node. It can be shown that the electrical quantities (voltages and currents) traveling in such a network and the field components propagating in the solution region satisfy the same type of equation, provided that the length of the transmission lines is much smaller than the minimum wavelength of the signal propagating in the region. The correspondence between the electrical voltages and currents propagating in a TLM mesh and the electromagnetic fields was first introduced in [29] for the two-dimensional case. Several TLM nodes have been proposed to represent three-dimensional problems; among these, the most widely used is certainly the symmetrical condensed node. The analogy between Maxwell's equations

and the three-dimensional symmetrical condensed node has been first demonstrated in [30].

Once the field problem has been replaced by the equivalent TLM network problem, and the appropriate analogy between field and network quantities has been established, the field evolution is obtained by iteratively solving the equivalent network in the time domain.

The TLM algorithm, repeated iteratively for each node of the transmission line mesh and for each time step of the numerical simulation, is naturally split into two parts: scattering and propagation. At each time step, the voltage pulses incident upon a node from each of the transmission lines are then scattered to produce a new set of pulses. The relationship between the incident pulses and the scattered pulses is determined by the scattering matrix, which is set to be consistent with Maxwell's equations. We refer to this as the scattering process.

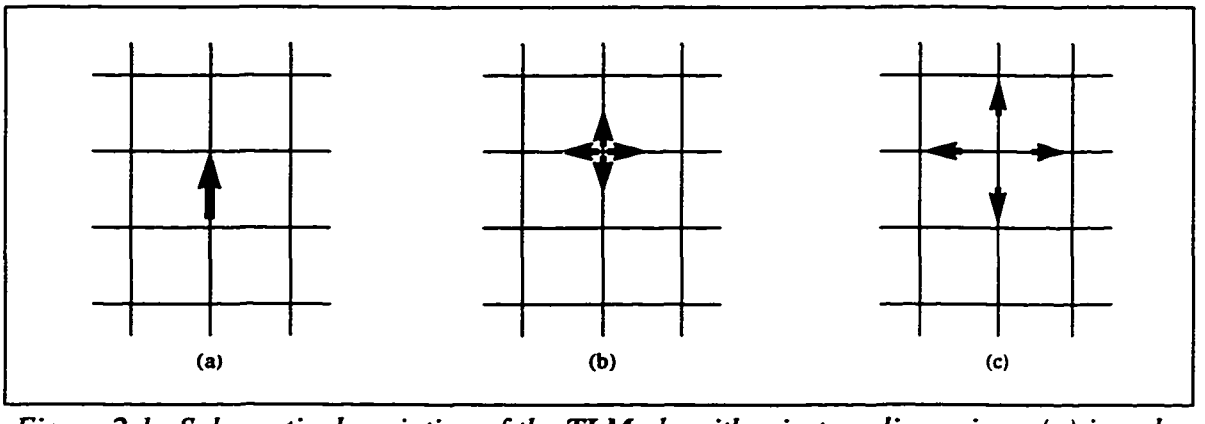

Figure 2.1 Schematic description of the TLM algorithm in two dimensions: (a) impulse excitation, (b) scattering at the node, (c) propagation

Each scattered pulse becomes then incident on the adjacent nodes at the next time-step, during the so-called propagation (or connection) process. In Figure 2.1 these two steps, and the initial excitation of a TLM mesh, are illustrated for the two-dimensional case.

In a compact form, the TLM algorithm can be described by:

$$_{k}[V^{r}] = [S]_{k}[V^{i}] \tag{2.1}$$

$$_{k+1}[V^{i}] = [P]_{k}[V^{r}] \tag{2.2}$$

The first expression indicates that the array of incident voltages $[V^i]$ is scattered at the TLM nodes at the time step $k\Delta t$ according to the scattering matrix [S], thus producing the reflected voltages $[V^r]$. The scattering process is supposed to be instantaneous. Similarly, the reflected voltages $[V^r]$ propagate to the neighboring nodes according to the connection matrix [P], thus giving the new incident voltages upon these nodes at the time step $(k+1)\Delta t$. The size and shape of the scattering and connection matrices depend on the dimensions of the problem under study (two- or three-dimensional) and on the material properties to be modeled (type of dielectric, lossless or lossy medium).

If we assume that the nodes are all equally spaced and that the interconnecting transmission lines are dispersionless, the time required for the impulses to travel from one node to the next, Δt_{line}, is related to the discrete space step, Δl, by:

$$\Delta t_{line} = \frac{\Delta l}{v_{line}} \tag{2.3}$$

where v_{line} represents the speed of the wave in the transmission lines.

The equivalent electric and magnetic field quantities at each node are approximated, according to the relationship between fields and voltages, by suitable combinations of the incident pulses. The continuous field evolution in time is therefore sampled at periodic time intervals Δt_{line}, and the field values are assumed to be spatially and temporally constant over each TLM cell, during a given time step.

It is important to underline that, since the TLM discretization of the real field problem generates a periodic structure consisting of a Cartesian mesh of lines intersecting at periodic nodes, the discretized version of the continuous problem can be considered as a slow-wave structure [31, 29]. For this reason, we can anticipate two basic properties of the TLM network, namely, passband-stopband characteristics and support of waves with phase velocities reduced with respect to the velocity in the link lines [31]. The first property limits the frequency range for which the model can be considered accurate; the second property reveals that an appropriate mapping between the velocity in the link lines and the velocity of propagation in the network must be performed [32].

In those situations where the electromagnetic fields can be assumed to be TE (electric field perpendicular to the direction of propagation) or TM (magnetic field perpendicular to the direction of propagation) [33], a simple two-dimensional analysis of the problem can be carried out. Two types of TLM nodes have been developed to model

these possible field configurations: the shunt node describes the propagation of TE waves on a plane, while the series node is suitable to model TM fields [10, 34].

When the complexity of the problem rules out the assumption of simple TE or TM propagation, a three-dimensional model of the structure must be used. Several forms of three-dimensional TLM nodes have been proposed in the literature; the most commonly used is the so called "Symmetrical Condensed Node" (SCN), introduced by P. B. Johns [30]. In the following sections, we will describe the two-dimensional shunt node and the symmetrical condensed node. An extensive review of the TLM method and its applications can be found in [10], [32] and [34-35].

2.2 The two-dimensional TLM shunt node

The electrical network used to model TE electromagnetic fields in the TLM method is constituted by an array of building blocks called "shunt nodes". The shunt node occupies a volume (also called TLM cell) of dimensions Δx, Δy, and Δz (for convenience we can assume they are all equal to Δl), and consists of the intersection of two transmission lines, as indicated in Figure 2.2.a. The lumped element equivalent circuit of the node can also be derived (Figure 2.2.b), assuming that the transmission lines have a distributed inductance L per unit length, and a distributed capacitance C per unit length.

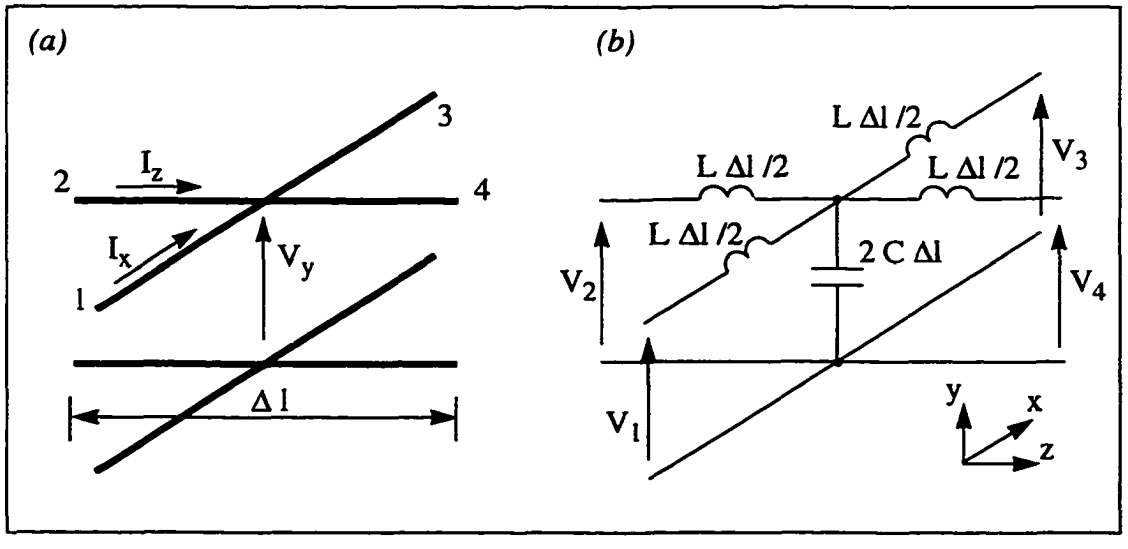

Figure 2.2 2D-TLM Shunt Node. a) Representation of the node as intersection of transmission lines. b) Lumped element equivalent circuit.

By writing the circuit equations for the shunt transmission lines and comparing them to Maxwell's equations, it is possible to demonstrate that this electrical model represents the TE-modes propagating on the x-z plane, having as non-zero field components E_y, H_x and H_z [34]. Assuming no variations of the fields in the y-direction, the differential form of Maxwell's equations reduces to:

$$\begin{aligned} \frac{\partial E_y}{\partial x} &= -\mu \frac{\partial H_z}{\partial t} \\ \frac{\partial E_y}{\partial z} &= \mu \frac{\partial H_x}{\partial t} \\ -\frac{\partial H_z}{\partial x} + \frac{\partial H_x}{\partial z} &= \varepsilon \frac{\partial E_y}{\partial t} \end{aligned} \tag{2.4}$$

Examining the circuit in Figure 2.2, and applying transmission line theory [33], we can derive the following equations for the electrical quantities V_y, I_x and I_z:

$$\begin{aligned} \frac{\partial V_y}{\partial x} &= -L \frac{\partial I_x}{\partial t} \\ \frac{\partial V_y}{\partial z} &= -L \frac{\partial I_z}{\partial t} \\ \frac{\partial I_x}{\partial x} + \frac{\partial I_z}{\partial z} &= -2C \frac{\partial V_y}{\partial t} \end{aligned} \tag{2.5}$$

There is an evident correspondence between equations (2.4) and (2.5). In particular, the relation between the field and circuit quantities is given by:

$$\begin{gathered} -V_y = E_y \qquad -I_x = H_z \qquad I_z = H_x \\ L = \mu \qquad C = \varepsilon/2 \end{gathered} \tag{2.6}$$

Were $\Delta x = \partial x$ and $\Delta z = \partial z$ infinitesimally small, the TLM shunt node would perfectly represent Maxwell's equations. Since in all practical cases (because of the finite memory capabilities of digital computers) the cell size is of finite value Δl, the discretized version of equations (2.5) must be considered, and the mapping (2.6) will be affected by an error. An brief overview of the causes of error in the TLM method will be offered in Section 2.4.

To conclude the analogy between electromagnetic fields and electric quantities, we will now compare the wave equation for the electric field component obtained from (2.4):

$$\frac{\partial^2 E_y}{\partial x^2} + \frac{\partial^2 E_y}{\partial z^2} = \mu\varepsilon \frac{\partial^2 E_y}{\partial t^2} = \frac{1}{c^2} \frac{\partial^2 E_y}{\partial t^2} \tag{2.7}$$

and the wave equation for the voltage V_y traveling in the TLM mesh. Differentiating the first two equations in (2.5) with respect to x and z, respectively, and the third with respect to t, and substituting, we obtain:

$$\frac{\partial^2 V_y}{\partial x^2} + \frac{\partial^2 V_y}{\partial z^2} = 2LC \frac{\partial^2 V_y}{\partial t^2} = \mu\varepsilon \frac{\partial^2 V_y}{\partial t^2} = \frac{1}{c^2} \frac{\partial^2 V_y}{\partial t^2} \tag{2.8}$$

In the last equation we have made use of the mapping between the distributed inductance and capacitance per unit length of the transmission lines, and the medium properties, μ and ε.

Comparing the two wave equations, it is apparent that the voltage V_y propagates with the same velocity, c, as that of the electric field, provided that the velocity of propagation of the link lines, $v_{line} = (1/\sqrt{LC})$ be equal to $\sqrt{2}c$. This means that the 2D-TLM network supports phase velocities reduced by $\sqrt{2}$ with respect to the velocity in the link lines.

In order to derive the scattering matrix of the TLM node, the circuit (Figure 2.2) must be examined from a transmission line theory point of view. The node constitutes a four-port device, for which we can define a scattering matrix, relating the vectors of the incident and reflected voltages, $[V^i]$ and $[V^r]$:

$$[V^i] = \begin{bmatrix} V_1^i \\ V_2^i \\ V_3^i \\ V_4^i \end{bmatrix} \qquad [V^r] = \begin{bmatrix} V_1^r \\ V_2^r \\ V_3^r \\ V_4^r \end{bmatrix} \tag{2.9}$$

The scattering matrix of equation (2.1) can be obtained by simple energy conservation considerations. Assuming that all the lines have the same characteristic impedance $Z_{l0}=\sqrt{L/C}$, a unitary voltage pulse incident on the node along the line *i* will see a load

impedance given by the parallel combination of three characteristic impedances; therefore, part of the pulse will be reflected back into the same line, according to the coefficient Γ_i, while a portion equal to T_i will be transferred to each of the connected lines:

$$\Gamma_i = \frac{1/3 - 1}{1/3 + 1} = -\frac{1}{2} \qquad T_i = 1 + \Gamma_i = \frac{1}{2} \tag{2.10}$$

Hence, applying expression (2.10) for all the ports, the linearity of the system allows us to write:

$$\begin{bmatrix} V_1 \\ V_2 \\ V_3 \\ V_4 \end{bmatrix}_k^r = \frac{1}{2}\begin{bmatrix} -1 & 1 & 1 & 1 \\ 1 & -1 & 1 & 1 \\ 1 & 1 & -1 & 1 \\ 1 & 1 & 1 & -1 \end{bmatrix} \begin{bmatrix} V_1 \\ V_2 \\ V_3 \\ V_4 \end{bmatrix}_k^i \qquad [S] = \frac{1}{2}\begin{bmatrix} -1 & 1 & 1 & 1 \\ 1 & -1 & 1 & 1 \\ 1 & 1 & -1 & 1 \\ 1 & 1 & 1 & -1 \end{bmatrix} \tag{2.11}$$

where [S] is the scattering matrix for the two-dimensional TLM shunt node.

The reflected pulses will then propagate in the TLM network, becoming impulses incident on the neighboring nodes, according the following propagation rules:

$$\begin{aligned} {}_{k+1}V_1^i(z, x) &= {}_kV_3^r(z, x-1) & {}_{k+1}V_2^i(z, x) &= {}_kV_4^r(z-1, x) \\ {}_{k+1}V_3^i(z, x) &= {}_kV_1^r(z, x+1) & {}_{k+1}V_4^i(z, x) &= {}_kV_2^r(z+1, x) \end{aligned} \tag{2.12}$$

where x and z describe the discrete coordinates of the nodes in the 2D-TLM network.

The correspondence between field and network quantities (2.6) can also be expressed as a function of the incident and reflected voltages; the node voltage V_y at the time $k\Delta t$ can be expressed as the sum of the incident and reflected impulses on one (m-*th*) of the link lines:

$${}_kV_y = {}_kV_m^i + {}_kV_m^r \tag{2.13}$$

Substituting the relation (2.11) and recalling that V_y is mapped into $-E_y$, we obtain:

$${}_kE_y = -\frac{1}{2}\sum_{m=1}^{4} {}_kV_m^i \tag{2.14}$$

Similarly, the magnetic field components can be determined as a function of the

incident voltages and of the characteristic impedance of the link lines [34]:

$$
\begin{aligned}
{}_kH_x = {}_kI_z &= \frac{{}_kV_2^i - {}_kV_4^i}{Z_{l0}} \\
{}_kH_z = -{}_kI_x &= \frac{{}_kV_3^i - {}_kV_1^i}{Z_{l0}}
\end{aligned}
\tag{2.15}
$$

Heterogeneous materials with different permittivities can be modeled with the 2D-TLM node. An additional open-circuited stub of length $\Delta l/2$ is used to increase the energy storage in the node, thus slowing down the wave propagation and simulating a medium with higher permittivity. The stub is shunt-connected to the node intersection, and its electrical characteristics are directly related to the permittivity ε_r that we want to realize. Specifically, $\hat{Y}_s = 4(\varepsilon_r - 1)$ is the admittance of the adjoint stub, normalized to the admittance of the link lines.

The derivation of the scattering properties for such a stub-loaded node follows the same procedure used to determine the scattering matrix of the un-loaded shunt node, as described in [10]; for brevity, the complete scattering matrix for this case is given here:

$$
[S] = \frac{1}{4+\hat{Y}_s}
\begin{bmatrix}
-2-\hat{Y}_s & 2 & 2 & 2 & 2\hat{Y}_s \\
2 & -2-\hat{Y}_s & 2 & 2 & 2\hat{Y}_s \\
2 & 2 & -2-\hat{Y}_s & 2 & 2\hat{Y}_s \\
2 & 2 & 2 & -2-\hat{Y}_s & 2\hat{Y}_s \\
2 & 2 & 2 & 2 & \hat{Y}_s-4
\end{bmatrix}
\tag{2.16}
$$

2.3 The three-dimensional TLM symmetrical condensed node (SCN)

The modeling of complex problems, where the assumption of TE or TM wave propagation is not sufficient, requires the development of three-dimensional TLM cells carrying information about all the six field components. The first three-dimensional TLM node, the so called "expanded node", was introduced in [36] and consisted in a combination of 2D series and shunt nodes, placed at the corners of a cube. Since then, many efforts have been made to develop new three-dimensional nodes and to increase the ver-

satility and efficiency of the TLM method [37-43]. Among the several formulations presently available, the most commonly used is the symmetrical condensed node (SCN) [30]. With respect to the original expanded node, its main advantage is that it yields all the electromagnetic field components in the same space/time point, thus simplifying the enforcement of boundary conditions.

In Figure 2.3 we have reported the structure of the Symmetrical Condensed Node. It is composed of 12 ports to represent two polarizations in each coordinate direction. The voltage pulses corresponding to the two polarizations are carried on transmission line pairs, shown schematically in heavy line. The two lines, such as 8 and 9, do not directly couple with each other. To achieve synchronism, the block of space represented by the SCN is chosen to be a cube of dimensions $\Delta x = \Delta y = \Delta z = \Delta l$.

As for the two-dimensional case, it can be demonstrated that the propagation of voltages in a three-dimensional network of symmetrical condensed nodes approximates the wave propagation in free-space, and that the finite discretization is accurate to the second order of the cell size Δl [44-46].

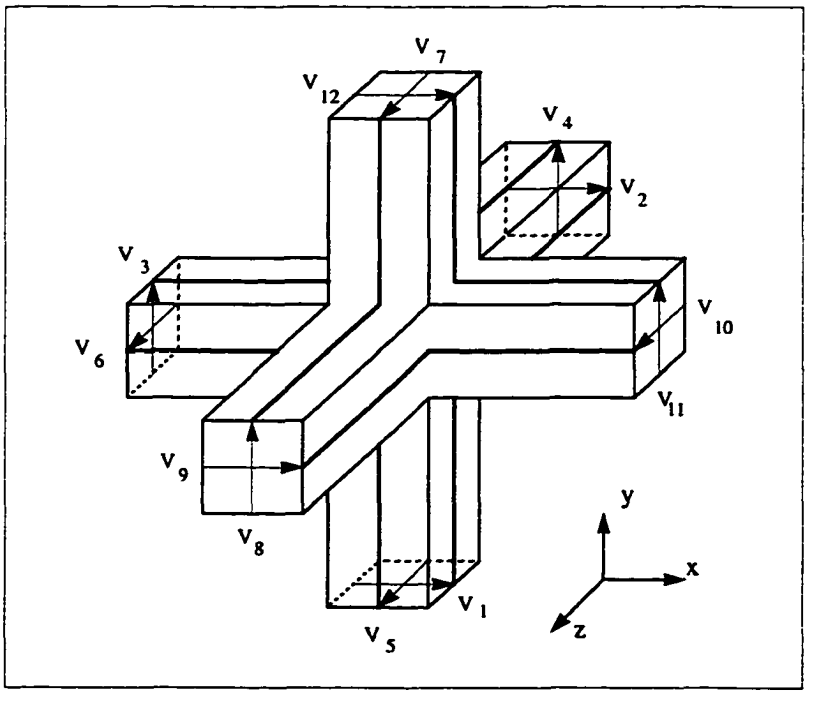

Figure 2.3 Elementary Symmetrical Condensed Node (SCN)

The scattering properties of the SCN are not as easily determined as those of the 2D node; instead, they are obtained from general energy and charge conservation principles, as described in [30, 10].

The scattering matrix [S], relating the reflected voltages [V^r] to the incident voltages [V^i], is described by the following 12x12 matrix:

$$[S] = \frac{1}{2}\begin{bmatrix} 0 & 1 & 1 & 0 & 0 & 0 & 0 & 0 & 1 & 0 & -1 & 0 \\ 1 & 0 & 0 & 0 & 0 & 1 & 0 & 0 & 0 & -1 & 0 & 1 \\ 1 & 0 & 0 & 1 & 0 & 0 & 0 & 1 & 0 & 0 & 0 & -1 \\ 0 & 0 & 1 & 0 & 1 & 0 & -1 & 0 & 0 & 0 & 1 & 0 \\ 0 & 0 & 0 & 1 & 0 & 1 & 0 & -1 & 0 & 1 & 0 & 0 \\ 0 & 1 & 0 & 0 & 1 & 0 & 1 & 0 & -1 & 0 & 0 & 0 \\ 0 & 0 & 0 & -1 & 0 & 1 & 0 & 1 & 0 & 1 & 0 & 0 \\ 0 & 0 & 1 & 0 & -1 & 0 & 1 & 0 & 0 & 0 & 1 & 0 \\ 1 & 0 & 0 & 0 & 0 & -1 & 0 & 0 & 0 & 1 & 0 & 1 \\ 0 & -1 & 0 & 0 & 1 & 0 & 1 & 0 & 1 & 0 & 0 & 0 \\ -1 & 0 & 0 & 1 & 0 & 0 & 0 & 1 & 0 & 0 & 0 & 1 \\ 0 & 1 & -1 & 0 & 0 & 0 & 0 & 0 & 1 & 0 & 1 & 0 \end{bmatrix} \tag{2.17}$$

The propagation process follows the principle described in (2.12) for the 2D case, repeated for all the 12 ports. Considering for example the ports 1 and 5, we have:

$$\begin{aligned} {}_{k+1}V_1^i(x, y, z) &= {}_kV_{12}^r(x, y-1, z) & {}_{k+1}V_5^i(x, y, z) &= {}_kV_7^r(x, y-1, z) \\ {}_{k+1}V_{12}^i(x, y-1, z) &= {}_{k+1}V_1^r(x, y, z) & {}_{k+1}V_7^i(x, y-1, z) &= {}_kV_5^r(x, y, z) \end{aligned} \tag{2.18}$$

At each node of the TLM network it is possible to establish a mapping between the incident voltages on the link lines and the fields in the center of the node; in general the relationship is described by suitable combinations of the incident pulses, and can be expressed in a compact way by means of a matrix notation as shown in (2.19).

$$\Delta l \begin{bmatrix} \mathbf{E} \\ Z_0\mathbf{H} \end{bmatrix}_k = [M]\,{}_kV^i \tag{2.19}$$

In this expression, Z_0 is the characteristic impedance of the homogeneous medium, **E** and **H** are the electric and magnetic field components, and the mapping matrix [M] is a 6x12 matrix (2.20).

$$[M] = \frac{1}{2}\begin{bmatrix} 1 & 1 & 0 & 0 & 0 & 0 & 0 & 0 & 1 & 0 & 0 & 1 \\ 0 & 0 & 1 & 1 & 0 & 0 & 0 & 1 & 0 & 0 & 1 & 0 \\ 0 & 0 & 0 & 0 & 1 & 1 & 1 & 0 & 0 & 1 & 0 & 0 \\ 0 & 0 & 0 & 1 & -1 & 0 & 1 & -1 & 0 & 0 & 0 & 0 \\ 0 & -1 & 0 & 0 & 0 & 1 & 0 & 0 & 1 & -1 & 0 & 0 \\ 1 & 0 & -1 & 0 & 0 & 0 & 0 & 0 & 0 & 0 & 1 & -1 \end{bmatrix} \tag{2.20}$$

The inverse mapping, to move from fields to voltages, is provided by the pseudo-inverse of the matrix [M] that is equal to its transpose, thus maintaining the consistency between mappings.

Because of the periodic nature of the discretized computational domain, a three-dimensional network of TLM SC nodes behaves like a slow-wave structure. In particular, it can be shown that waves propagate in the 3D-TLM mesh with a velocity equal to 1/2 the velocity of propagation on the link lines. The SCN, as the 2D shunt and series nodes, can be equipped with capacitive and inductive stubs, which will account for the different permittivities and permeabilities. The addition of stubs does not affect the connection process, but modifies the scattering matrix of the node. The three open-circuited stubs (having port numbers 13 to 15) modify the three electric components E_x, E_y, and E_z, while the three short-circuited stubs (with port number 16 to 18) influence the three magnetic components. These stubs also take into account the variations in the dimensions of the cells, used to model graded meshes.

The scattering matrix is determined again according to the laws of energy conservation [30], and is described by the 18x18 matrix in Figure 2.4, where:

$$a = -\frac{\hat{Y}}{2(4+\hat{Y})} + \frac{\hat{Z}}{2(4+\hat{Z})} \qquad b = \frac{4}{2(4+\hat{Y})}$$

$$c = -\frac{\hat{Y}}{2(4+\hat{Y})} - \frac{\hat{Z}}{2(4+\hat{Z})} \qquad d = \frac{4}{2(4+\hat{Z})} \tag{2.21}$$

$$e = b \qquad f = \hat{Z}d \qquad g = \hat{Y}b$$

$$h = \frac{\hat{Y}-4}{4+\hat{Y}} \qquad i = d \qquad j = \frac{4-\hat{Z}}{4+\hat{Z}}$$

[S]=

	1	2	3	4	5	6	7	8	9	10	11	12	13	14	15	16	17	18
1	*a*	*b*	*d*						*b*		*-d*	*c*	*g*					*i*
2	*b*	*a*				*d*			*c*	*-d*		*b*	*g*				*-i*	
3	*d*		*a*	*b*				*b*			*c*	*-d*		*g*				*-i*
4			*b*	*a*	*d*		*-d*	*c*			*b*			*g*		*i*		
5				*d*	*a*	*b*	*c*	*-d*		*b*					*g*	*-i*		
6		*d*			*b*	*a*	*b*		*-d*	*c*					*g*		*i*	
7				*-d*	*c*	*b*	*a*	*d*		*b*					*g*	*i*		
8			*b*	*c*	*-d*		*d*	*a*			*b*			*g*		*-i*		
9	*b*	*c*				*-d*			*a*	*d*		*b*	*g*				*i*	
10		*-d*			*b*	*c*	*b*		*d*	*a*					*g*		*-i*	
11	*-d*		*c*	*b*				*b*			*a*	*d*		*g*				*-i*
12	*c*	*b*	*-d*						*b*		*d*	*a*	*g*					*-i*
13	*e*	*e*							*e*			*e*	*h*					
14			*e*	*e*				*e*			*e*			*h*				
15					*e*	*e*	*e*			*e*					*h*			
16				*f*	*-f*		*f*	*-f*								*j*		
17		*-f*				*f*			*f*	*-f*							*j*	
18	*f*		*-f*								*f*	*-f*						*j*

Figure 2.4 Scattering matrix for the stub-loaded SCN.

The values of $\hat{Y}$ and $\hat{Z}$ used in these expressions are chosen to correspond to the relevant stubs [30]. If an isotropic medium in a cubic region is represented, then all the admittances and impedances are respectively the same for the three coordinates, and equal to

$$\hat{Y} = \hat{Y}_x = \hat{Y}_y = \hat{Y}_z = 4(\varepsilon_r - 1)$$
$$\hat{Z} = \hat{Z}_x = \hat{Z}_y = \hat{Z}_z = 4(\mu_r - 1) \tag{2.22}$$

In general, since the dimensions of the TLM cell and the values of relative permittivity and permeability can be different for the three Cartesian coordinates, three different admittances and impedances must be taken into account in the determination of the scattering matrix. The general expressions for the stub characteristic admittances and impedances are given by:

$$\hat{Y}_x = \frac{2\varepsilon_r}{v\Delta t}\frac{\Delta y \Delta z}{\Delta x} - 4 \qquad \hat{Z}_x = \frac{2\mu_r}{v\Delta t}\frac{\Delta y \Delta z}{\Delta x} - 4$$

$$\hat{Y}_y = \frac{2\varepsilon_r}{v\Delta t}\frac{\Delta x \Delta z}{\Delta y} - 4 \qquad \hat{Z}_y = \frac{2\mu_r}{v\Delta t}\frac{\Delta x \Delta z}{\Delta y} - 4 \tag{2.23}$$

$$\hat{Y}_z = \frac{2\varepsilon_r}{v\Delta t}\frac{\Delta x \Delta y}{\Delta z} - 4 \qquad \hat{Z}_z = \frac{2\mu_r}{v\Delta t}\frac{\Delta x \Delta y}{\Delta z} - 4$$

For example, the coefficient $d_{2,6}$ is related to the electric fields E_x and E_z, and to the magnetic field H_y (Figure 2.3). Therefore the correct value of impedance to be used in the formula of d is that of Z_y, since the short-circuited stub in the y direction is the one responsible for the modifications to the magnetic field component in that direction (H_y).

2.4 Errors in TLM

The solution of an electromagnetic problem by means of numerical techniques is inevitably affected by several sources of errors, the reason being that all these methods solve a discrete approximation of the continuous problem. The knowledge of the possible causes of error in a numerical simulation is important to gain "a priori" confidence in the accuracy of the results. A fundamental branch of research for all the numerical methods is the error analysis, the objective of which is to identify and quantify the sources of error. By understanding the differences between the exact and numerical solutions of a problem, it is possible to define and improve the accuracy of the method. In general, the sources of error cannot be totally eliminated, but their influence can be kept to acceptable levels [32].

In the last years, extensive studies have been performed to identify and reduce the errors in the TLM method. In the following, a brief review of the sources of error in TLM is presented. Possible solutions to reduce the entity of the errors are also introduced.

- Roundoff error

The roundoff error is due to the implementation of the TLM algorithm on a computer with finite precision. The imprecision introduced is always negligible compared with the other sources of error which affect the TLM procedure. For this reason the use of single precision variables is generally sufficient to implement the TLM algorithm on a computer.

- Velocity or dispersion error

The velocity error results from the discretization of the continuous problem. In Section 2.2, it has been shown that the TLM algorithm emulates Maxwell's equations when the cell size Δl is infinitesimally small. In this case, the voltages propagate isotropically in the discrete network, which behaves like a virtual nondispersive medium. This assumption can be made as long as the wavelength λ of the signal of interest is much larger than Δl. As the wavelength of the signal decreases, the assumption $\Delta l << \lambda$ is no longer acceptable, and the voltages will travel with different velocities in different directions, thus producing a dispersion error of the signal. The simulation of the continuous propagation of an electromagnetic wave is therefore only correctly modeled in a frequency range where $\Delta l << \lambda$. A simple way to reduce the dispersion error is therefore to use a fine TLM mesh, compatible with the computer memory resources and computational time.

The dispersion characteristics of electromagnetic waves propagating in an infinite homogeneous TLM mesh have been extensively investigated for various 2D and 3D TLM schemes [44-46]. It can be seen that the TLM model (both two- and three-dimensional) is accurate within the second order. It is important to underline that, since the dispersion error refers to the specific case of waves propagating in free-space, this will constitute the minimum error affecting a TLM simulation. The accuracy of the field representation can be further degraded in the presence of obstacles and heterogeneous media.

Another important factor related to the periodic nature of the TLM network and to its anisotropic properties, is that for some directions of propagation a cut-off frequency is present. The critical direction of propagation is the axial direction for the two-dimensional case and the main diagonal direction for waves propagating in a 3D-SCN network; in both cases, the cutoff frequency corresponds to one quarter of the sampling frequency of the mesh, $f_s = \frac{1}{\Delta t}$ [10].

- Spurious solutions

The mapping of the electromagnetic fields onto the electric voltages and currents propagating in the TLM network gives rise to spurious modes, that are solutions of the discretized system but not of the continuous problem. The presence of these non-physical solutions is a problem affecting many numerical methods, and TLM is not immune. Other numerical techniques in the time domain, such as FDTD, do not present spurious solutions, since they use only six variables to map the six field components.

Much effort has been devoted to the investigation of spurious solutions in TLM, from their first discovery [44], to their analysis with the Hilbert space formulation [45]. From these investigations it appears that spurious solutions arise because of the mapping between the voltages on the TLM network and the electromagnetic field quantities. For example, in the standard 3D-SCN, twelve voltages are mapped into six field components: the mapping is therefore not unique and voltages configurations exist that are mapped into a null electromagnetic field. Their excitation occurs in the presence of discontinuities, where the physical and spurious modes couple, as any discontinuity in a waveguide would cause the coupling among its possible modes; in this case, the presence of spurious modes primarily affects the field distribution in the vicinity of corners, thus producing a shift in the frequency domain results. Alternatively, they may be generated by the excitation (source) itself.

From a dispersion analysis of the 3D-SCN, it is possible to demonstrate that these voltages may either have a high spatial frequency (wavelength of the order of $2\Delta l$) or appear as a static voltage configuration. This suggests that a technique to reduce the incidence of spurious solutions consists in avoiding sharp excitations both in space and time. In space, a-priori information on the field distribution is useful to excite only the physical field configurations [47]; in the time domain, the excitation is chosen to cover only the frequency range of interest, rather than using a single impulse.

- Truncation error

Another source of imprecision in a TLM simulation comes from the need of truncating the output impulse response in the time domain. This is equivalent to multiplying the time-domain data stream by a rectangular window. Hence, the frequency domain response will be given by the convolution of the desired frequency spectrum with a $\frac{\sin x}{x}$ function, giving rise to the Gibbs' phenomenon [48]. In order for the frequency response to resemble the desired spectrum, the $\frac{\sin x}{x}$ function must be as narrow as possible; this is obtained by taking a sufficiently long number of time steps. This type of error is more severe when resonating structures are analyzed, because there is a significant time response even after a very large number of time steps. In these cases, appropriate windowing techniques may be used to improve the frequency response [49]. When open, propagating or naturally lossy structures are examined, the time response decays naturally, and the truncation error is easily kept under control.

A further improvement in the convergence of the output response is obtained by using a band-limited signal, such as a Gaussian pulse, rather than impulsive excitation. While band-limited signals are necessary in FDTD in order to avoid instabilities at high frequencies, they are also useful in TLM, although stability issues do not arise; in this way, more control on the frequency range in which energy is injected in the mesh is achieved.

Another form of truncation, in this case in the computational space, occurs when open or propagating structures are analyzed. While dispersionless walls are easily implemented in TLM and in other time domain techniques, the modeling of dispersive boundaries, simulating an outgoing wave, constitutes a critical issue since the frequency dispersive load retains memory of the past field evolution. The spurious reflections generated by these artificial boundaries may interact with the field evolution thus compromising the accuracy of the analysis. In the recent years, many efforts have been devoted to develop high quality, efficient and stable absorbing boundary conditions based on the application of diakoptics [50-51]. Another form of absorbing boundaries, based on the Perfectly Matched Layer (PML) approach first introduced in FDTD [52], have also been proposed by [53-54].

2.5 Conclusions

In this Chapter, the fundamental theory of the TLM algorithm has been reviewed and the scattering characteristics of the two-dimensional shunt node and of the three-dimensional symmetrical condensed node have been presented. The introduction of stubs to model heterogeneous media with different permeabilities and permittivities has also been shown. Finally, some of the typical causes of error encountered in the resolution of electromagnetic problems by means of numerical techniques, and in particular with the TLM method, have been discussed.

Chapter 3

Modeling of Nonlinear Devices

3.1 Introduction

In this Chapter a brief overview of the models of nonlinear active and passive devices that will be included in the TLM algorithm is presented.

In the last few years, numerical techniques have been used to characterize semiconductor devices for high-frequency applications. While standard semiconductor modeling is based on a drift-diffusion picture of electron and hole transport coupled to a quasi-static electromagnetic model, the simulation of high-frequency semiconductor devices is better described by more complex transport models, possibly coupled to a full-wave electromagnetic model [55]. Numerical methods in the time domain are particularly attractive for the characterization of such devices, because they are suitable for large signal or transient analysis, and because they can be coupled with other physical models (thermal, mechanical and so forth). The application of these techniques is becoming increasingly important to predict the behavior of a semiconductor device in the presence of high-frequency fields; unfortunately, they are also extremely expensive in terms of computational intensity. As an example, the full electromagnetic simulation coupled with the transport model of a GaAs MESFET studied in [9], required a discretization time step of the order of 10^{-17} s, and parallel computing resources.

Since the objective of this thesis is to model and predict the response of full circuits containing also semiconductor devices, the above mentioned time step would be several orders of magnitude smaller than the discretization time step required to describe the electromagnetic wave propagation, thus imposing prohibitive computational requirements on the simulation.

As long as the smallest wavelength of the signal of interest is large compared with the TLM cell size, and the volume of the nonlinear device is comparable with one or few TLM cells, the interaction between the electromagnetic field and the behavior of the device can be neglected. For the purposes of this thesis, the characterization of a semiconductor device by means of its equivalent circuit is therefore preferred.

A large variety of devices (diodes, field effect and bipolar junction transistors) has been extensively studied in the past years, and therefore well-established equivalent circuit models, including package and thermal effects, are now available. These models are extremely useful for the design of integrated circuits, and have been incorporated in a computer CAD tool called SPICE (Simulation Program with Integrated Circuit Emphasis) [7]. As the frequencies of operation and the need for integration have increased, new components have been developed, such as metal-semiconductor field effect transistors (MESFETs), heterojunction bipolar transistors (HBTs) and high electron mobility transistors (HEMTs) [56, 57]. Since the typical range of applications for such devices is quite different from that of the usual SPICE simulations, and since these devices are typically embedded in complex electromagnetic structures (that SPICE would not be able to characterize), their equivalent models are not included in SPICE.

In the following, the basic characteristics of the p-n junction diode and bipolar transistor will be briefly reviewed, and SPICE-like models will be derived. For a more extensive review of the characteristics of these and other semiconductor devices, the reader is referred to [56]. The equivalent models of these devices will be then embedded into the TLM mesh, with the procedure explained in the next Chapter. The potentiality for the TLM method to include nonlinear circuits will be demonstrated, opening new possibilities for the characterization of high-frequency active devices.

3.2 P-N junction diode

The simplest nonlinear semiconductor device consists of the junction of a p-type material (a material doped with an impurity that can capture free electrons from the crystal) and a n-type material (a material doped with an impurity that can provide free electrons to the crystal) (Figure 3.1).

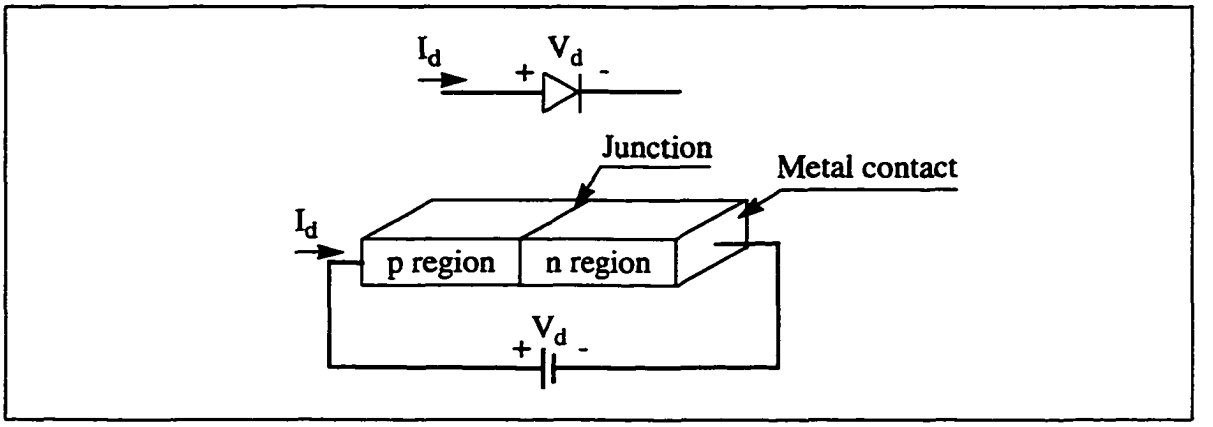

Figure 3.1 The p-n junction diode and its one-dimensional physical model

When the two doped materials are placed in contact, the p-n junction is formed and diffusion takes place in its vicinity. Electrons diffuse from the n to the p region, leaving behind a donor atom with a net positive charge, and the opposite happens for the holes in the p region. A space-charge (or depletion) region is thus created; the built-in field ($\mathcal{E}_0$) generated at the junction makes the free charges drift in the opposite direction until equilibrium is reached (Figure 3.2). Assuming that the charge density is zero everywhere except in the depletion region, where it takes the value of the ionized dopant concentration, the potential variation across the junction is determined by solving Poisson's equation [58].

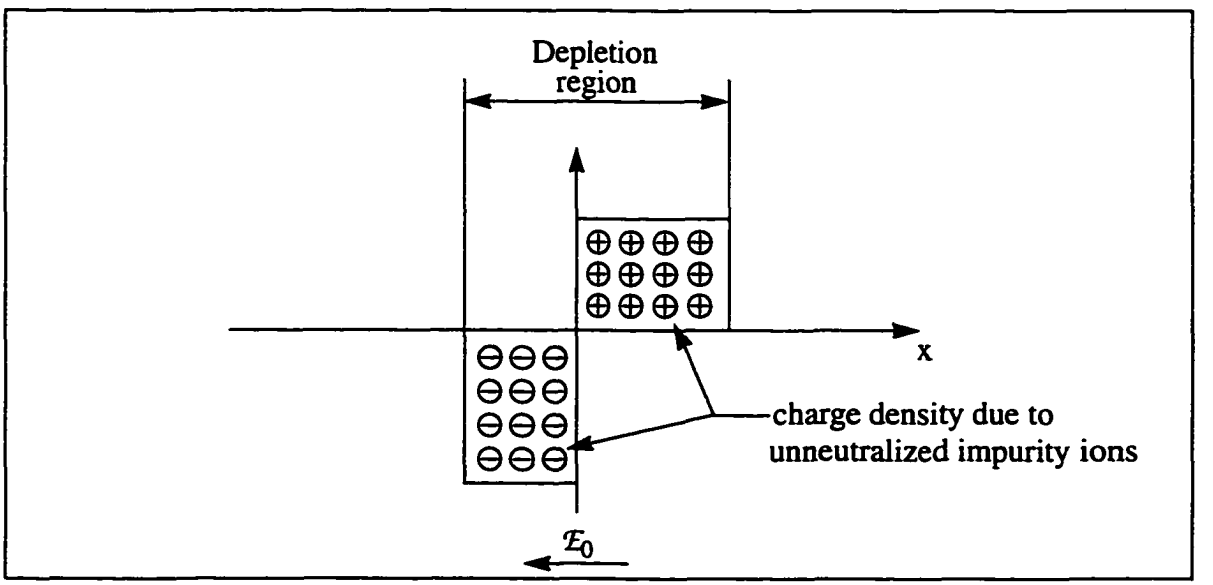

Figure 3.2 Abrupt p-n junction diode in thermal equilibrium: space charge distribution

When a positive V_d is applied to the junction (forward-bias) the voltage barrier decreases, the depletion region is narrowed and appreciable currents can flow even for small values of V_d. If a negative voltage is applied the depletion region widens and the junction is reverse-biased. In this case very little current can flow in the device.

In order to determine the current flow in the p-n junction as a function of the applied voltage, the continuity equation for the free carriers must be derived [58]. This must take into account the hole and electron drift currents and the hole and electron diffusion currents. It can be shown that the ideal current-voltage relation governing the diode behavior can be expressed as:

$$I_d = I_s\left[e^{qV_d/(kT)} - 1\right] \tag{3.1}$$

where I_s is the reverse saturation current, q is the electronic charge, k is Boltzmann's constant and T the temperature of the device in Kelvin. Equation 3.1 is called *Shockley equation*. In the reverse-biasing condition, the current asymptotically approaches $-I_s$.

In order to obtain the large-signal model of the diode, the charge storage effects of the device must be taken into account. These represent the inertia of the diode in changing the current flow. The junction capacitance arises from the depletion region where there is a dipole of fixed positive and negative charge; the diffusion capacitance is due to the region outside the depletion region, where minority carrier injection has introduced charges.

The presence of a dipole of fixed positive and negative charge in the depletion region gives rise to a "junction" capacitance C_j. Since the number of charges resident in the depletion region varies with the applied voltage V_d, the value of C_j depends on V_d. It can be found that, for an abrupt junction:

$$\begin{aligned} C_j(V_d) &= \frac{C_j(0)}{\sqrt{1-\dfrac{V_d}{\phi_0}}} \qquad \text{for} \qquad V_d < 0.5\cdot\phi_0 \\ C_j(V_d) &= \frac{C_j(0)}{0.5^{1.5}}\left(0.25+\frac{V_d}{2\phi_0}\right) \qquad \text{for} \qquad V_d \geq 0.5\cdot\phi_0 \end{aligned} \tag{3.2}$$

where $C_j(0)$ is the zero-bias junction capacitance and ϕ_0 is the built-in voltage [58-59]. This capacitance is dominant for reverse or small forward bias.

When the diode is forward-biased the dominating process is the diffusion of free carriers (electrons moving from the n to the p region, and holes moving in the opposite direction) and the charge storage is proportional to the total current injected across the junction:

$$Q_d = \tau_d I_d(V_d) \tag{3.3}$$

where τ_d (transit time of the diode) represents the minimum time required to store or remove charge. When a time varying voltage is applied, a diffusion capacitance C_d must be taken into account:

$$C_d(V_d) = \frac{dQ_d}{dV_d} = \frac{q}{kT}\tau_d I_s e^{qV_d/(kT)} \tag{3.4}$$

The large signal diode model can be represented by:

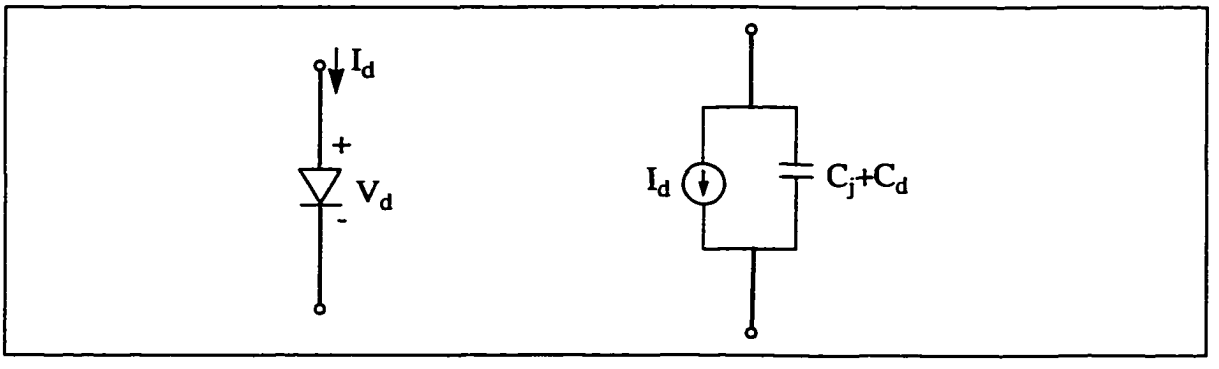

Figure 3.3 Equivalent large signal model of the p-n junction diode

Other effects can cause the performance of the diode to differ from the ideal behavior described above. The assumption that no carriers are lost in the depletion layer is not correct, and the real diode may produce a smaller current than that reported in (3.1) for low levels of forward-bias condition [58]. If the voltage applied in reverse-bias is too large, strong reverse currents are generated and breakdown occurs. Finally, a ohmic resistance r_s due to the voltage drop across the neutral regions affects the forward bias behavior for high levels of voltage.

It is worth noting that the p-n junction diode model is also useful for representing Schottky diodes, once the diffusion capacitance is neglected. Schottky diodes thus offer faster responses to signal variations; moreover, they have almost no recombination in the depletion region [58].

3.3 Bipolar junction transistor (BJT)

In the previous section it has been shown that a p-n junction diode conducts currents under forward bias conditions because the majority carriers present in one of the doped regions of the device are injected into the adjacent region. Under reverse bias the current is much smaller because it is carried only by the minority charges present either in the space-charge region or in the nearby regions. This current can be increased if the minority carrier concentration is increased in the vicinity of the reverse-biased p-n junction. This can be done by locating a forward-biased p-n junction close to it. The current flow in one p-n junction is hence modified by changing the bias in a nearby junction (Figure 3.4).

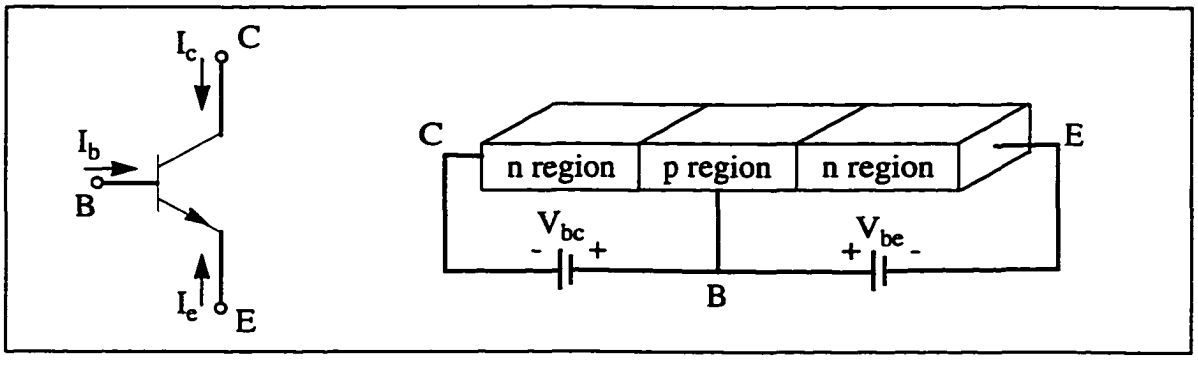

Figure 3.4 The n-p-n bipolar junction transistor and its physical one-dimensional model

In order to determine the behavior of the BJT in static conditions, the interaction between the two p-n junctions must be considered. Four different modes of operation are defined by the base-emitter and base-collector biasing voltages (V_{be} and V_{bc}):

- $V_{be}>0$ and $V_{bc}<0$. *Normal active region.*

  In this case the base-emitter junction is forward polarized, therefore a current flows from B to E. If the emitter region is more heavily doped than the base region (n^+-p junction), the current is made up essentially of electrons injected into the base [58]. The base-collector junction is reverse-biased, therefore the current in this junction is determined by the minority carriers that reach the depletion region. If the base length is small compared with the diffusion length of the electrons (minority carriers in the p region) most of them reach the BC depletion region and are then swept out to form the collector current. The intensity of the current I_C is proportional to the quantity of electrons in the emitter current, according to a factor α_F.

- $V_{be}>0$ and $V_{bc}>0$. *Saturated region.*

  In this case both the junctions are forward-biased. A current due to the majority carriers flows from B to E and from B to C; a current due to the minority carriers is also present and flows in the opposite directions. The net current flowing from the base to the two other terminals is therefore reduced.

- $V_{be}<0$ and $V_{bc}>0$. *Inverse region.*

  This situation is symmetrical to the normal bias case. The BC region is forward biased and a current of majority carriers from B to C is generated. The BE junction is reverse biased but the vicinity of a forward biased junction allows a flow of current from the emitter to the base, due to the minority carriers.

- $V_{be}<0$ and $V_{bc}<0$. *Cutoff region.*

  In this case both the junctions are reverse-biased and practically no current flows in the device.

This qualitative description can be modeled with the following equivalent circuit, called the Ebers-Moll static model of the n-p-n ideal transistor:

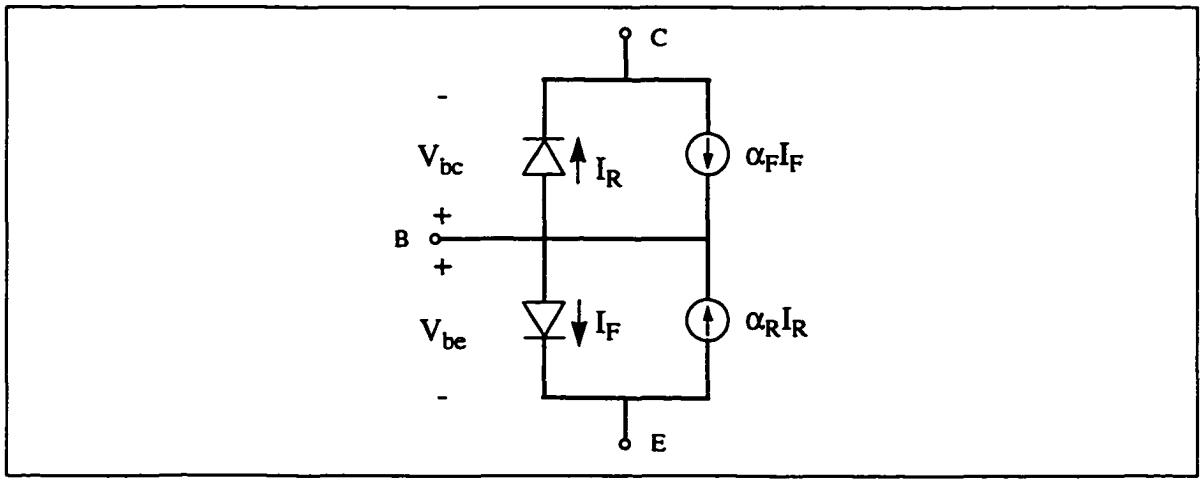

Figure 3.5 Ebers-Moll static model for an ideal n-p-n bipolar junction transistor

In Figure 3.5, I_F and I_R are the currents flowing through the p-n regions (base-emitter and base-collector, respectively), when the effect of the adjacent junction is neglected:

$$I_F = I_{ES}\left[e^{qV_{be}/(kT)} - 1\right]$$
$$I_R = I_{CS}\left[e^{qV_{bc}/(kT)} - 1\right] \tag{3.5}$$

while α_F and α_R are the large-signal forward and reverse current gain of a common-base BJT, and represent the interaction between the two junctions [56, 58]. It can be shown that the following relation must also be satisfied [58]:

$$\alpha_F I_{ES} = \alpha_R I_{CS} = I_S \tag{3.6}$$

where I_S is the BJT saturation current.

Applying Kirchoff's current equations to the terminals of the transistor and introducing the following quantities, an equivalent representation of the circuit can be obtained (Figure 3.6):

$$I_{cc} = I_S\left[e^{qV_{be}/(kT)} - 1\right]$$
$$I_{ec} = I_S\left[e^{qV_{bc}/(kT)} - 1\right] \tag{3.7}$$
$$\beta_f = \frac{\alpha_F}{1-\alpha_F} \qquad \beta_r = \frac{\alpha_R}{1-\alpha_R}$$

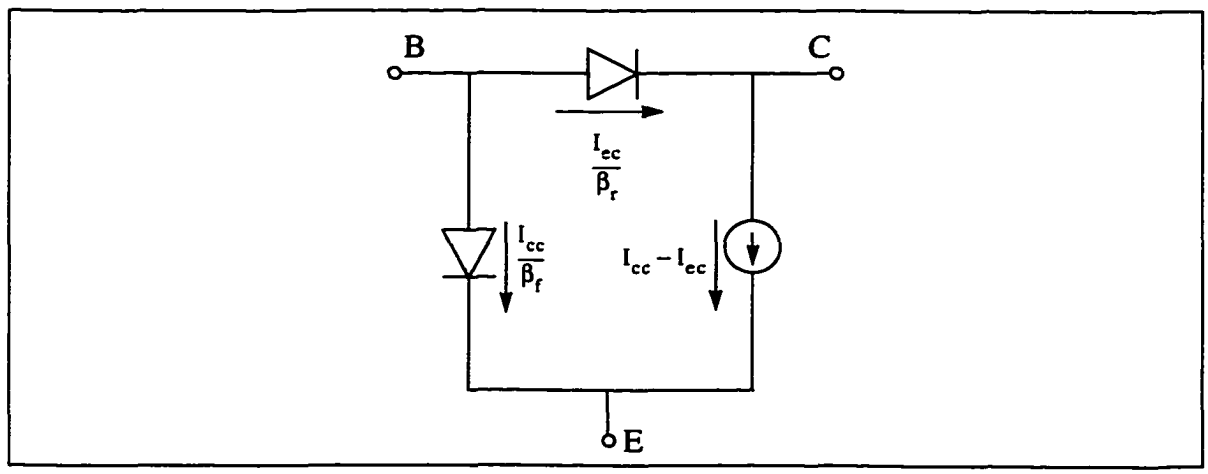

Figure 3.6 Rearrangement of the bipolar junction transistor in a common-emitter configuration

The large signal model of the bipolar transistor can be similarly derived by considering the coupling between two nonideal p-n junctions.

The dominating capacitive effect in each p-n junction when it is reverse biased, is due to the space charges stored in the BJT space-charge layers. A good approximation for the junction emitter-base junction capacitance is given by [59]:

$$C_{JE}(V_{be}) = \frac{C_{JE}(0)}{(1 - V_{be}/\phi_e)^{m_e}} \qquad \text{for} \qquad V_{be} < 0$$
$$C_{JE}(V_{be}) = C_{JE}(0)\left(1 + m_e \frac{V_{be}}{\phi_e}\right) \qquad \text{for} \qquad V_{be} \geq 0 \tag{3.8}$$

where $C_{JE}(0)$ is the zero-bias emitter-base junction capacitance and ϕ_e is the emitter-base barrier potential and m_e is a factor taking into account the doping profile of the junction (0.5 for an abrupt junction, 0.33 for a linearly graded junction). Similar expressions are derived for the collector-base junction, substituting the subscripts "E" with "C".

As in the diode model, the charge storage associated with the mobile carriers in the BJT, dominating in forward biasing conditions, will be represented by diffusion capacitances (one for the BE junction and one for the BC junction). The value of these nonlinear capacitors is given by [59]:

$$C_{dE} = \frac{q}{kT}\tau_F I_S e^{qV_{be}/(kT)}$$
$$C_{dC} = \frac{q}{kT}\tau_R I_S e^{qV_{bc}/(kT)} \tag{3.9}$$

where τ_F and τ_R are the total forward and reverse transit times and represent the mean time for the carriers to cross the neutral base region from the emitter to the collector, and vice versa.

The simplified model described so far can be improved by including other effects. For example, ohmic resistances can be introduced in the three terminals to improve the dc characterization of the model, and a substrate capacitance can be connected to the collector. Moreover, the variations of I_S, α_F and α_R with the applied voltages may be also considered [59]. All these factors are taken into account in the SPICE model of the bipolar transistor [59].

3.4 Conclusions

In this Chapter, a brief overview of the models of nonlinear passive and active

devices have been presented. In particular, the lumped element equivalent circuits for the p-n diode and the bipolar junction transistor, including some of their nonideal characteristics, have been described.

Since the purpose of this thesis is to demonstrate the ability of the TLM method of describing structures containing also nonlinear devices, the lumped equivalent circuits have been intentionally maintained simple. More sophisticated models available in the literature [57-59] can be incorporated in the TLM algorithm at a later time.

Chapter 4

Embedding of Lumped Equivalent Circuits in Three-Dimensional TLM Networks

4.1 Introduction

The TLM method has proved to be a very versatile and accurate tool to model complex electromagnetic problems in the time-domain. After several years of studies, the algorithm has proved to be inherently stable [10, 30] and to offer high quality absorbing boundaries ([50-51] and [54]). As the confidence in the method was increasing, the time was also mature to empower the TLM algorithm with other features, in order to increase the range of applications in which the method can be employed.

For example, in the framework of applying the TLM approach to electromagnetic compatibility problems, special nodes have been developed to model elements (such as thin wires and small apertures) smaller than a TLM cell [60-62]; in the same direction of reducing the discretization error and, in general, of modeling arbitrary geometries, the infinitely adjustable boundaries [63-65], the multigrid scheme [66] and finally the "adaptive cell" [6] have been developed. Special TLM cells to reduce the coarseness error in the presence of thin metallic wedges [46] have also been presented in [44, 67, 68]

The inclusion of lumped equivalent circuits into the TLM algorithm goes also in the direction of extending the possibilities of application of the method. Numerous situations are encountered where some of the subvolumes of the electromagnetic structure under study can be simply described by means of a lumped element equivalent circuit. In some cases it can be feasible to extract the equivalent circuit from the full-wave analysis of a complex problem [8, 69], and to use it in equivalent circuit based microwave solvers, such as MDS™ or Touchstone™. In other situations it can be useful to use the equiv-

alent circuit of the subvolume, provided for example by SPICE or other circuit CAD tools, and to integrate it into the full-wave simulation. Since equivalent circuits can be derived not only for real devices, but also for other properties (the TLM method itself is an equivalent circuit representation of the wave propagation in a medium), a recent application of the link between equivalent circuits and full-wave simulators consisted in the modeling of anisotropic dispersive materials (represented by a suitable equivalent circuit) in TLM [70].

In the present chapter we will explore the possibility of introducing lumped equivalent circuits into three-dimensional TLM networks, composed by symmetrical condensed nodes. The possible ways of linking a general one-port equivalent circuit to a TLM mesh will be discussed, and the discretization of the Kirchoff equations describing the circuit will be then presented, with emphasis on the problem of nonlinear active devices. The procedure will be then extended to include two-port devices.

4.2 Modeling of one-port equivalent circuits with the 2D TLM shunt node

The concept of incorporating lumped elements into the 2D-TLM mesh has already been addressed in several contributions [14-17]. In the following, the principle of general lumped element modeling in 2D-TLM will be reviewed and, in particular, the procedure used in [15] will be examined. In that approach, the active nonlinear subregions are connected to the TLM nodes by means of stubs and the reflection coefficient of these stubs is updated according to the explicit integration of the nonlinear differential equation describing the lumped circuit.

In general, a lumped element can be directly connected either to the TLM node or to the link lines of the TLM mesh [17]; or it can also be connected to the TLM node by means of a stub of length $\Delta l/2$ [15]; these possibilities are shown in Figure 4.1. A major drawback of the first approach (Figure 4.1.a) is that the scattering matrix of the node must be modified at each time step; moreover, in the case of circuits with memory, not only the past information about the circuit must be stored, but also the information about the old values of the incident and reflected voltages in each of the link lines must be retained. The second approach (Figure 4.1.b) requires the modification of the connection matrix at each time step and involves less TLM quantities (only the voltages for two link lines); it is therefore a preferable solution, compared to the previous one. In this case, the

reflected voltages generated at the interface with the lumped circuit travel toward the node and part of them may be reflected back into the link line (this happens for example in the 2D nodes and in the stub-loaded SCN). When a nonlinear device is modeled, this reflection creates an undesirable coupling between the linear and nonlinear part of the circuit [15-16]. In the last approach (Figure 4.1.c) an extra stub is added to the TLM node to provide the connection to the lumped circuit. The length of the stub is fixed at $\Delta l/2$ to ensure synchronism of the impulses in the entire TLM network. With this technique, the scattering matrix is modified to include the stub, but must not be changed at each iteration. On the other hand, the reflection coefficient of the adjoint stub must be updated at each time step, but this must be done for a single TLM quantity (the voltage in the stub). The main advantage of this approach is that, by choosing the appropriate value of the stub admittance, a decoupling between the linear and nonlinear parts of the circuit is obtained. For this reason, and because the interaction between the TLM mesh and the nonlinear device is limited to a single TLM voltage, it is easier to link the TLM algorithm to other lumped element circuit simulators, such as SPICE. The only disadvantage of this technique is that the stub introduces an extra capacitance in the equivalent model of the device; the error thus introduced is known "a priori" and in some situations it can also be compensated. In this work the last configuration will be adopted.

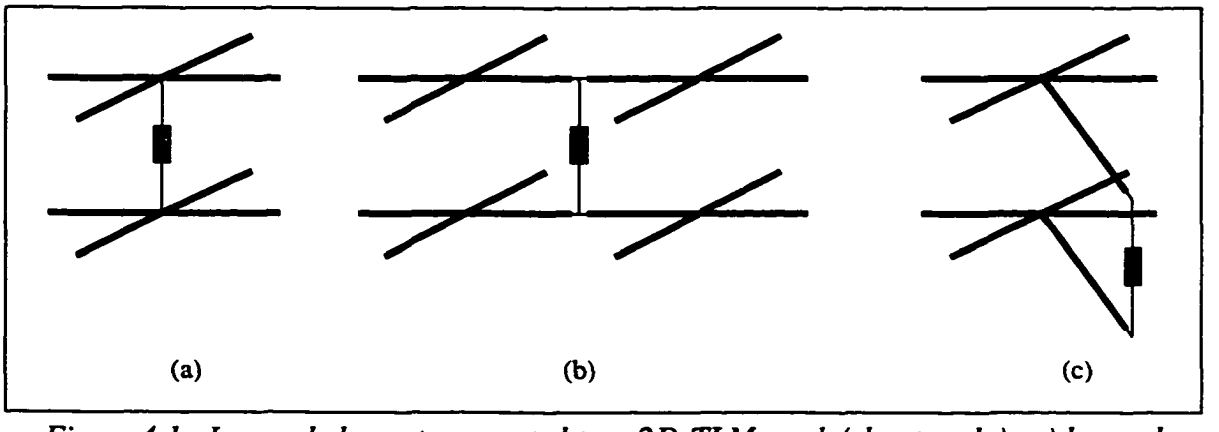

Figure 4.1 Lumped element connected to a 2D-TLM mesh (shunt node): a) lumped element directly connected to the TLM node; b) lumped element directly connected to a TLM link line; c) lumped element connected to the TLM node by a stub

In the following, the modeling of a one-port lumped device in a 2D-TLM scheme (shunt node) will be examined (Figure 4.2); this will be the basis for the development of more complex models, including biasing circuits and 3D schemes.

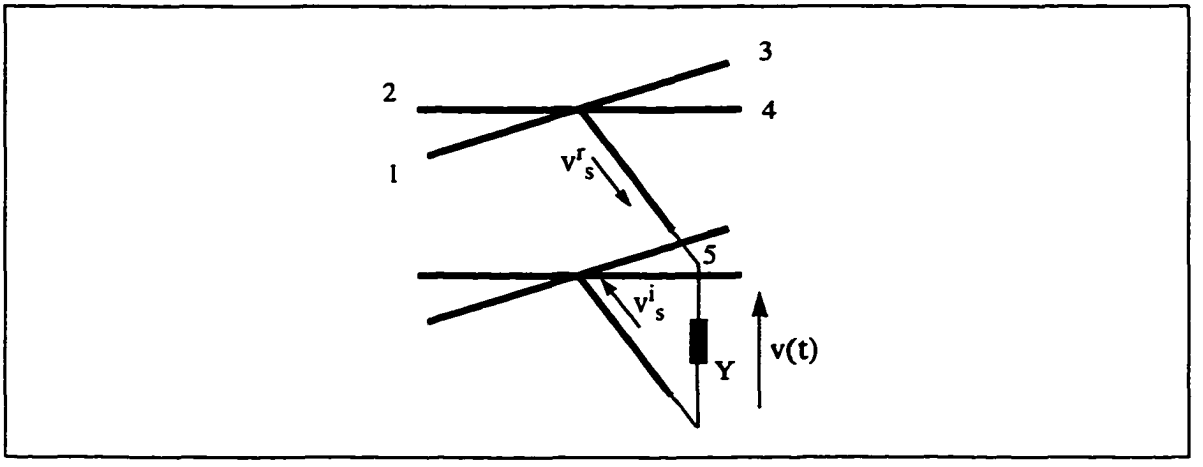

Figure 4.2 Lumped element circuit connected to a 2D-TLM shunt node

From the transmission line theory, the total voltage v(t) across the lumped circuit at the instant t is given by the superposition of the reflected and incident voltages traveling along the stub transmission line, while the current i(t) flowing towards the device is given by their difference, weighted by the stub admittance Y_s. We therefore obtain:

$$\begin{aligned} v(t) &= v^r_s(t) + v^i_s(t) \\ i(t) &= Y_s \cdot [v^r_s(t) - v^i_s(t)] \end{aligned} \tag{4.1}$$

In general, the admittance of the stub can be chosen arbitrarily, but by an appropriate choice the calculations may be simplified. The value of the admittance is determined by examining the scattering matrix of stub-loaded shunt TLM node; its expression was given in Section 2.2 (eq. (2.16)).

By inspection of the above-mentioned matrix, it is easily verified that for a normalized stub admittance $\hat{Y}_s = 4$ the element S_{55} vanishes, and therefore the reflected voltage v^r_s does not depend on the incident voltage v^i_s; in this way the linear and nonlinear parts of the TLM node are decoupled [15-16].

The total voltage v(t) and current i(t) must also satisfy the current-voltage equations describing the circuit. For example, for a one-port first-order device, this can generally be expressed as:

$$i(t) = f\left[v(t), \frac{dv}{dt}\right] \quad \text{or} \quad v(t) = f\left[i(t), \frac{di}{dt}\right] \tag{4.2}$$

For simplicity, the first of the two possible cases reported in eq. (4.2) will be treated. In order to obtain a discretized model of the circuit, an appropriate discretization scheme must be employed. In the case of band limited signals, where all signals are completely determined by discrete sample values at time intervals Δt, we may introduce the time discrete description ${}_kV_s^r = v_s^r(k\Delta t)$ and ${}_kV_s^i = v_s^i(k\Delta t)$.

For the development of the procedure to link the TLM mesh to a lumped circuit, it is most convenient to assume that the scattering at the nodes involves a delay Δt, and that transfer from one node to the next is instantaneous. Although this differs from the convention in eqs. (2.11-2.12) where the propagation of the impulses from one cell to the next is delayed by Δt and the scattering is instantaneous, the two approaches lead to identical algorithms.

If a central difference scheme is used, the following substitutions must be done for the half time step (k-1/2)Δt:

$$\begin{aligned} {}_{k-1/2}V &= ({}_kV + {}_{k-1}V)/2 \\ {}_{k-1/2}I &= ({}_kI + {}_{k-1}I)/2 \\ \left(\frac{dV}{dt}\right)_{k-1/2} &= \frac{{}_kV - {}_{k-1}V}{\Delta t} \\ \left(\frac{dI}{dt}\right)_{k-1/2} &= \frac{{}_kI - {}_{k-1}I}{\Delta t} \end{aligned} \tag{4.3}$$

Substituting the expressions for the current and for the voltage (4.1) in the equation describing the lumped circuit (4.2) and applying the above-mentioned discretization scheme, we obtain a finite difference equation which is solved for ${}_kV_s^i$, the unknown voltage impulse reflected by the device towards the node. For first-order circuits this recursive formulation can be written as:

$${}_kV_s^i = F[{}_kV_s^r,\ {}_{k-1}V_s^i,\ {}_{k-1}V_s^r] \tag{4.4}$$

Note that for first-order circuits the values of V_s^i and V_s^r at the previous time-step must be stored. When nonlinear devices are modeled, the determination of the new incident voltage requires the resolution of a nonlinear equation (F in eq. (4.4) is nonlinear).

4.3 Modeling of one-port equivalent circuits with the 3D TLM symmetrical condensed node

In the following, this method to include lumped-element devices in two dimensional networks will be extended to three-dimensional situations. At the beginning, we will assume that the device occupies a single TLM cubic cell; this assumption is generally acceptable, since the physical volume occupied by the device is small, compared with the other dimensions of the electromagnetic problem. Moreover, the device will be embedded in a homogenous structure. Successively, these assumptions will be removed and the general case of devices occupying more TLM cells in a heterogenous medium will be considered.

4.3.1 Device volume equal to a single TLM cell

In Section 2.3 it has been shown that the standard SCN can be equipped with three capacitive (shunt-connected) stubs, which modify the three electric components E_x, E_y, and E_z, and three inductive (series-connected) stubs, which influence the three magnetic components. These stubs are generally used to modify the electric and magnetic field storage in the volume occupied by the TLM cell, in order to model heterogenous media. If the subvolume to be modeled is constituted by an isotropic material, the characteristic admittances and impedances of the stubs in the three directions are the same, as reported in eqs. (2.22).

If a lumped device is connected to the node, then only one of the field components is affected by its presence; in this case, the TLM cell must be modified "anisotropically". This situation is reported in Figure 4.3; the lumped device will only affect the E_y component or, in terms of TLM quantities, only the voltages directed in the y direction: V_3, V_4, V_8 and V_{11}.

As in the two-dimensional case, the proposed technique to modify these voltages is to simply add a shunt-connected stub in the y-direction. Referring to the general stub-loaded scattering matrix shown in Figure 2.4, the inclusion of this stub corresponds to the case where all the stub admittances and impedances are null, except for $\hat{Y}_y$.

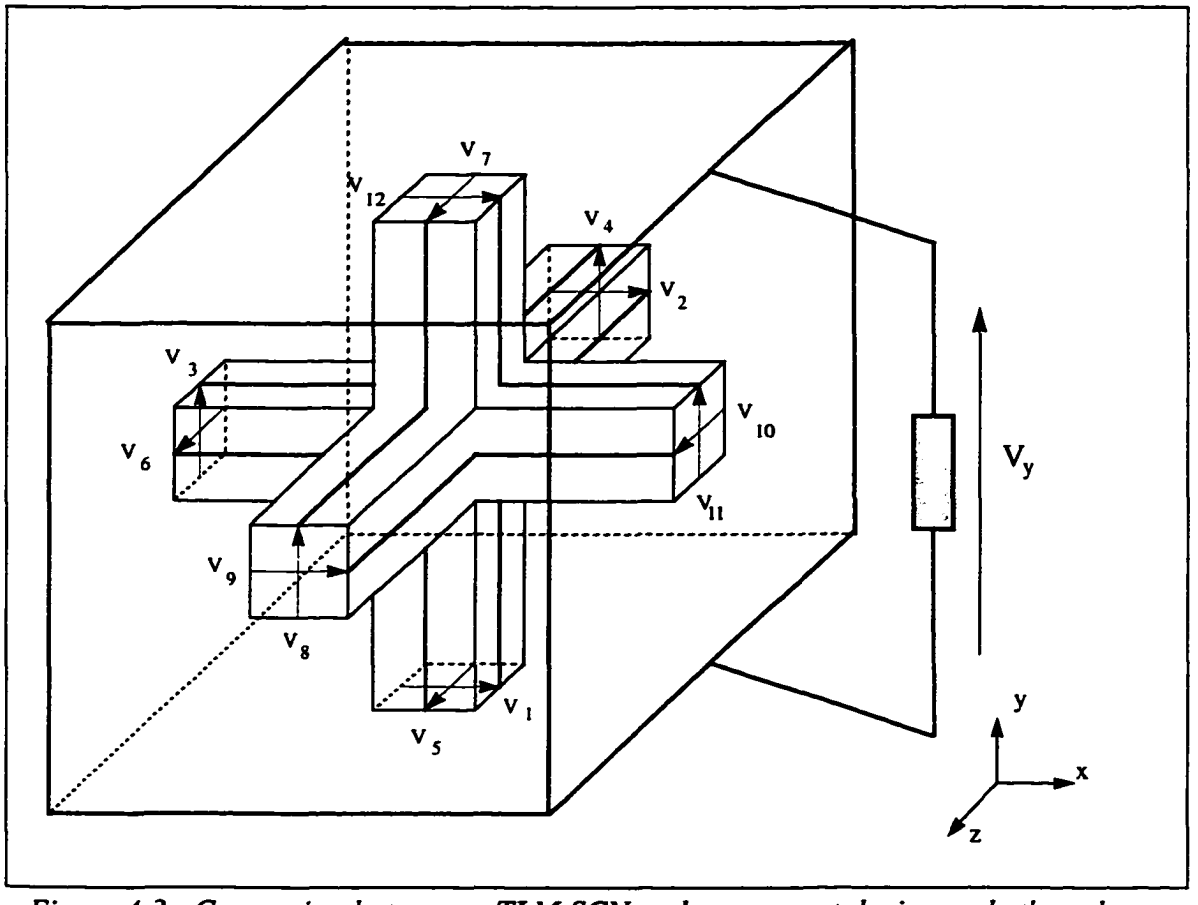

Figure 4.3 Connection between a TLM SCN and a one-port device: only the voltages along the y-direction are affected by the presence of the lumped circuit.

Again, by choosing appropriately the value of the normalized stub admittance, the incident and reflected voltages at the transmission line connecting the device to the TLM node can be decoupled; since the stub relative to the E_y component corresponds to voltage 14 in the scattering matrix, it can be seen that the decoupling is achieved if $h_{14,14}$ is zero, and this happens for:

$$\hat{Y}_y = 4 \tag{4.5}$$

The connection algorithm between the device and the TLM algorithm proceeds as in the two-dimensional case: the voltage and current at the circuit plane can be expressed respectively as sum and difference of the reflected and incident voltages traveling in the TLM stub (4.1). The current-voltage relation describing the circuit is hence substituted by a reflected voltage-incident voltage relation which is then discretized; a recursive formulation yielding the new incident voltage propagating form the device to the node is

obtained (4.4).

4.3.2 Device volume occupying more than one TLM cell in the three directions

In the previous Section, the proposed technique to connect the device to a TLM mesh was restricted to cases where the circuit volume was equal to the space occupied by a TLM node. While this assumption is not too restrictive in most of the cases, it is useful to develop a more general model, capable of representing larger elements.

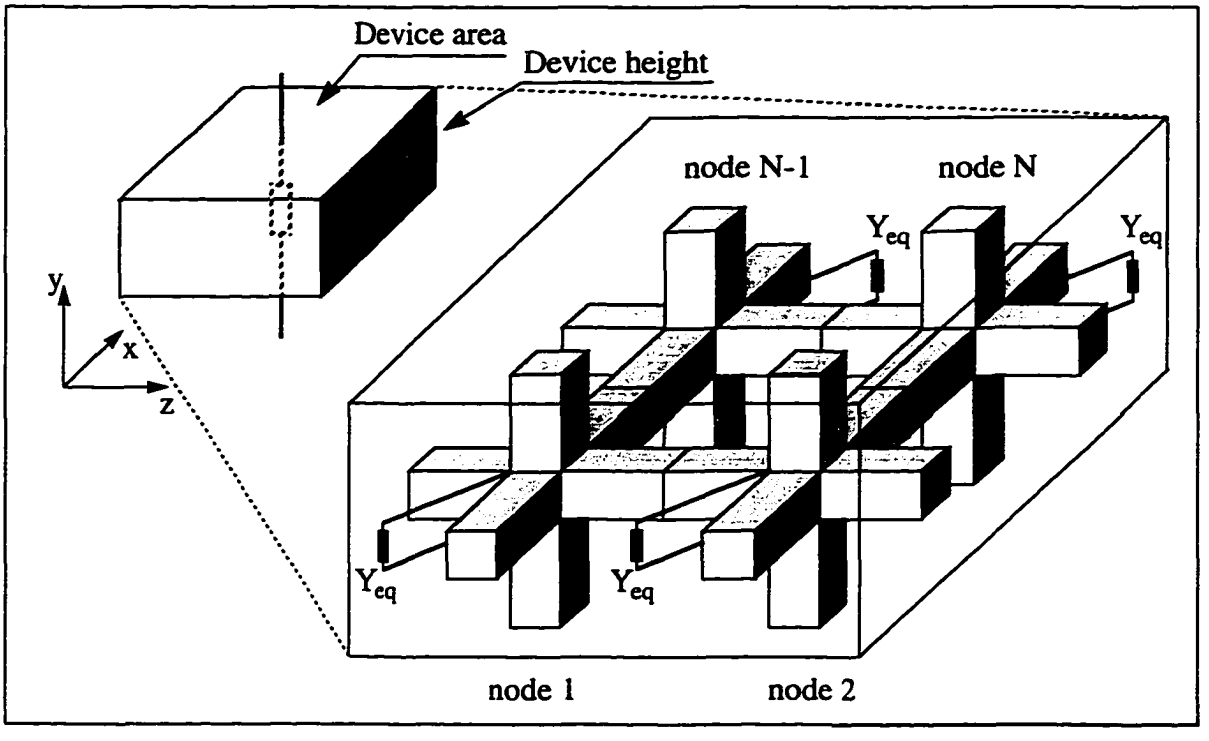

Figure 4.4 Equivalent TLM model of a lumped device occupying more than one cell in the plane perpendicular to the direction of the feeding voltage (xz-plane, in this example)

When dealing with the lumped component, it is important to distinguish whether the circuit occupies more cells in the direction of the feeding voltage, or in the plane perpendicular to it. First, let us consider the situation when the "area" of the device is larger than the cross-section of a single TLM cell; this corresponds to the second case. The lumped device can be modeled as the parallel combination of identical equivalent sub-elements, the properties of which are obtained by simple application of Kirchoff's equations. Each of these sub-elements will then be connected to one of the TLM nodes

enclosed in the device volume by means of a shunt stub. This situation is depicted in Figure 4.4.

In order to determine the sub-element characteristics, all the impedance values must be multiplied by the number (N) of nodes occupying the device area, while all the admittance and current source values must be divided by N.

In principle, a similar procedure can be applied to connect a lumped device to several TLM nodes in the direction of the feeding voltage. In this case, the total device is split-up into the series connection of lumped sub-elements, the characteristics of which are obtained by dividing all the impedance and voltage source values by the number (M) of nodes occupying the device height, and multiplying all the admittance values by M (Figure 4.5).

With this approach, the behavior of each sub-element depends only on the local field at the corresponding TLM cell. This assumption is acceptable in most situations, and it does offer the advantage of being easy to implement; unfortunately, it may create instabilities in the modeling of nonlinear, active devices such as Tunnel or Gunn diodes. In this case, each cell will then act as a separate active device, and therefore the connection of cells in the direction of the feeding voltage will have the effect of a series of diodes, which is DC-unstable. Another disadvantage occurs when the device to be modeled is a nonlinear element. For such situations, the determination of the unknown voltages V_m^i requires the resolution of M nonlinear equations at each time step.

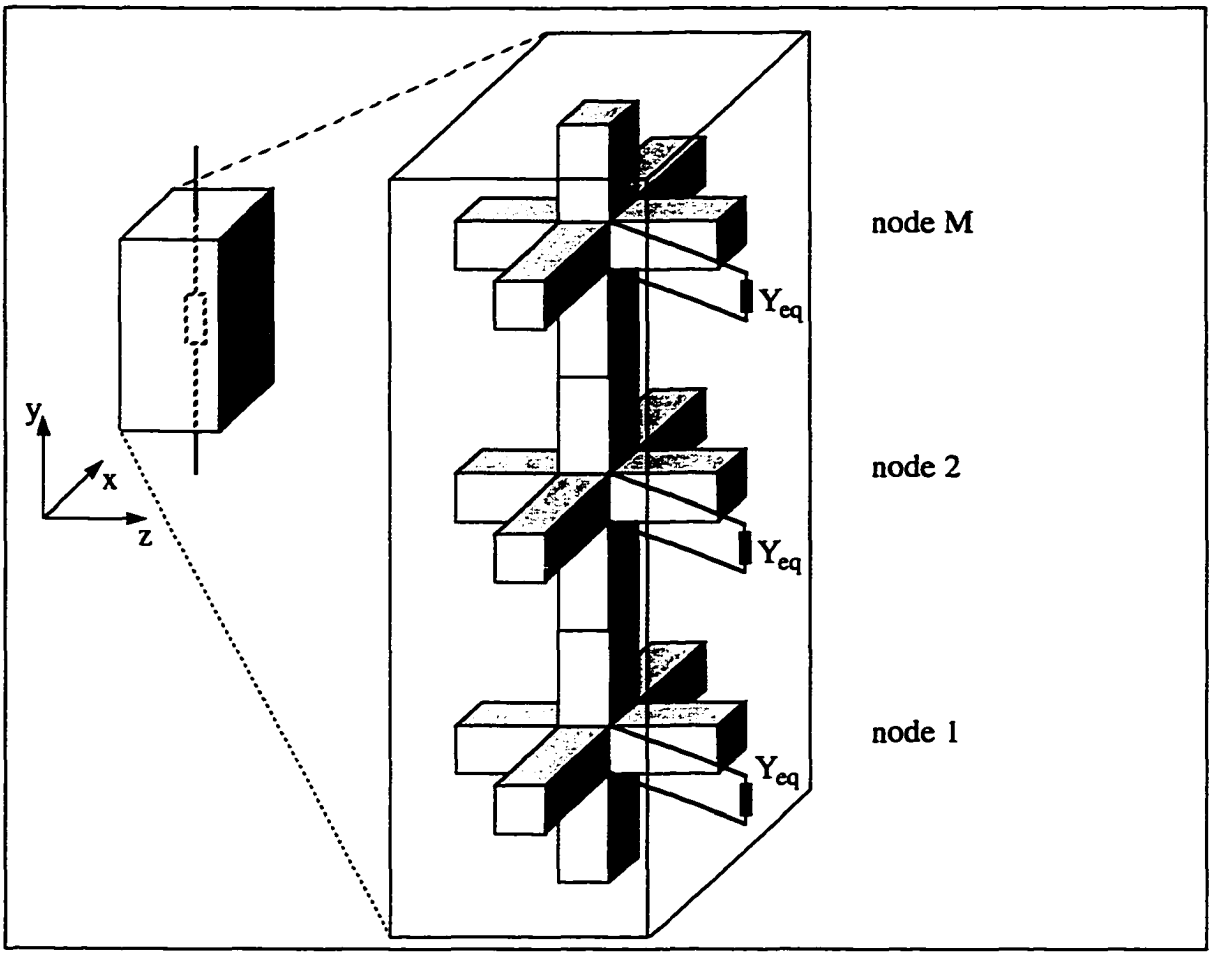

Figure 4.5 Equivalent TLM model of a lumped device occupying more than one cell in the direction of the feeding voltage (y-direction, in this example)

From the above discussion, it is evident that instabilities arise only in the case of decomposition of the element in the direction of the feeding voltage, while in the plane perpendicular to it no problems are generated by the subdivision into parallel circuits.

In order to circumvent this problem, a new technique must be developed to introduce nonlinear active elements in the three-dimensional TLM mesh. Such a technique must model the entire active region as a single device in the direction of the feeding voltage, while in the other two directions it will be still considered as the parallel combination of sub-circuits.

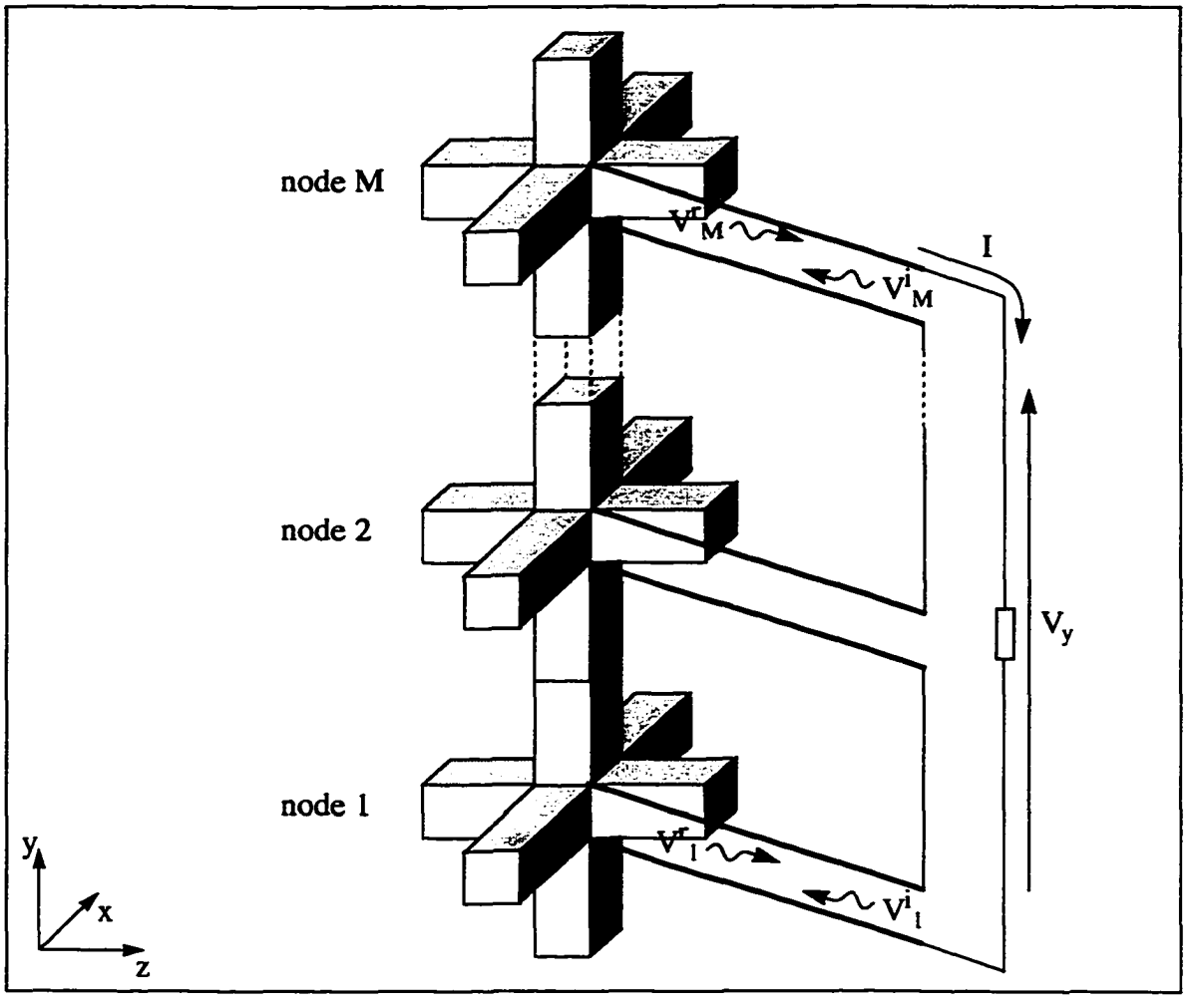

Figure 4.6 Schematic connection of the active device to the three-dimensional TLM mesh: the active region is modeled as a single element in the direction of the voltage

The proposed approach is based on the procedure presented in [17] for the connection of lumped sources to a two-dimensional network of series nodes; in that case the lumped source was placed across a set of series connected link lines and the new incident voltages in each transmission line, determined during the connection process, were dependent on the reflected voltages in the other link lines as well as on the source behavior. A similar idea has also been applied in FDTD [24] for the modeling of Gunn diodes: the voltage across the diode was a function of the sum of the local fields of all the FDTD cells in the active region; the standard FDTD algorithm had thus to be modified so that the updated field at each cell depended on the previous fields in all the cells of the active region.

The same concept can be applied to model nonlinear active devices in the three-dimensional TLM mesh.

Assuming that the connection between the TLM nodes and the device is still provided by shunt stubs, for the reasons explained in Section 4.2, at each time step the voltage across the device must be equal to the sum of the voltage drops across each TLM stub in the active region. This model is physically equivalent to arranging all the stub lines in a series connection, as displayed in Figure 4.6. For the sake of simplicity, we have also made the assumption that the area of the device is equivalent to a single TLM cell.

The connection procedure (4.4) must then take into account the new stub configuration. In particular, eqs. (4.1) takes the following form:

$$\begin{aligned} v(t) &= \sum_{m=1}^{M} [v_m^r(t) + v_m^i(t)] \\ i(t) &= Y_s \cdot [v_m^r(t) - v_m^i(t)] \qquad m = 1, \ldots, M \end{aligned} \tag{4.6}$$

where M is the number of TLM cells into which the height of the device is discretized, m indicates the node to which the stub belongs, and Y_s represents the stub admittance (assumed to be equal for all the stubs in the active region). In the present example $Ys = \hat{Y}_y Y_0$, where Y_0 is the admittance of the TLM link lines. It is important to observe that, due to the series connection of the stubs, the same current i(t) will flow in all the TLM stubs and in the device. Thanks to this important condition, all the (unknown) incident voltages $v^i_m(t)$ can be expressed as a function of only one of them, for example $v^i_1(t)$. Thus, from the second of eqs. (4.6) we can derive the relation:

$$v_m^i(t) = v_m^r(t) + v_1^r(t) - v_1^i(t) \qquad m = 2, \ldots, M \tag{4.7}$$

which can be substituted in the first of eqs. (4.6), so that both the voltage and current at the device plane depend only on a single unknown voltage, $v^i_1(t)$:

$$\begin{aligned} v(t) &= M \cdot v_1^i(t) + (2 - M)\, v_1^r(t) + 2 \sum_{m=2}^{M} v_m^r(t) \\ i(t) &= Y_s \cdot [v_1^r(t) - v_1^i(t)] \end{aligned} \tag{4.8}$$

These relations are substituted in the current-voltage equation and then discretized,

as described for the two-dimensional approach (Section 4.2). A finite difference equation is thus obtained, which can be solved for ${}_kV_1^i$, the unknown voltage impulse traveling from the device towards the node number 1. The other unknown voltages are then determined by using eq. (4.7).

For first order circuits, the general recursive formulation to obtain the new incident voltages as a function of the reflected impulses can be expressed as:

$$
\begin{aligned}
{}_kV_1^i &= F\left[{}_kV_1^r \,,\; {}_{k-1}V_1^i \,,\; {}_{k-1}V_1^r \,,\; \sum_{m=2}^{M} {}_kV_m^r \,,\; \sum_{m=2}^{M} {}_{k-1}V_m^r \right] \\
{}_kV_m^i &= {}_kV_m^r + {}_kV_1^r - {}_kV_1^i \qquad m = 2, \ldots, M
\end{aligned}
\tag{4.9}
$$

From the above expression, it appears that a secondary advantage of this approach is that, when nonlinear devices are modeled, the determination of the new incident voltages ${}_kV_m^i$ requires the resolution of a single nonlinear equation (F) at each time step, rather than M.

In general, when the device volume is larger than a single TLM cell, the combination of the techniques described in this Section is adopted. The device is first split-up in the shunt combination of equivalent sub-elements across the device area; each sub-element will then be described by the same equivalent circuit as that of the original device, but with scaled impedances and admittances. Each sub-element will then be interfaced to a cluster of nodes in the direction of the feeding voltage.

4.4 Modeling of one-port lumped devices in heterogenous media using the stub-loaded TLM node

In the previous Section, the connection of one-port lumped elements to 3D-TLM symmetrical condensed nodes has been discussed. This technique can be adopted when the device is embedded in a homogenous medium or in the dielectric region with the lowest permittivity (in the case of heterogenous problems). Only in these situations the standard SCN can be used, and additional stubs (traditionally used to model the material characteristics of the region and the cell geometry) can be provided to connect the device

to the nodes. If this conditions cannot be met, then the lines 13-18 are used to model the medium properties (Section 2.3), and other stubs, from now on identified as "device stubs", must be added to the node to link the device to the TLM mesh.

If a lumped device is connected to the node, then only one of the field components is affected by its presence; in this case, as for the connection of lumped circuits to the SCN, the TLM cell must be modified "anisotropically". In general, assuming that the device can be oriented in any one of the three Cartesian directions, three stubs with appropriate admittances must be added to the node; only one of them will be then effectively used in connection with the device, while the others will be eliminated by setting their admittance to zero (anisotropic modification of the node).

The scattering matrix of the new node, now taking into account the interaction between 21 lines (12 link lines and 9 stubs), must be determined according to the laws of energy conservation, and assumes a form similar to that of the SCN for the modeling of electrical losses [10]. In that case, since the additional lossy stubs are assumed to be matched, no incident voltages are coming from them towards the node, and a 18x21 matrix is sufficient to describe the situation. When using the device stubs to connect the lumped element equivalent circuit, voltages will travel from the device to the node, hence the interaction between these impulses and the rest of the node must be taken in consideration. A full 21x21 matrix is therefore needed to model the material properties of the node in conjunction with the presence of the lumped device.

The coefficients of the new scattering matrix are given by:

$$a = -\frac{\hat{Y}+\hat{Y}_s}{2(4+\hat{Y}+\hat{Y}_s)} + \frac{\hat{Z}}{2(4+\hat{Z})} \qquad b = \frac{4}{2(4+\hat{Y}+\hat{Y}_s)}$$

$$c = -\frac{\hat{Y}+\hat{Y}_s}{2(4+\hat{Y}+\hat{Y}_s)} - \frac{\hat{Z}}{2(4+\hat{Z})} \qquad d = \frac{4}{2(4+\hat{Z})}$$

$$e = b \qquad f = \hat{Z}d \qquad g = \hat{Y}b \tag{4.10}$$

$$h = \frac{\hat{Y}-\hat{Y}_s-4}{4+\hat{Y}+\hat{Y}_s} \qquad i = d \qquad j = \frac{4-\hat{Z}}{4+\hat{Z}}$$

$$m = \frac{\hat{Y}_s-\hat{Y}-4}{4+\hat{Y}+\hat{Y}_s} \qquad n = \hat{Y}_s b$$

where $\hat{Y}$ is the normalized stub admittance for the modeling of the material permittivity, $\hat{Z}$ is the normalized stub impedance for the modeling of the material permeability (eqs. 2.22), and $\hat{Y}_s$ is the normalized device stub admittance, which is different for the three directions ($\hat{Y}_{sx}$, $\hat{Y}_{sy}$, $\hat{Y}_{sz}$), according to the orientation of the device. In this case $\hat{Y}_{sx} = \hat{Y}_{sz} = 0$.

The global scattering matrix, modified to take into account the presence of device stubs, is given by:

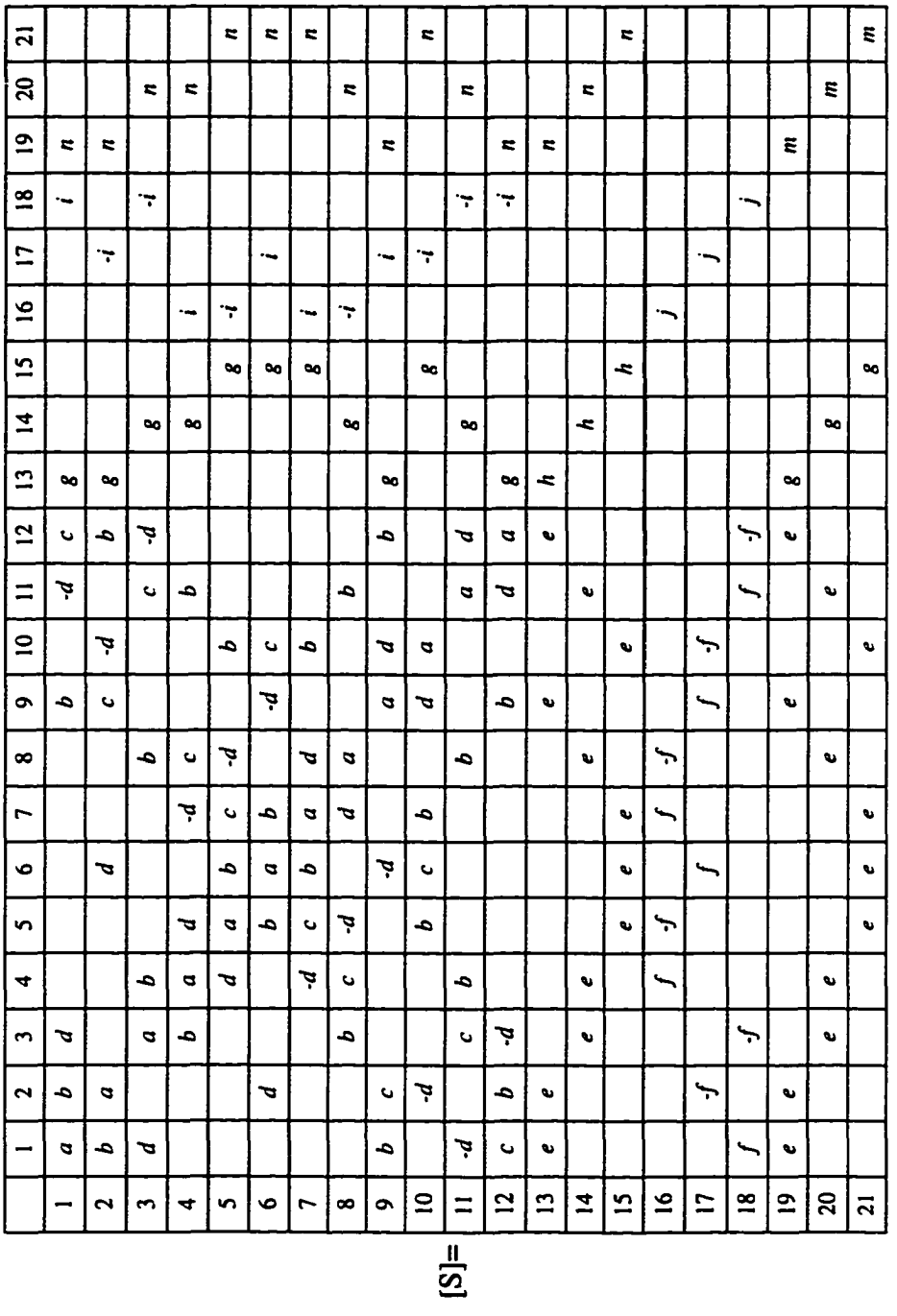

$$[S] =$$

Figure 4.7 Scattering matrix for the stub-loaded SCN equipped with device stubs in the three directions. With this matrix, both heterogeneous material properties and lumped circuits can be included in the TLM simulation.

With respect to the lossy SCN (for the case of electrical losses only), the coeffi-

cients *m* and *n* are added, to take into account the portion (*m*) of the voltage traveling in the device stub that is reflected back towards the device, and the fraction (*n*) that is transmitted to the link lines and the capacitive stub related to the same voltage.

In order to decouple the linear and nonlinear behavior of the circuit, the value of the device stub admittance can be chosen appropriately. This corresponds to the value of $\hat{Y}_s$ that annihilates the value of the m coefficient for the relative stub. For example, if the device is placed in the y-direction (Figure 4.3), the element $m_{20,20}$ must be null. By inspection of the scattering matrix coefficients (4.10), it is evident that this is obtained when:

$$\hat{Y}_{sy} = \hat{Y}_y + 4 \tag{4.11}$$

The general procedure to determine the new incident voltages, as explained in the previous Section, remains invariate in the case of stubs with same characteristic admittance; for those situations in which the lumped device is placed across materials with different permittivities, eqs. (4.7-4.8) become:

$$v_m^i(t) = v_m^r(t) + \frac{Y_{s1}}{Y_{sm}}\left[v_1^r(t) - v_1^i(t)\right] \qquad m = 2, \ldots, M \tag{4.12}$$

$$\begin{aligned} v(t) &= \left[v_1^i(t) - v_1^r(t)\right] \cdot \sum_{m=1}^{M} \frac{Y_{s1}}{Y_{sm}} + 2\sum_{m=1}^{M} v_m^r(t) \\ i(t) &= Y_{s1} \cdot \left[v_1^r(t) - v_1^i(t)\right] \end{aligned} \tag{4.13}$$

where Y_{sm} indicates the characteristic admittance for the m-th device stub.

4.5 Modeling of two-port lumped devices in 3D-TLM networks

In the following, an extension of the procedure described above to include two-port nonlinear active and passive devices in the TLM network will be presented. In order to simplify the analysis, the device will be assumed to occupy two adjacent clusters of TLM nodes in the z-direction, and M nodes in the y-direction (Figure 4.8). As in the previous cases (Section 4.3.2), the device is modeled as a single element in the direction of the feeding voltages; in this way, instabilities are avoided when the device is active and non-

linear. The device is thus linked to the mesh by means of two sets of device stubs, which are series connected in the y-direction. In order to ensure that the only interaction between the two sets of nodes occurs because of the presence of the device, the link lines normally connecting the set of nodes in the z-direction are terminated by open circuits (see top view in Figure 4.8).

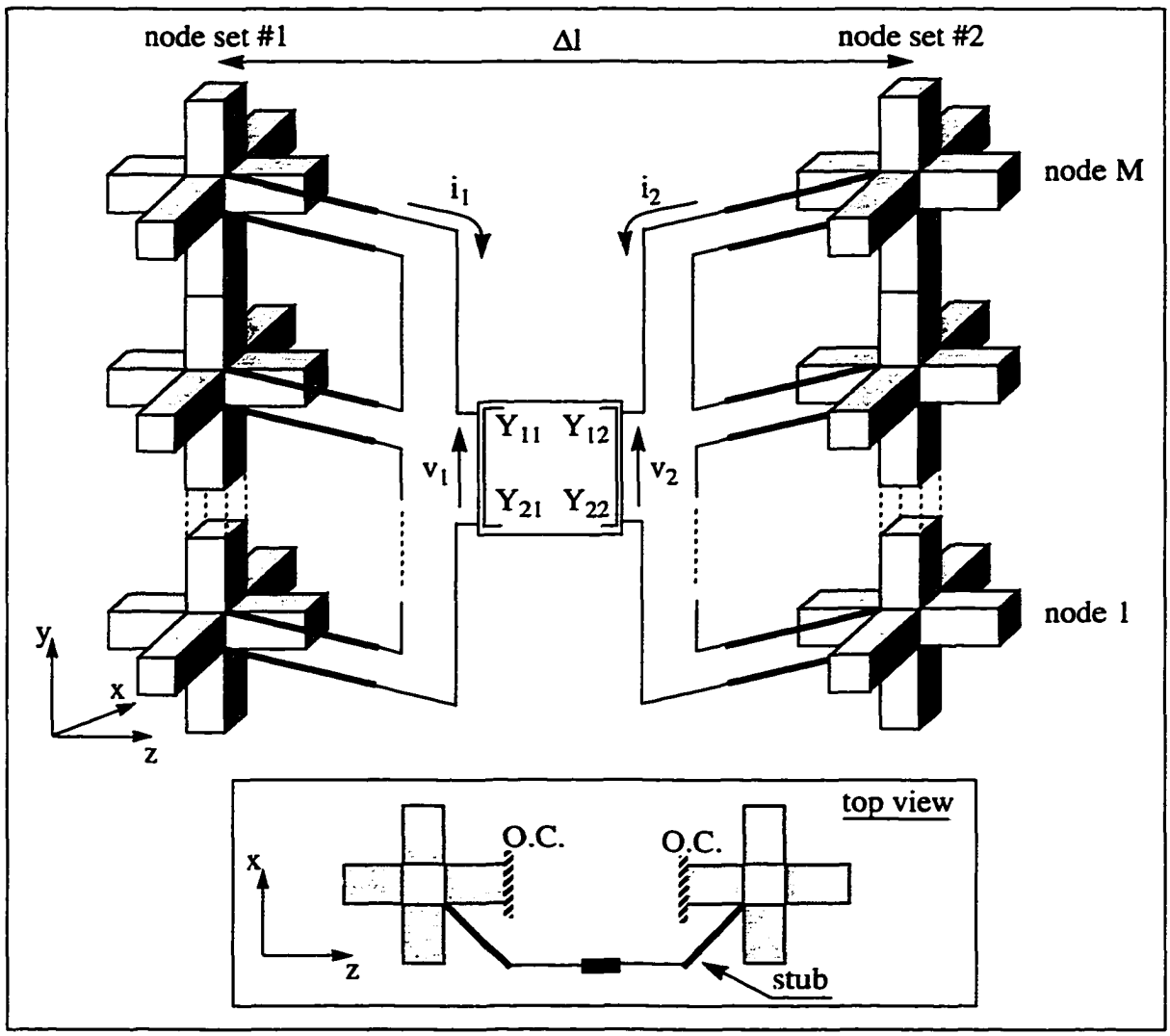

Figure 4.8 The connection of a two-port lumped device to a 3D TLM network. The device is described by a generic 2x2 Y matrix and is connected to two clusters of TLM nodes by means of device stubs. The link lines, which are normally connected in the z-direction during the propagation process, are terminated by open circuits (top view).

The admittance of the stubs is determined according to the same considerations in Sections 4.3 and 4.4, and therefore is not discussed here. The electrical quantities in the

lumped circuit are now $v_1(t)$, $i_1(t)$, $v_2(t)$ and $i_2(t)$; in general, the device behavior can be represented by a set of coupled nonlinear equations:

$$\begin{aligned} i_1(t) &= f_1[v_1(t), v_2(t)] \\ i_2(t) &= f_2[v_1(t), v_2(t)] \end{aligned} \tag{4.14}$$

The currents and voltages can be also expressed in terms of the incident and reflected voltages traveling in the device stubs; eqs. (4.8) can be rewritten as:

$$\begin{aligned} v_{l,2}(t) &= M \cdot v^i_{l_{1,2}}(t) + (2-M)\, v^r_{l_{1,2}}(t) + 2 \sum_{m=2}^{M} v^r_{m_{1,2}}(t) \\ i_{l,2}(t) &= Y_s \cdot \left[v^r_{l_{1,2}}(t) - v^i_{l_{1,2}}(t) \right] \end{aligned} \tag{4.15}$$

where the subscripts 1,2 indicate which set of nodes the voltages refer to.

Proceeding as for the inclusion of one-port devices, eqs. (4.15) are substituted into the coupled equations relating the currents and voltages in the device (eq. (4.14)), and an appropriate discretization scheme is used. In this way, making also use of the relation (4.7) imposed by the series connection of the stubs, a set of coupled finite difference equations are obtained, describing the new incident voltages for the two sets of device stubs. For first order circuits, these can be written in the following general form:

$$\begin{aligned} {}^{k+1}V^i_{l_{1,2}} = F_{l,2}\Bigg[& {}^{k}V^r_{l_1},\ {}^{k}V^i_{l_1},\ {}^{k-1}V^r_{l_1},\ \sum_{m=2}^{M} {}^{k}V^r_{m_1},\ \sum_{m=2}^{M} {}^{k-1}V^r_{m_1} \\ & {}^{k}V^r_{l_2},\ {}^{k}V^i_{l_2},\ {}^{k-1}V^r_{l_2},\ \sum_{m=2}^{M} {}^{k}V^r_{m_2},\ \sum_{m=2}^{M} {}^{k-1}V^r_{m_2} \Bigg] \end{aligned} \tag{4.16}$$

$$ {}^{k+1}V^i_{m_{1,2}} = {}^{k}V^r_{m_{1,2}} + {}^{k}V^r_{l_{1,2}} - {}^{k+1}V^i_{l_{1,2}} \qquad m = 2, \ldots, M$$

4.6 Evaluation of the capacitive effect produced by the device stubs

As briefly mentioned in Section 4.2, the main disadvantage of the proposed technique is that a parasitic capacitance is introduced in the analysis of the circuit. If the wavelengths of the signal are sufficiently larger than the stub length (this assumption is

generally true, to maintain the dispersion error below acceptable values), the stub behaves like a parallel plate capacitor shunt-connected to the device model (Figure 4.4). In the following a quantitative evaluation of this effect will be given.

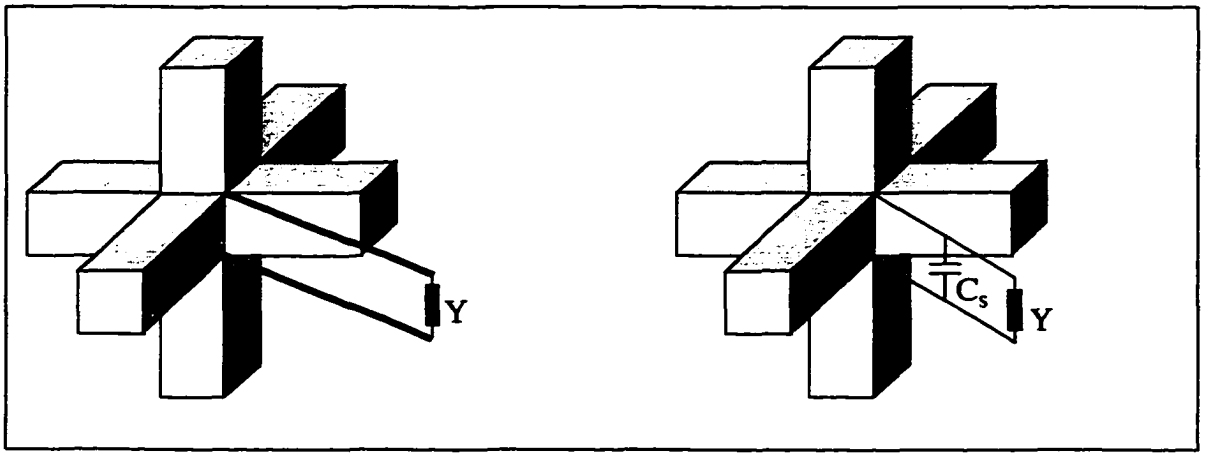

Figure 4.9 a) Connection of a lumped device to the TLM node by means of a stub. b) The stub is modeled by an equivalent lumped capacitance C_s.

Before proceeding with the analytical determination of the parasitic capacitance, it is worthwhile mentioning that such a capacitance has also been included in FDTD [27] in order to link the FDTD algorithm to SPICE. The value of the additional capacitance was given by:

$$C = \varepsilon \cdot \frac{A}{\Delta x} \tag{4.17}$$

where A was the area of the finite difference cell and Δx its height.

In order to determine the value of the parasitic capacitance C_s introduced in the TLM algorithm, we will first examine the case when the device is connected to a single SCN (Figure 4.3), according to the procedure discussed in Section 4.3. From transmission line theory, the value of capacitance is determined examining the stub when this is terminated by an open circuit. For low frequencies, the input admittance of the open-circuited stub can be approximated by:

$$Y_{in} = j \cdot Y_s \tan(\beta \cdot \Delta l_{stub}) \approx j \cdot Y_s \cdot \frac{\omega}{v_{stub}} \Delta l_{stub} = j\omega C_s \tag{4.18}$$

In this expression, Δl_{stub} represents the length of the device stub and v_{stub} repre-

sents the velocity of propagation in the stub. In order to maintain the synchronism of the impulses, the following relations must be satisfied:

$$\begin{aligned} v_{stub} &= v_{line} \\ \Delta l_{stub} &= \frac{\Delta l_{line}}{2} \end{aligned} \tag{4.19}$$

where Δl_{line} is the spatial discretization step of the TLM mesh and v_{line} is the velocity of propagation of the impulses in the link lines.

Substituting the expressions for Y_s, Δl_{line} and v_{line} in (4.18) we finally obtain the desired value for the parasitic capacitance introduced by the device stub:

$$C_s = \varepsilon \cdot \Delta l_{line} \tag{4.20}$$

It is straightforward to verify that the value of the additional capacitance (4.17) used to link the SPICE model to an FDTD cell reduces to eq. (4.20), for the case of a cubic FDTD cell of size Δl_{line}.

For those situations in which the device area is larger than the area of a single TLM cell (Figure 4.4) the capacitive load is increased because all the additional capacitances of the device stubs are connected in parallel. In this case the total capacitance is given by $N \cdot C_s$. The opposite happens when the device height is larger than the height of a single TLM cell (Figures 4.5-4.6). In this case the total capacitance is reduced because of the series combination of the stubs, and is equal to C_s/M.

When the device is embedded in a heterogenous medium, the additional capacitance introduced by the device stubs can be determined with a similar procedure. Assuming that the lowest permittivity in the electromagnetic problem under study is air, the admittance of the device stub is given by $Y_s = 4 \cdot \varepsilon_r Y_0$ (obtained combining eqs. (4.11) and (2.22)). After some algebraic manipulations the value of the capacitance is obtained:

$$C_s = \varepsilon_0 \varepsilon_r \cdot \Delta l_{line} \tag{4.21}$$

The correctness of these expressions will be verified with numerical experiments in the next Chapter.

4.7 Conclusions

In this Chapter, a new technique to embed lumped equivalent circuits into 3D-TLM meshes has been proposed. The procedure consists in linking the nonlinear devices to the nodes of the TLM network by means of stubs of length $\Delta l/2$. The stubs related to the electric field components, traditionally employed to model the material dielectric properties, have been used for this purpose. The new stub voltages incident upon the nodes are modified by the presence of the lumped circuit connected to TLM cell. The procedure does not impose restrictions regarding the number of cells occupied by device, and can be applied to both one- and two-port devices.

A modification of the stub-loaded SCN scattering matrix has also been proposed, to model lumped circuits in heterogeneous media and graded meshes. With this generalization, arbitrary structures containing nonlinear devices can be analyzed.

Finally, the capacitive effect introduced by the device stubs has been determined. Since the value of the extra capacitance is known 'a priori', the error introduced may in many cases be compensated.

Chapter 5

Validation of the Device Stub Approach for One- and Two-port Lumped Devices

5.1 Introduction

In the previous Chapter, a general procedure to embed lumped element circuits into a TLM network has been examined. The procedure requires the addition of device stubs with appropriate characteristic admittance to link the lumped circuit to the SCN nodes, and the modification of the connection matrix for such nodes to take into account the presence of the device. The general expressions for the modification of the new incident voltages in the case of one-port (4.4) and two-port devices (4.16) have been determined for first-order lumped circuits. Unfortunately, these expressions are not directly applicable to the TLM algorithm, since they must be formulated for each specific component embedded in the TLM mesh.

In the following, the expressions will be specified for several types of elements, and their validity will be tested against analytical solutions (when available) or compared with SPICE simulations. The testing procedure will be performed for one-dimensional problems for two reasons: the behavior of the problem can be easier to obtain analytically, and the numerical results determined with the TLM simulations are not affected by a dispersion error. In this way the accuracy of the procedure will be more easily determined.

First, simple linear devices such as resistive voltage and current sources will be implemented. The models of linear first-order circuits such as RL and RC circuits, will then be considered. In this context, the presence of a capacitive effect due to the device stubs will be also verified (Section 4.6). Successively, the inclusion of nonlinear passive

and active devices will be examined; in this framework, the importance of the discretization scheme will be discussed. Finally, a fully 3D example is presented, to test the method in the presence of graded meshes, heterogenous media and lumped devices. In this case, the modeling results are compared to measurements available in the literature.

5.2 Modeling of lumped resistive sources in 3D-TLM

An electromagnetic problem can be often decomposed into distributed and lumped components. The simplest lumped components that can be identified are the voltage sources, generally used to bias the circuit and/or to produce a RF signal. These sources can be included either by simulating a distributed source with an appropriate source impedance (this approach is generally used to model matched sources), or by including a suitable model to interface lumped sources to the TLM network (this method is preferred when arbitrary source impedances are to be modeled). In the following we will pursue this second approach. In this way, the proposed method will be first tested for a simple linear situation, before approaching circuits with memory and nonlinear problems. It is worthwhile mentioning that, unlike FDTD [13], since in the TLM method both voltages and currents are defined simultaneously, no time-averaging is necessary when circuits without memory are treated.

In the following, both voltage and current sources will be embedded in the TLM network. As demonstrated in the previous Chapter, lumped devices occupying a volume larger than a single TLM cell are split-up into N equivalent sub-elements in the device cross-section (Section 4.3.2), which are then assumed to be interfaced to a cluster of M nodes along the device height. Each sub-element is described by the same equivalent circuit of the device, provided that its electrical components are appropriately scaled. For this reason, the recursive formulation will only be derived for lumped components occupying M cells in the direction of the device voltage, and having an area equivalent to a single TLM cell. In this case, the connection between the device and the TLM mesh is provided by M stubs, arranged as in Figure 5.1 (the reader is also referred to Figure 4.6 for the full representation of the connection). The admittance of the stubs is given by (4.5) if the electromagnetic problem is embedded in a homogeneous medium, or by (4.11), in the presence of a heterogenous medium.

The essence of the method is to determine the relation imposed by the device between the voltage v(t) and the current i(t), and to replace it with a relation between the

reflected and incident voltages traveling in the device stubs, according to eqs. (4.6).

In the case of a simple voltage source, the relation between the voltage and the current is given by:

$$v(t) - v_s(t) = R_{int} \cdot i(t) \tag{5.1}$$

Note that in the previous equation no assumptions have been made about the time-domain behavior of the voltage source, therefore the same expression describes both DC and RF sources.

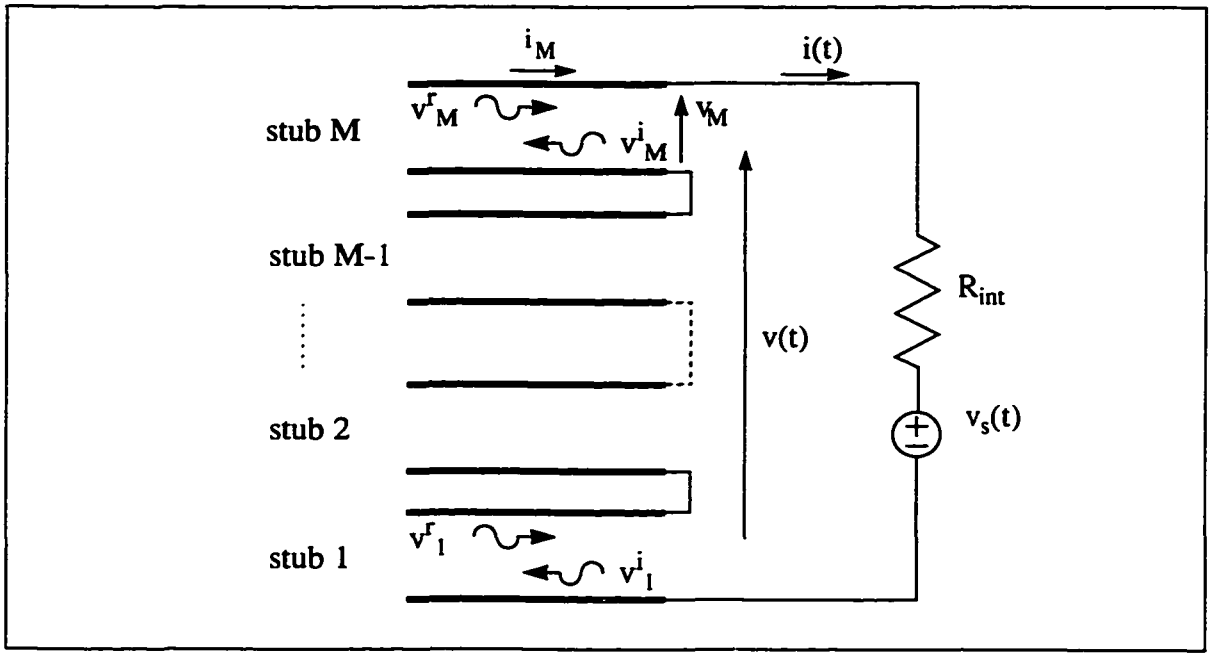

Figure 5.1 Connection of a lumped voltage source across M device stubs in the direction the feeding voltage

By making use of the expressions (4.1), the previous formula can be rewritten as:

$$(M + R_{int}Y_s)\, v^i_1(t) = (M - 2 + R_{int}Y_s)\, v^r_1(t) - 2 \sum_{m=2}^{M} v^r_m(t) + v_s(t) \tag{5.2}$$

and since there are no time derivatives, this can be easily translated into its discretized form for the time step $k\Delta t$:

$$ {}_kV_1^i = \frac{1}{(M+R_{int}Y_r)} \left[(M-2+R_{int}Y_r) \cdot {}_kV_1^r - 2 \sum_{m=2}^{M} {}_kV_m^r + {}_kV_s \right] $$

$$ {}_kV_m^i = {}_kV_m^r - {}_kV_1^r + {}_kV_1^i \qquad m = 2, \ldots, M \tag{5.3} $$

Equations (5.3) represent the recursive formulation providing the new incident voltages V^i_m as a function of the voltages reflected into the nodes V^r_m and of the source behavior (discretized at the time step k). Note that the second of the equations (5.3) gives the new incident voltages for m = 2, ..., M and is due to the imposition of a series connection among the stubs; thus it is not dependent on the particular device that is connected to the TLM mesh. For this reason it will be omitted in the following examples.

A similar set of equations are obtained for the modeling of a resistive current source, as the one represented in Figure 5.1.

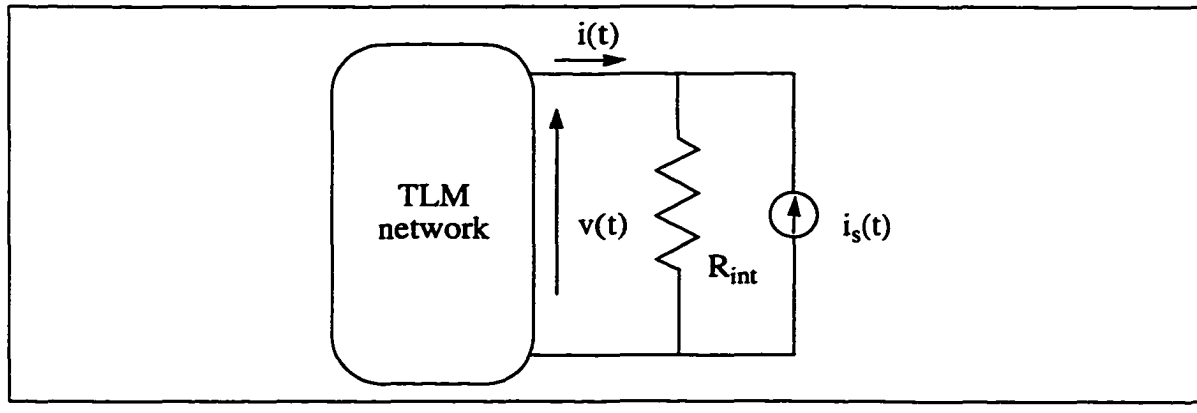

Figure 5.2 Connection of a lumped current source to a TLM network; the source is assumed to occupy M cells in the direction the feeding voltage

In this case the device equation is given by:

$$ v(t) = R_{int}[i(t) + i_s(t)] \tag{5.4} $$

The substitution of eqs. (4.1) now gives:

$$ {}_kV_1^i = \frac{1}{(M+R_{int}Y_r)} \left[(M-2+R_{int}Y_r) \cdot {}_kV_1^r - 2 \sum_{m=2}^{M} {}_kV_m^r + (R_{int} \cdot {}_kI_s) \right] \tag{5.5} $$

In order to verify the validity of the method, a lumped voltage source has been connected to a field model of an air-filled parallel plate capacitor (Figure 5.3.b), having plate length l = 10 mm, width w =3 mm, and plate separation h =3 mm (C = 0.974pF); the sides of the capacitor have been terminated by open-circuit boundaries. The source provides a sinusoidally oscillating voltage with amplitude 10 V and frequency of 1GHz, and is connected to an internal series resistance of 1.5 KΩ. The chosen spatial discretization step is Δl = 1mm; therefore the capacitor width is described by 3 TLM cells. In order to simulate a one-dimensional problem, the voltage source is assumed to occupy the full width (N=3) and height (M=3) of the capacitor. A schematic representation of the problem is given in the following picture:

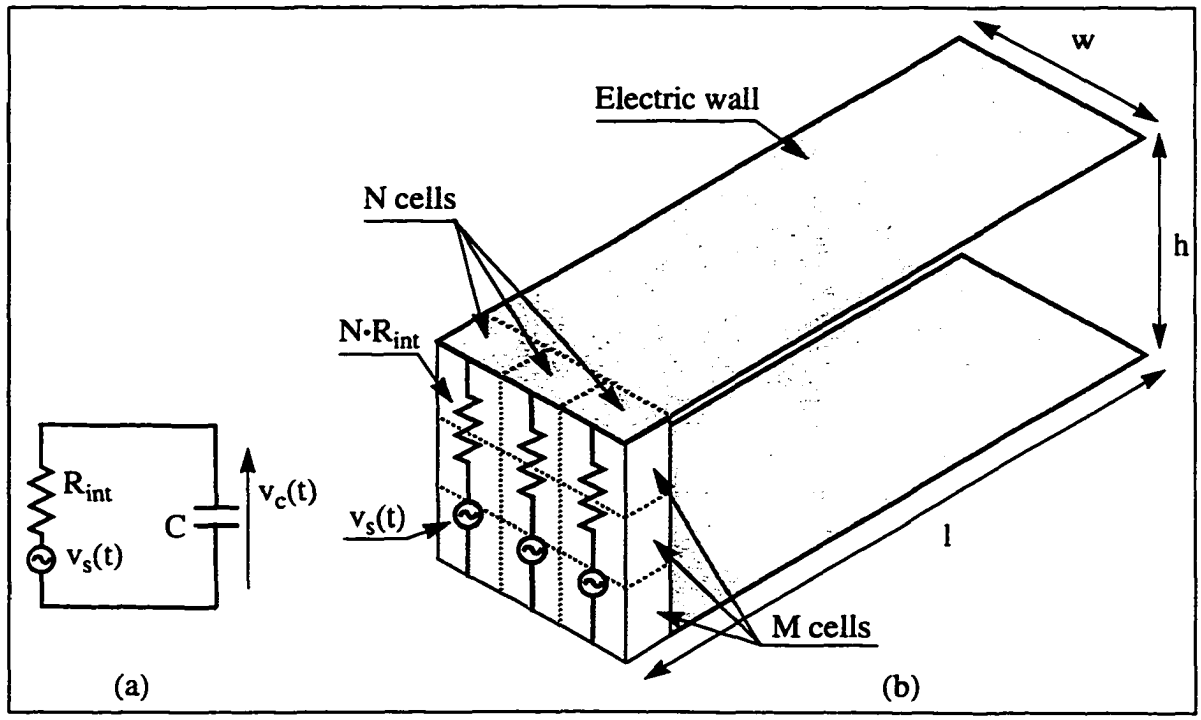

Figure 5.3 a) Lumped element representation of a capacitor connected to a resistive RF voltage source and b) its three-dimensional representation in a TLM network: the capacitor has been modeled with a parallel plate waveguide and the lumped voltage source has been distributed over the capacitor cross-section.

In order to determine the analytical response of the circuit, the capacitor must be sufficiently small with respect to the wavelength of the RF source, so that it is possible to neglect the voltage variations across the capacitor. If this assumption is correct, the transient response of the circuit can be determined by analyzing the equivalent lumped ele-

ment circuit of Figure 5.3.a and using the Laplace transform:

$$v_s(t) = V_0 \sin(\omega_s t) \qquad t \geq 0$$

$$v_c(t) = \frac{V_0}{[1 + (\omega_s R_{int} C)^2]} \{\omega_s R_{int} C \left[\exp(-\frac{t}{R_{int} C}) - \cos(\omega_s t) \right] + \sin(\omega_s t) \} \quad (5.6)$$

To verify the validity of eq. (5.3), the voltage across the capacitor, $v_c(t)$, has been determined with a TLM simulation and compared with the analytical solution. The comparison between the analytical and the numerical results shows a very good agreement (Figure 5.4); the small amplitude and phase differences are mainly due to the additional capacitance provided by the device stubs. This effect will be further investigated in the next Section.

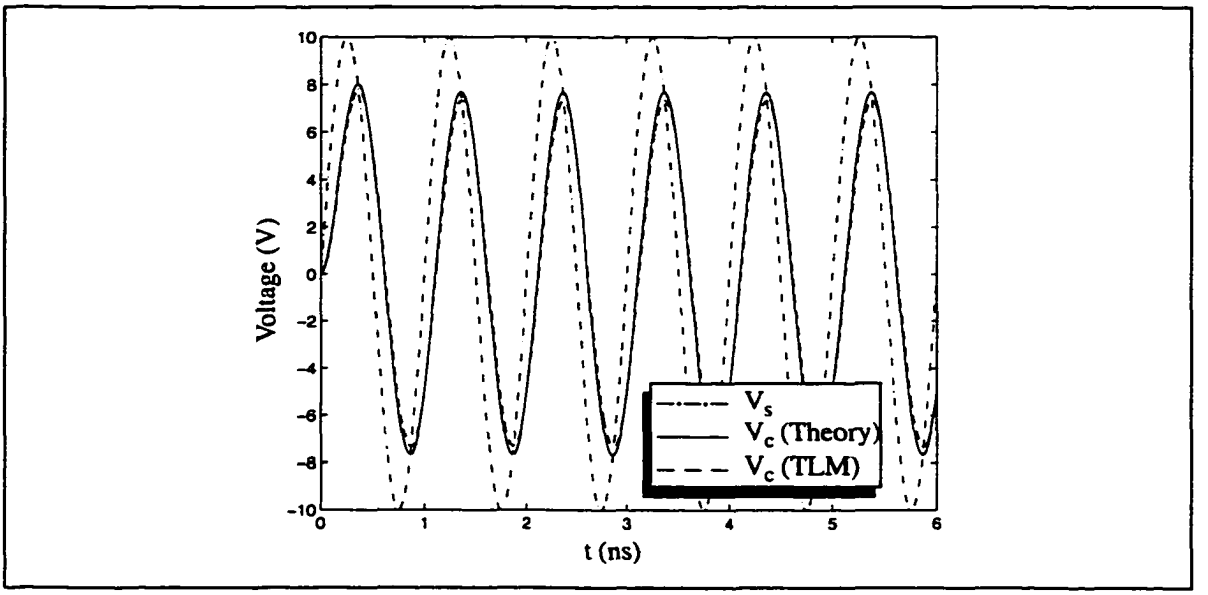

Figure 5.4 Validation of the lumped voltage source model $v_s(t)$: the transient behavior of the voltage produced across the distributed capacitor (Figure 5.3.b) is in very good agreement with the predicted response evaluated for the lumped circuit model of Figure 5.3.a.

5.3 Derivation of the recursive formulation for linear, first-order lumped circuits (RC and RL)

The successive step in the modeling of lumped devices in the TLM network consists in the inclusion of circuits with memory. Lumped capacitors can be easily found in

RF or microwave circuits alone (for example, they may be used as DC blocks) or in combination with resistive elements, for example in the lumped equivalent circuit of a diode. Lumped inductors are less frequently used at high frequencies, where distributed inductors are usually preferred; yet, their modeling as lumped elements can in some cases be useful, for example in the design process of a RF switch (RF chokes).

When circuits with memory are modeled, information about the circuit state at the previous time steps must be retained in order to predict the device response to the impinging TLM voltages. Recalling that the recursive expression for the new incident voltages depends on the particular equivalent circuit that is interfaced to the TLM mesh, the following RC network will be now examined:

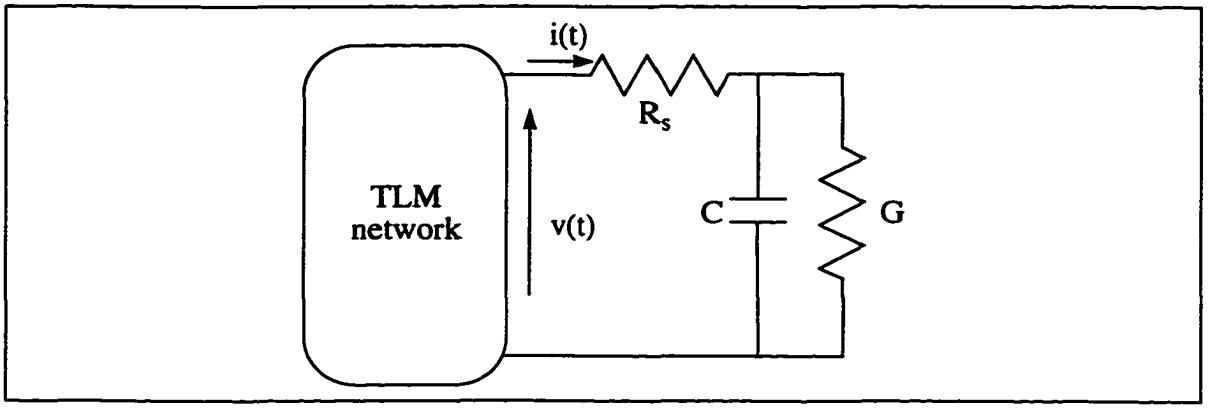

Figure 5.5 Connection of a sample lumped RC network to a 3D-TLM mesh

The circuit is composed of a series resistance R_s connected to the shunt combination of a capacitor C and another resistance of value 1/G. As in the source example, the circuit is assumed to be interfaced to M symmetrical condensed nodes in the direction of v(t), the connection being provided by the usual device stubs. The area of the lumped circuit is assumed to be equal to that of a TLM cell. From now on, these conditions will be assumed for each device modeled in the TLM network; therefore, they will not be reiterated in the successive examples.

The current-voltage equation for the circuit represented in Figure 5.5 is easily obtained by applying Kirchoff's laws:

$$(1 + R_s G)\, i(t) = G \cdot v(t) + C \cdot \frac{d}{dt}[v(t) - R_s \cdot i(t)] \tag{5.7}$$

This expression must now be discretized according to eqs. (4.3), thus giving:

$$\alpha I_k = \beta V_k - \gamma I_{k-1} + \delta V_{k-1} \tag{5.8}$$

where:

$$\begin{aligned} \alpha &= \frac{1}{2}(1 + R_s G) + \frac{CR_s}{\Delta t} & \beta &= \frac{G}{2} + \frac{C}{\Delta t} \\ \gamma &= \frac{1}{2}(1 + R_s G) - \frac{CR_s}{\Delta t} & \delta &= \frac{G}{2} - \frac{C}{\Delta t} \end{aligned} \tag{5.9}$$

By replacing V_k and I_k according to eqs. (4.6), the recursive formulation yielding the new incident voltages is finally obtained:

$${}_kV_l^i = \frac{[\alpha \cdot Y_s + (M-2)\beta]\,{}_kV_l^r - 2\beta \cdot \sum_{m=2}^{M} {}_kV_m^r + \gamma \cdot {}_{k-1}I - \delta \cdot {}_{k-1}V}{\alpha \cdot Y_s + M \cdot \beta} \tag{5.10}$$

where Y_s is the device stub admittance.

From the previous equation (5.8), it appears that in order to obtain the new incident voltages the previous values of the total voltage ($_{k-1}V$) and current ($_{k-1}I$) must be stored.

As an example of first-order RL circuit, a resistive voltage source with a series lumped inductor will be connected to the TLM mesh. If the source models a switching voltage, this circuit can be used for example to bias a diode switch. In this case the inductor prevents the RF signal from propagating into the biasing circuit (RF choke).

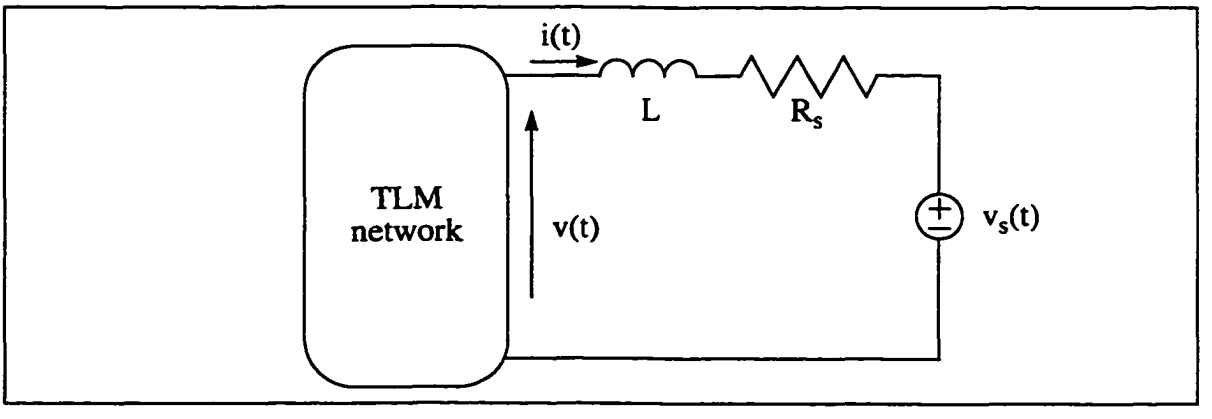

Figure 5.6 Connection of a sample lumped RL network to a 3D-TLM mesh

In this case the voltage-current equation can be written as:

$$R_s \cdot i(t) + L\frac{di}{dt} = v(t) - v_s(t) \tag{5.11}$$

Proceeding as for the previous example, the recursive formulation for this kind of circuit is given by:

$${}_kV_l^i = \frac{\left[M - 2 + (R_s + \frac{2L}{\Delta t})\,Y_s\right]{}_kV_l^r - 2\sum_{m=2}^{M} {}_kV_m^r - {}_kV + {}_kV_s + {}_{k-1}V_s}{M + (R_s + \frac{2L}{\Delta t})\,Y_s} \tag{5.12}$$

where ${}_kV_s$ represents the source voltage value, sampled at the time step $k\Delta t$. As for the RC network shown above, since the circuit contains an element with memory, the previous value of the voltage across the device (${}_{k-1}V$) is necessary to determine the unknown incident voltages and must be stored during the computation.

5.3.1 Validation of the RC and RL equations

With the method described above, we are able to include in the three-dimensional TLM mesh the circuit shown in Figure 5.5, as well as parts of it. Hence, as preliminary verification of the procedure, we have analyzed a simple low-pass filter, constituted by a lumped capacitance (R_s=0, G=0) placed between two metallic conductors forming a transmission line (Figure 5.7).

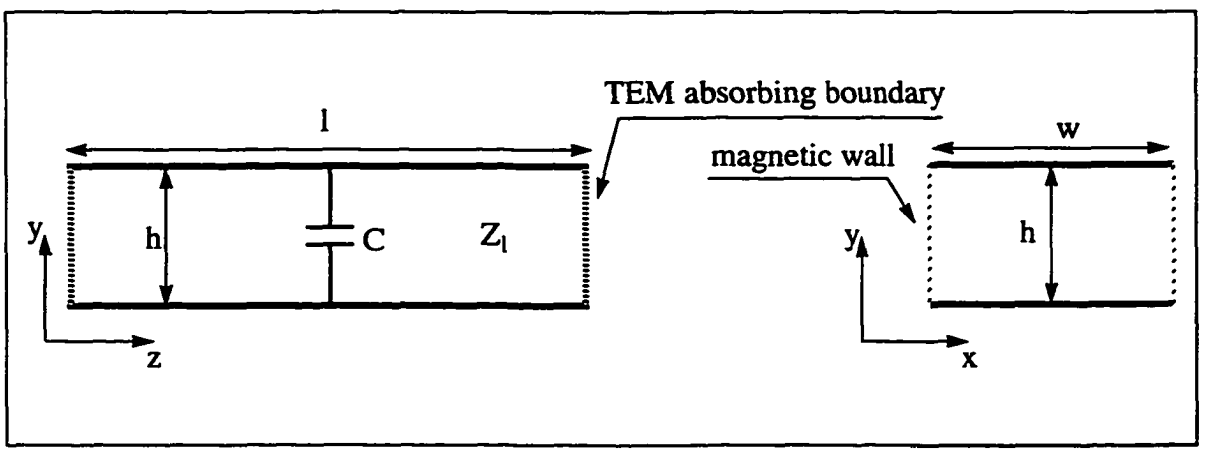

Figure 5.7 Geometry of the transmission line low-pass filter: a) cross-section of the transmission line. b) position of the capacitor in the direction of propagation

The characteristics of the transmission line are: w = 3 mm, h = 3 mm, l = 20 mm

and the dielectric is air; the characteristic impedance of the transmission line is therefore $Z_l = 377\ \Omega$. The chosen spatial discretization is $\Delta l = 1$ mm and the capacitance, of value C = 2 pF, is distributed over 3 cells along the x- and y-directions, and 1 cell along the z-direction; in this way the problem is kept one-dimensional for the frequency range of interest.

The S-parameters have been computed for the three-dimensional distributed structure and for the equivalent one-dimensional problem, showing also in this case an excellent agreement between the simulated and analytical results. Examining Figure 5.8, it is evident that the parameter most afflicted by error at high frequencies is $|S_{21}|$. In this case the relative error between the simulated and theoretical values of $|S_{21}|$ ranges from 0% at DC to approximately 20% at 6GHz.

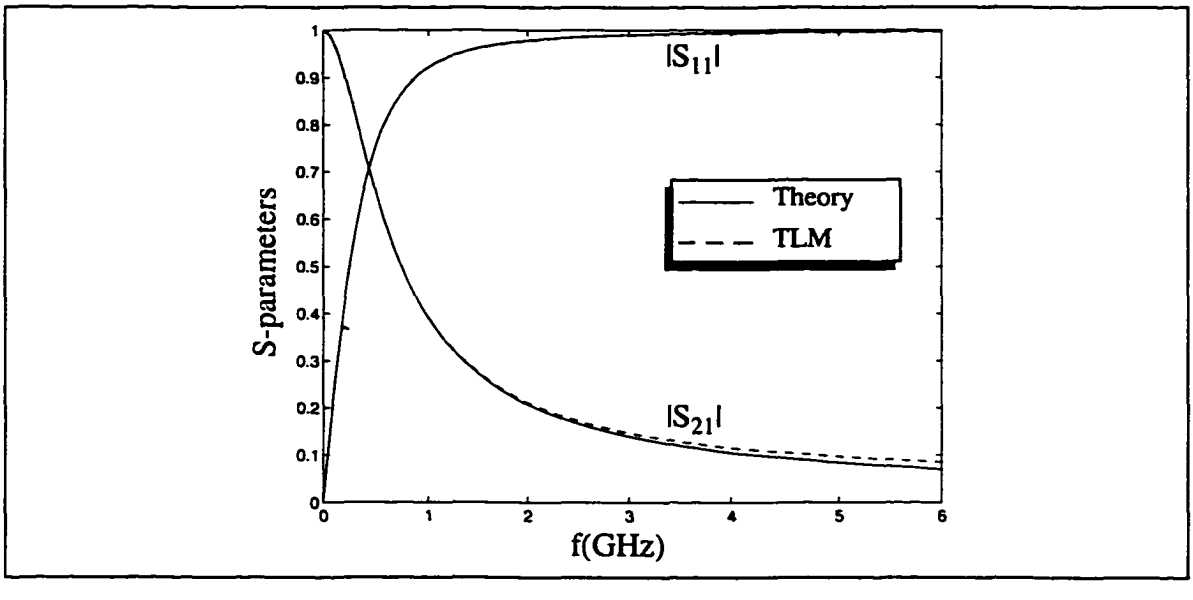

Figure 5.8 S-parameters for the low-pass filter illustrated in Figure 5.7. Comparison between the analytical solution (solid line) and the computed results for the three-dimensional TLM model (dashed line)

In this case the parasitic effect of the stub capacitance is negligible, compared to the lumped capacitance value of 2 pF.

The effect of the additional capacitance provided by the stub can be evaluated with the same model described above, provided that also the lumped capacitor is eliminated (C=0). In this way, the low-pass effect detected in the propagation of the wave is only due to the capacitive behavior of the stubs; for this particular structure, this is described

by:

$$C_s = \frac{N}{M}\varepsilon \cdot \Delta l_{line} = 8.854 \text{ fF} \tag{5.13}$$

The comparison between the computed S-parameters of the transmission line with C = 0 and the analytical solution of a low-pass filter with a shunt capacitance of value C_s are presented in the next diagram. A logarithmic scale has been used to increase the dynamic range of the plot for $|S_{11}|$. The graphs show that the scattering parameters are perfectly overlapping, thus confirming that the predicted value of the capacitance produced by the device stubs is correct. The computed relative error is smaller than 0.0016% for $|S_{21}|$ and smaller than 0.4% for $|S_{11}|$. This also excludes the possibility that the small discrepancy between the theoretical and the numerical results in Figure 5.8 is due to this capacitance; the difference can be rather explained by considering that the approximation of the time derivative in eq. (5.7) becomes less accurate for high frequency signals.

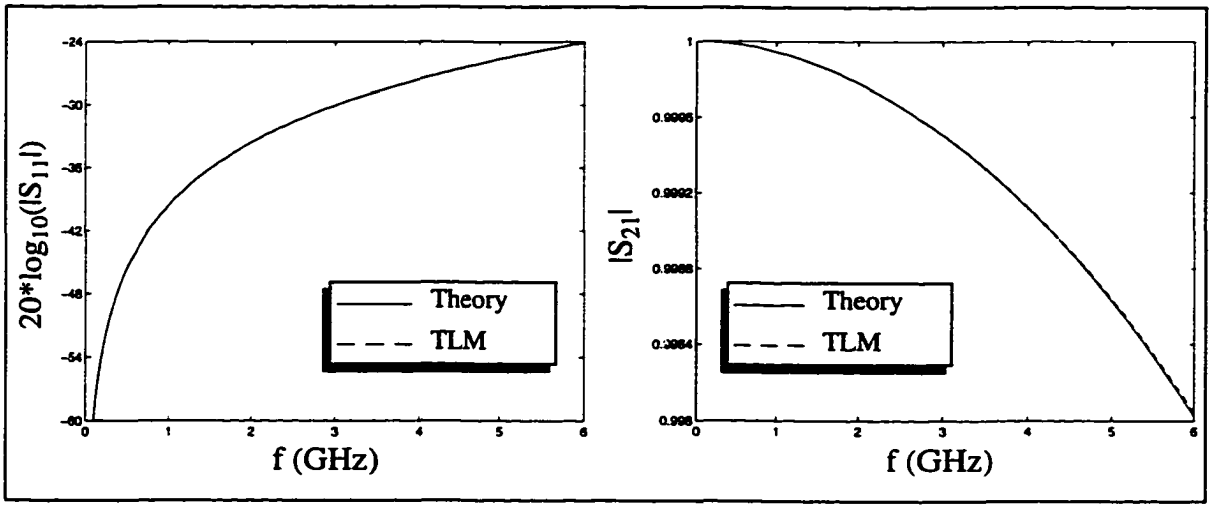

Figure 5.9 Determination of the capacitive effect introduced by the device stubs. A cluster of device stubs has been left open-circuited, thus producing a low-pass effect in the transmission line. In the plots, the solid line is to the analytical solution of the problem in Figure 5.7 with $C=C_s$, while the dashed line is to the TLM simulation.

A similar procedure has been adopted to verify the equations for the behavior of a lumped RL circuit. The lumped capacitor of Figure 5.7 has been replaced by a lumped inductor of value L = 0.1 μH; the structure thus constitutes a high-pass filter. With reference to the circuit described in Figure 5.5, the lumped element model is simplified by

considering $R_s = 0$ and $v_s(t) = 0$. Since the problem is one-dimensional, it is easy to determine the analytical response of the filter in the frequency domain.

The comparison between the analytical solution and the TLM simulation for this example is given in Figure 5.10. Examining the frequency behavior of $|S_{11}|$, it appears that the comparison is favorable in the low frequency range, but the results differ for higher frequencies, where nearly total transmission occurs. (Figure 5.10)

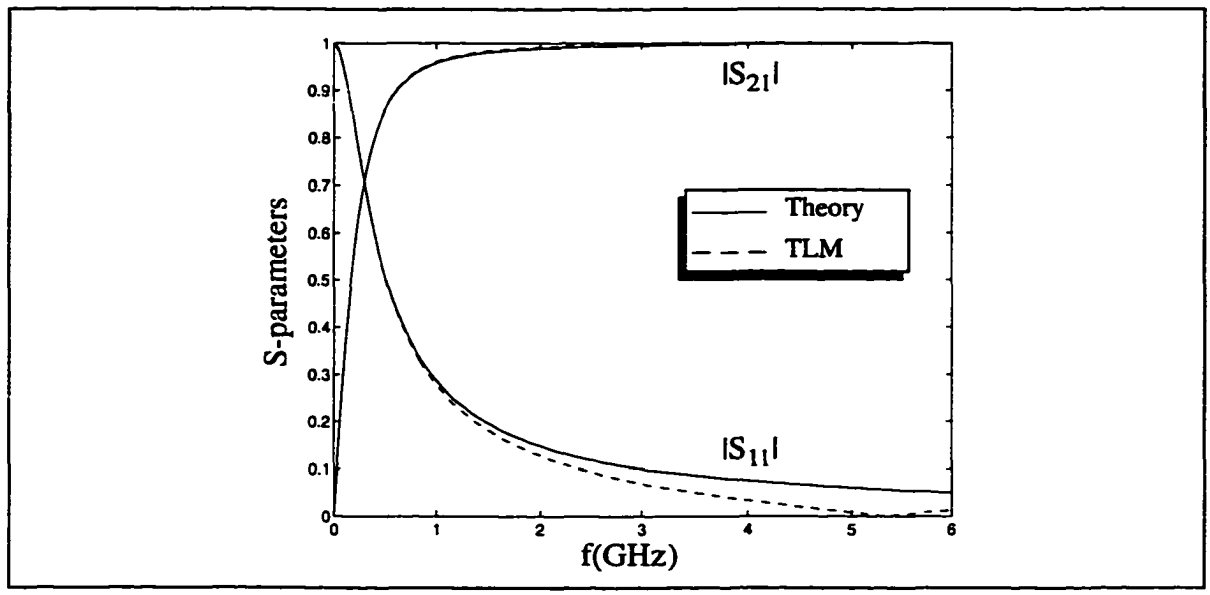

Figure 5.10 S-parameters of the high-pass filter consisting of a lumped inductor placed between the two conductors of the transmission line in Figure 5.7.

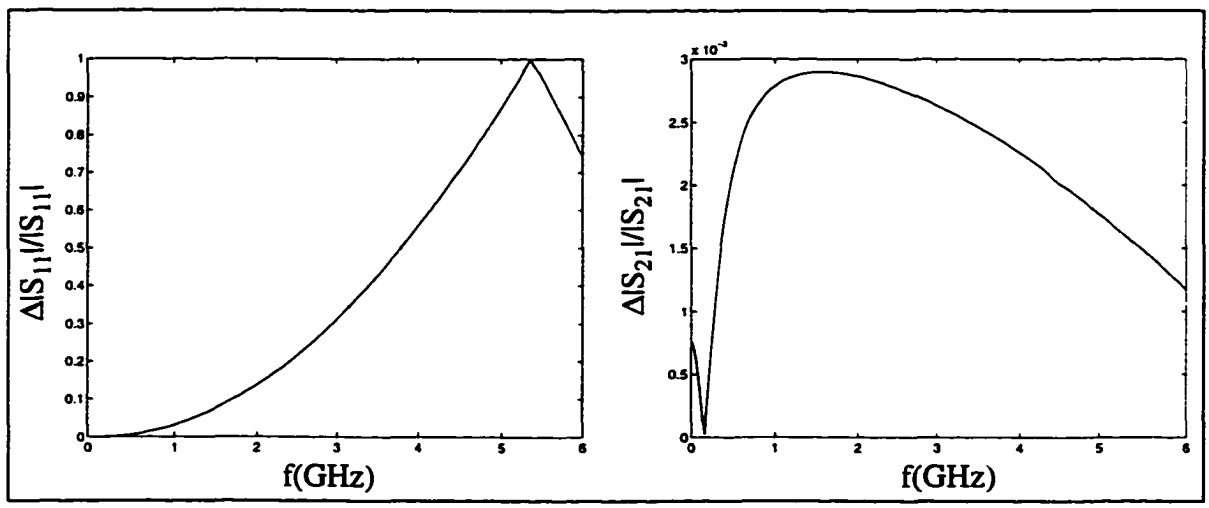

Figure 5.11 Relative error introduced in the scattering parameters of Figure 5.10 due to the parasitic capacitance introduced by the device stub.

This discrepancy is explained by taking into account the presence of the parasitic capacitance discussed above. This capacitance is placed in shunt with the lumped inductor, thus creating a resonance effect. At the resonant frequency, the total reactive impedance is null, and the signal is entirely transmitted.

Given the formula for the capacitance in (5.13), the resonant frequency can be determined analytically:

$$f_0 = (2\pi LC_s)^{-1} = 5.349 \text{ GHz} \tag{5.14}$$

which matches the frequency of total transmission at 5.340 GHz, obtained from the TLM simulation (error < 0.2%).

From the above discussion, it is evident that some care is necessary when modeling inductive elements, because of the parasitic capacitance produced by the device stubs. In the case where this capacitance is not negligible with respect to the other capacitance values in the problem, its combination with inductors will generate an undesired resonant effect, thus limiting the frequency range of applicability of the method. Figure 5.10 shows that acceptable results are obtained in the frequency range from DC to $f_0/5$ (error of 3.5% in $|S_{11}|$).

5.4 Inclusion of one-port nonlinear active and passive devices in the TLM network: p-n junction diode and Gunn diode

When dealing with nonlinear devices, the method described above becomes somewhat more complicated because the nonlinear equations must be solved. Therefore, appropriate algorithms must be adopted to obtain the new incident voltages at each time step. In general, two possible approaches can be taken to solve the problem of nonlinear devices:

- the nonlinear terms are updated according to the values of the voltage and current at the previous time step; with this procedure the new incident voltages are obtained in an explicit manner. This method can be successfully adopted for those situations in which the nonlinearity is not very strong.

- the nonlinear dependance is inserted in the voltage-current equation, which is then solved by means of numerical techniques; in this case the new voltages are given in an implicit manner. This procedure can be also applied to the case of strong nonlinearities, such as in the modeling of p-n junction diodes.

In the following, the two possibilities and their consequences will be discussed; the derivation of the formulae yielding the new incident voltages will be determined for a p-n junction diode and a Gunn diode.

When describing active devices such as Gunn diodes, particular care must be taken because the negative conductivity may cause spurious oscillations and instabilities at the TLM cut-off frequencies [15, 34]; this is also true for the FDTD method [23]. On the other hand, a real device exhibits an intrinsic cut-off frequency: an accurate TLM model must therefore take into account the cut-off behavior of the active device, while at the same time avoiding spurious oscillations. The natural cut-off effect of the active element can be represented by a capacitance in parallel to the device. To circumvent the problem of oscillations, the TLM mesh cut-off is chosen to be well above the active device cut-off frequency.

Traditionally, a capacitance is modeled in TLM by an open-circuited stub [10]; this works well for passive devices, but in this case suffers from the same instability problems mentioned earlier at the mesh cut-off frequencies. To avoid the excitation of the spurious oscillations, the capacitance must preserve its cut-off effect also at higher frequencies, and therefore is more effectively modeled by a lumped element.

The equivalent circuit of a Gunn diode is thus constituted by a nonlinear conductance $G(v_1)$, a linear series resistance R_s, a linear parallel capacitance C_p (responsible for the cut-off of the active device) (Figure 5.12). The diode is assumed to have a region with negative differential conductance.

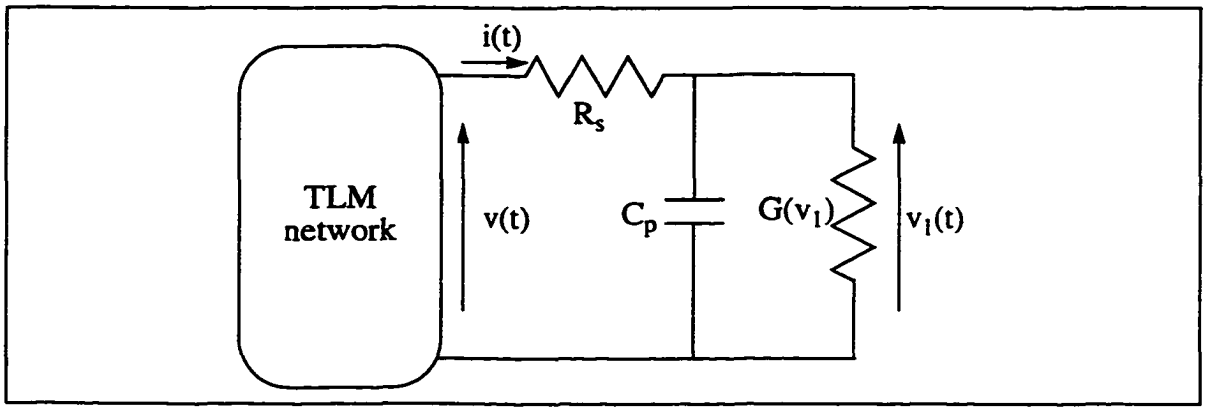

Figure 5.12 Connection of a Gunn diode equivalent circuit to a 3D-TLM mesh

So far, the typical Gunn diode model used in connection with the TLM (2D) or FDTD schemes [15, 23] exhibited a shifted I-V characteristic (Figure 5.13), so that the operating point was coincident with the origin and the presence of bias was thus avoided. A typical representation of such an active current source is given by the equation:

$$i_1(v_1) = -|G_{max}|\left[1 - \frac{1}{3}\left(\frac{v_1}{v_m}\right)^2\right]v_1 \tag{5.15}$$

where G_{max} is the maximum differential conductance, and $\pm\ v_m$ are the values of null differential conductance.

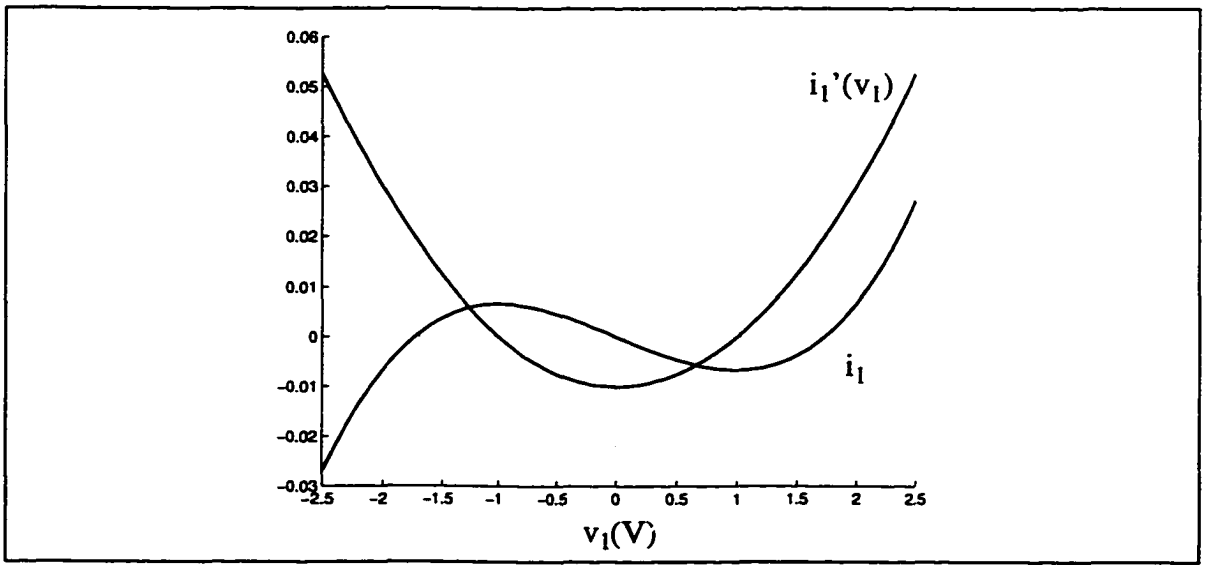

Figure 5.13 Typical current and differential conductance characteristics for the Gunn diode model, as described in eq. (5.15) (G_{max}=0.01 S, v_m=1V)

A serious limitation of this model is that it does not take in account the DC behavior of the diode. In fact, the characteristic I-V equation (5.15) describes sufficiently well the negative, differential conductance of the device, but erroneously amplifies any DC signal, because of the negative ratio i_1/v_1 in the region of operation of the diode. A more realistic model of active conductance should then be able to include the correct DC behavior of the diode, described by an I-V characteristic such as that in Figure 5.14.

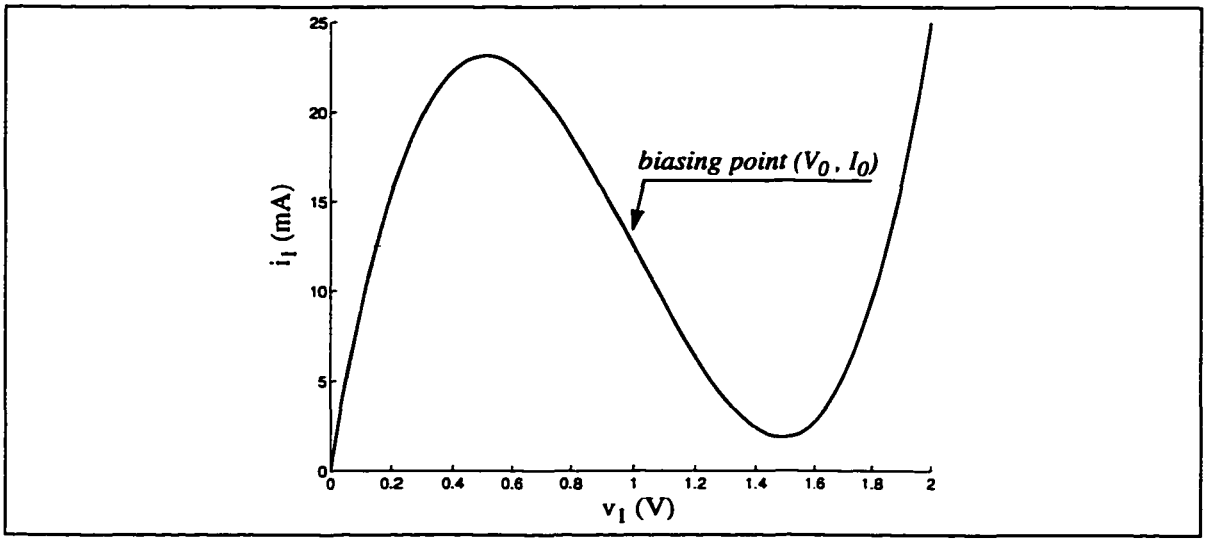

Figure 5.14 I-V characteristic of a Gunn diode having non-zero operating point

This I-V characteristic is generally described by a third order polynomial as:

$$i_1(t) = g_1 \cdot v_1(t) + g_2 \cdot [v_1(t)]^2 + g_3 \cdot [v_1(t)]^3 \qquad (5.16)$$

Considering now the problem of connecting a Gunn diode to the TLM network, by comparing Figure 5.12 with Figure 5.5 it appears that the diode is described by the same current-voltage equation (5.7) used to model the RC network. The only substantial difference is that in the Gunn diode the conductance G presents a nonlinear behavior with respect to the voltage v_1; in the time-domain, this means that the value of G evolves in time and must consequently be discretized.

$$G(v_1(t)) = \frac{i_1(t)}{v_1(t)} = g_1 + g_2 \cdot v_1(t) + g_3 \cdot [v_1(t)]^2 \qquad (5.17)$$

If the assumption that $G(v_1(t))$ does not vary dramatically from one time step to the next can be made (weak nonlinearity), it is legitimate to approximate its value with that assumed at the previous time-step:

$$ {}_{k}G \approx G({}_{k-1}V_1) = g_1 + g_2 \cdot {}_{k-1}V_1 + g_3 \cdot [{}_{k-1}V_1]^2 \tag{5.18} $$

where:

$$ {}_{k-1}V_1 = {}_{k-1}V - R_s \cdot {}_{k-1}I \tag{5.19} $$

and ${}_{k-1}V$ is the total voltage across the equivalent circuit at the time step $(k-1)\Delta t$, and ${}_{k-1}I$ is the current entering the device.

Under these conditions, the procedure to embed the diode into the TLM network is described by eqs. (5.9-5.10), once G is updated according to eq. (5.19) at each time step.

If the previous assumption cannot be made, then the nonlinear behavior of the conductance must be included in the voltage-current equation describing the diode. A nonlinear equation is thus obtained which can then be solved to determine the new incident voltages. Particular care must be taken in the time discretization of the nonlinear terms present in the equation, in order to obtain consistent results.

The equation is best treated if rewritten in the following way:

$$ i(t) = C\frac{dv_1}{dt} + i_1(v_1(t)) \tag{5.20} $$

The previous equation naturally leads to the correct discretized expression. If a central difference scheme is applied, the discretized version of the equation is given by:

$$ {}_{k}I + {}_{k-1}I = \frac{2C}{\Delta t}({}_{k}V_1 - {}_{k-1}V_1) + {}_{k}I_1 + {}_{k-1}I_1 \tag{5.21} $$

where ${}_{k}I_1 = i_1({}_{k}V_1)$ is the current flowing in the conductance at the time step $k\Delta t$, and is determined by substituting eq. (5.19) in (5.16). In this context, it is important to underline that the central difference scheme must be applied to the nonlinear term, i_1, and not to the voltage (v_1) on which i_1 depends; this second approach, suggested in [28, 25] would give:

$$ {}_{k}I + {}_{k-1}I = \frac{2C}{\Delta t}({}_{k}V_1 - {}_{k-1}V_1) + 2i_1\left(\frac{{}_{k}V_1 + {}_{k-1}V_1}{2}\right) \tag{5.22} $$

where the function i_1 (eq. (5.16)) is evaluated for the voltage value $({}_{k}V_1 + {}_{k-1}V_1)/2$.

The difference between the two procedures can be easily appreciated in the case

when C = 0. For such a situation, there must be an instantaneous relation between the electrical quantities; since

$$i_l\left(\frac{{}_{k+1}V_l + {}_kV_l}{2}\right) \neq \frac{1}{2}\left[i_l\left({}_{k+1}V_l\right) + i_l\left({}_kV_l\right)\right] \tag{5.23}$$

this condition is clearly met with the first approach, but is not verified in equation (5.21).

Since ${}_kI_l$ presents a nonlinear dependance on the voltages traveling in the device stubs, equation (5.21) must be solved numerically at each iteration to obtain the new incident voltages ${}_kV^i_m$. Details about the algorithm (*Brent's method*) used for the resolution of the nonlinear equation are given in [71].

A similar approach can be used in the determination of the nonlinear equation governing a p-n junction diode. As described in Chapter 3, the equivalent circuit of a diode can reach several levels of complexity, according to the degree of accuracy that must be achieved.

For the purpose of this thesis, that is to demonstrate the ability of the TLM method to model lumped nonlinear devices, the diode will be represented by a nonlinear voltage-controlled current source (3.1) and a nonlinear capacitance (3.2, 3.4):

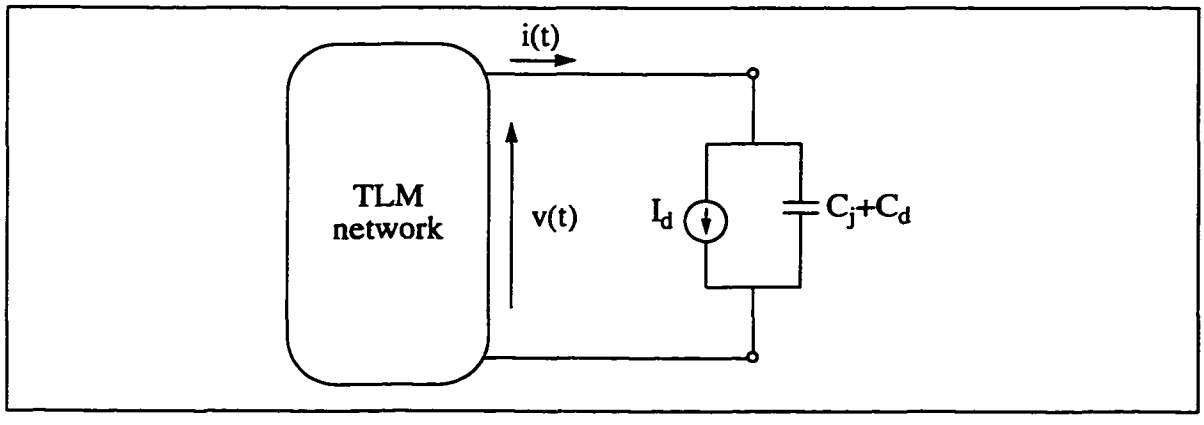

Figure 5.15 Equivalent large signal model of the p-n junction diode embedded in a TLM network

Both the current source and the diffusion component of the capacitance present a strong nonlinear behavior with respect to the applied voltage v(t). This suggests that the diode is best modeled by resolving the implicit nonlinear current-voltage equation at

each iteration. In this case, the current-voltage relation is simply given by:

$$i(t) = I_s\left[e^{qv(t)/(kT)} - 1\right] + \left[C_j(v(t)) + C_d(v(t))\right]\frac{dv}{dt} \tag{5.24}$$

When discretizing this expression, some care must be taken because of the presence of a multiplication of two terms depending on the voltage v(t). A possible approximation of this term is obtained by considering the average of the values of the capacitance at the time-steps $k\Delta t$ and $(k-1)\Delta t$; in this case the discretized version of eq. (5.4) is given by:

$$\begin{aligned} {}_kI + {}_{k-1}I &= I_s\left[e^{q_k V/(kT)} - 1\right] + I_s\left[e^{q_{k-1} V/(kT)} - 1\right] \\ &+ \left[C_j({}_kV) + C_d({}_kV) + C_j({}_{k-1}V) + C_d({}_{k-1}V)\right]\frac{{}_kV - {}_{k-1}V}{\Delta t} \end{aligned} \tag{5.25}$$

As for the model of the Gunn diode, eq. (5.25) must be solved numerically to obtain the new incident voltages traveling in the device stubs.

5.4.1 Validation results for the Gunn diode model

The validity of the techniques described above to embed Gunn and p-n junction diodes in the 3D-TLM network has been verified for the modeling of one-dimensional structures containing such devices. Due to the nonlinear nature of the problems, analytical solutions are not available for such structures and a comparison with other numerical solvers must be performed. Among all the available circuit simulators, SPICE has been chosen for the following reasons: it offers the transient response of the circuit, easily comparable with the TLM output; for the purpose of validation of the procedure, the electromagnetic part of the problem is quite elementary and can be accurately described by SPICE; finally, public domain versions of the SPICE software are available. Naturally, the final objective of this thesis will be to analyze structures that circuit simulators such as SPICE cannot accurately model, because of the complexity of their distributed electromagnetic subvolumes; for the purpose of validation of the coupled TLM - nonlinear lumped circuit model, the distributed part of the problem must be kept extremely simple.

In the following, a public domain version [72] of the PSPICE® software by Microsim Corp. will be used to obtain the validation results. A good introduction to SPICE can be found in [73-74]; information about the Graphical User Interface of PSPICE® (Schematics®) is given in [72].

In order to verify the accuracy of the Gunn diode circuit, a transmission line oscillator with its DC biasing circuit has been modeled. A complete three-dimensional layout of such an oscillator in microstrip technology would be more complex, requiring appropriate matching stubs, but for the objective of verifying the proposed technique the circuit can be simplified to the one shown in Figure 5.16.

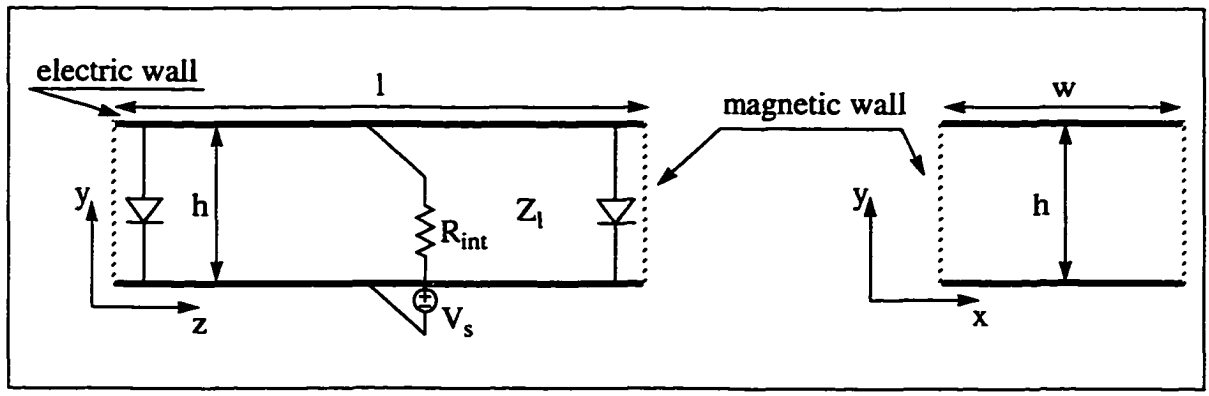

Figure 5.16 Transmission line oscillator with DC biasing circuit

The transmission line in the three-dimensional model has dimensions l = 20 mm, h = 3 mm and w = 5 mm and is discretized with cubic cells of size Δl=1mm; in order to keep the problem one-dimensional, all the lumped devices are assumed to occupy the full cross-section of the transmission line. They also extend over a single TLM cell in the z direction.

The two diodes are assumed to be identical, and to have as biasing point V_0 = 1 V and I_0 = 3.5 mA (Figure 5.14). The typical I-V characteristic of the diode has been approximated by the third-order polynomial:

$$i_1(v_1) = G(v_1)\,v_1 = (19.5 - 24.0v_1 + 8v_1^2)\,v_1 \qquad \text{(mA)} \qquad (5.26)$$

The active devices also comprise a series resistance of value R_s = 4 Ω, and a shunt capacitance C_p = 1 pF (Figure 5.12).

The source model represents a DC voltage supply of value V_s = 1.4 V, and is positioned slightly asymmetrically with respect to the length of the transmission line, to start the oscillations. Once the amplitude of the feeding voltage has been chosen, the source internal resistance, R_{int}, must be determined so that the operating point is the desired one. Analyzing the DC equivalent circuit in Figure 5.17, it is easy to verify that the value of

this resistance is given by the formula:

$$R_{int} = \frac{1}{2}\left(\frac{V_s - V_0}{I_0} - R_s\right) \tag{5.27}$$

which, for this problem, corresponds to 55.143 Ω.

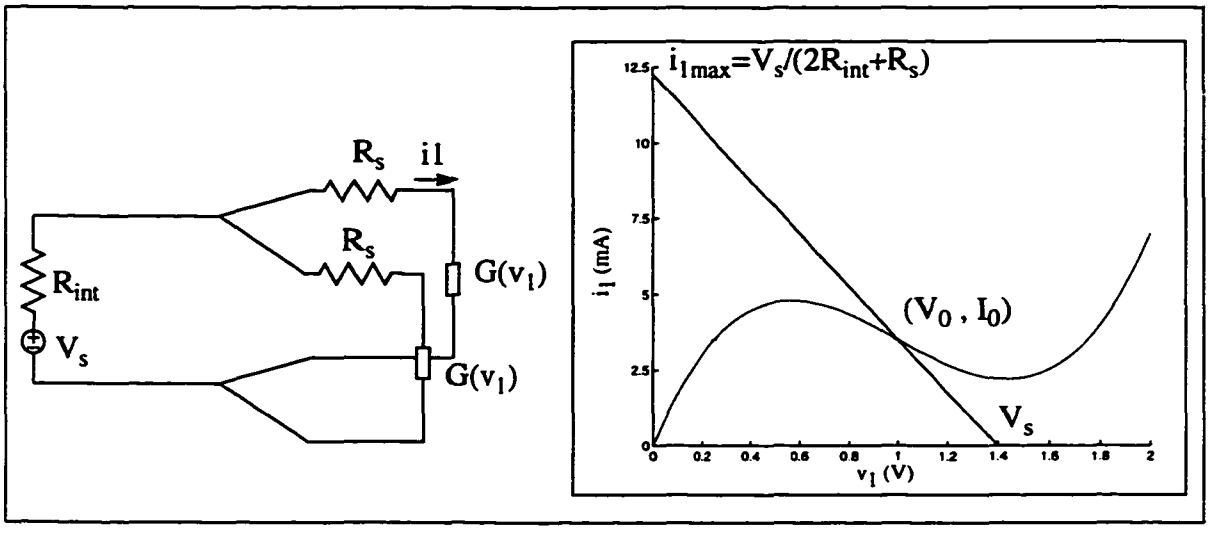

Figure 5.17 Equivalent DC circuit of the stripline oscillator, and determination of the internal resistance value

The objective of the validation is to determine the difference between the two possible Gunn diode models proposed in eqs. (5.10) and (5.21), and to compare them to SPICE; in particular, it is expected that the second of the proposed approaches will yield more accurate results. It is also desired to evaluate the effect of the device stub capacitance, with the purpose of compensating it.

The SPICE equivalent circuit is slightly different from the TLM model, since the lumped elements are actually in the center of the TLM cell in the direction of propagation of the fields. Therefore, the effective distance between the "lumped" TLM elements is respectively l_1=9mm and l_2=10mm. The determination of the exact distances is crucial in this example, because they affect the frequency of the generated oscillations. Moreover, each lumped element (the Gunn diodes and the lumped resistive source) has an associated parasitic capacitance, that can also be included in the SPICE model. For the problem under study the value of the extra capacitance is C_s=14.757 fF, which is approximately equivalent to 1.5% of the capacitance of the Gunn diode.

The equivalent one-dimensional SPICE model is thus given in Figure 5.18:

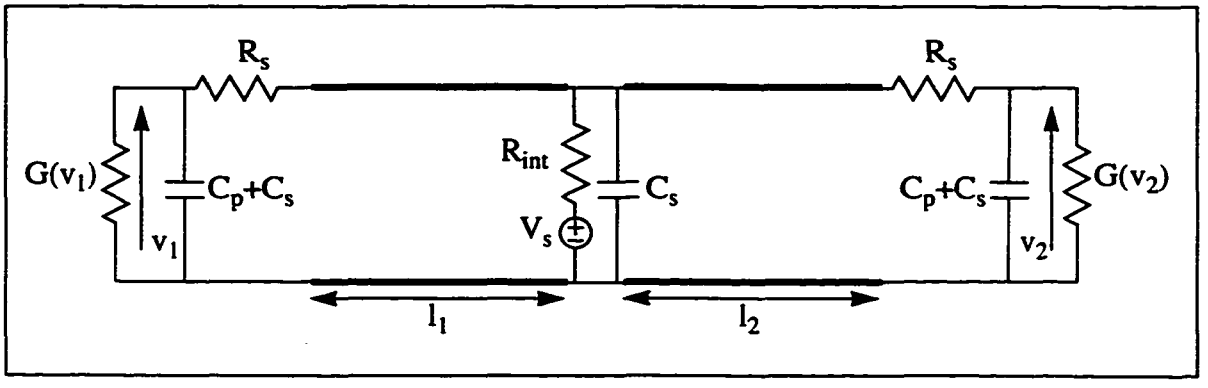

Figure 5.18 Equivalent one-dimensional SPICE model of the three-dimensional TLM circuit in Figure 5.17. The thick lines represent two sections of transmission line. Note the addition of the parasitic capacitances C_s, shunt connected to all the lumped devices.

In the following picture (Figure 5.19.a), the transient behavior of the voltage across one of the diodes (modeled according to eq. (5.21)) is shown for both the TLM model ("dash and dot" line) and the equivalent SPICE circuit including the parasitic capacitance effect (solid line). It appears that a good correspondence is achieved between the two circuit representations, since the curves are almost perfectly overlapping.

For completeness, the difference between the two results is also shown in Figure 5.19.b. Considering that even a little phase difference can produce considerable deviations for such rapidly varying signals, the graph confirms the good agreement between the two models. The noisy behavior observed in the signal difference during the transient response is due to the fact that SPICE uses an adaptive time discretization in the initial time steps of the simulation.

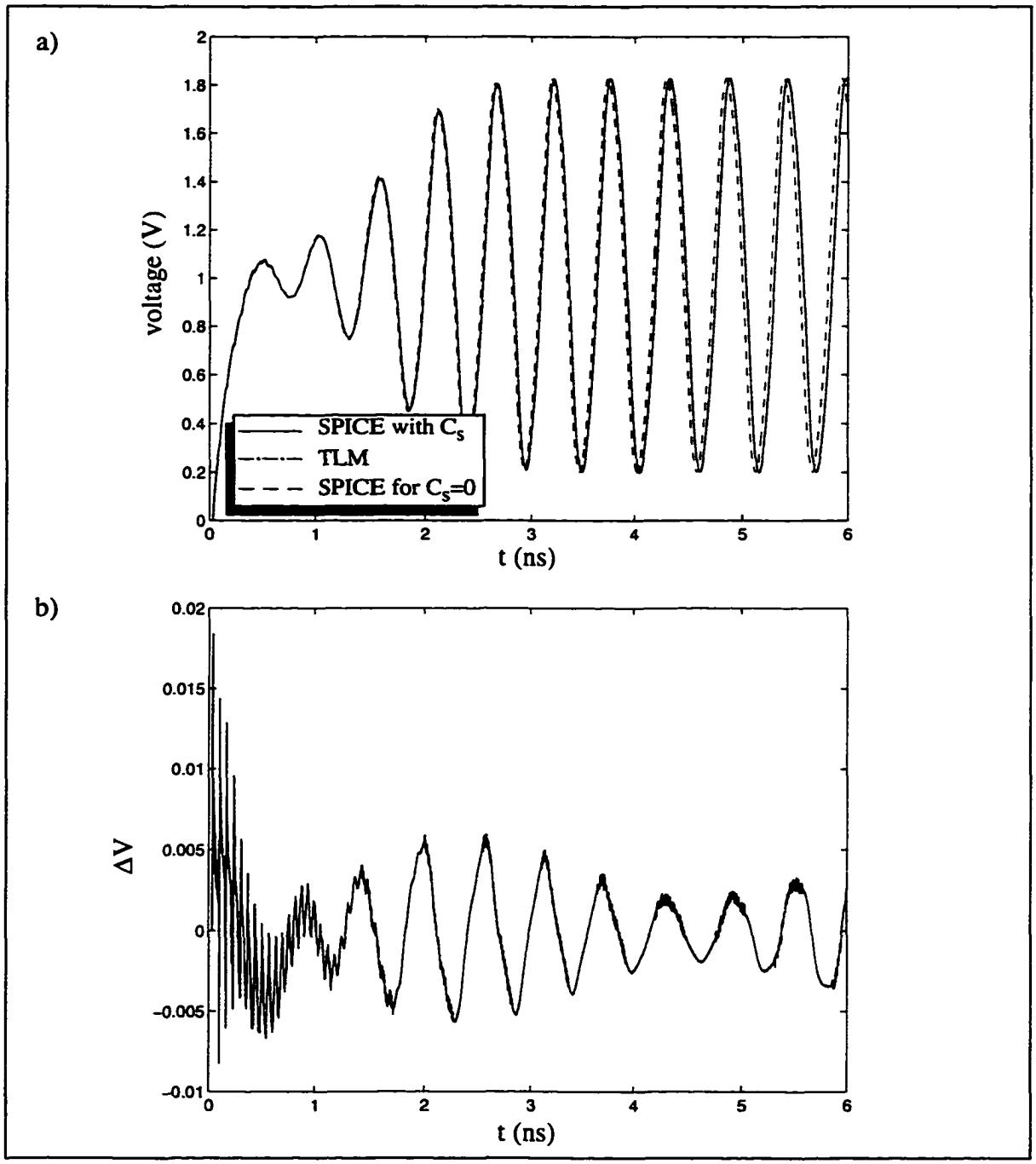

Figure 5.19 Transient behavior of the TLM and SPICE models for the transmission line oscillator. a) Transient response of the voltage $v_2(t)$ for the TLM model, the SPICE circuit including the parasitic capacitances, and the SPICE equivalent circuit without the stub capacitive effect (C_s=0). b) Deviation $v_2(t)|_{TLM}$-$v_2(t)|_{SPICE}$ for the SPICE model containing C_s

As a further comparison, the resulting voltage is also plotted for the circuit in Figure 5.18 when C_s = 0 F; it is clear that the capacitive effect introduced by the device stubs is small, but not negligible (Figure 5.19.a). This consideration leads to a possible way of reducing the parasitic capacitance effect: when the lumped circuit presents a lumped parallel capacitor larger than C_s, as in the example now considered, the capacitance value inserted in the TLM simulation must be reduced by C_s.

When the oscillations reach steady-state (t > 4 ns), the measured mean values of the voltage across the diode and of the current flowing into it, are respectively 1.014 V and 3.445 mA, and agree well with the imposed biasing point described above. The accuracy of the method has also been verified in the frequency domain, by comparing the Fourier transforms of the TLM and SPICE signals:

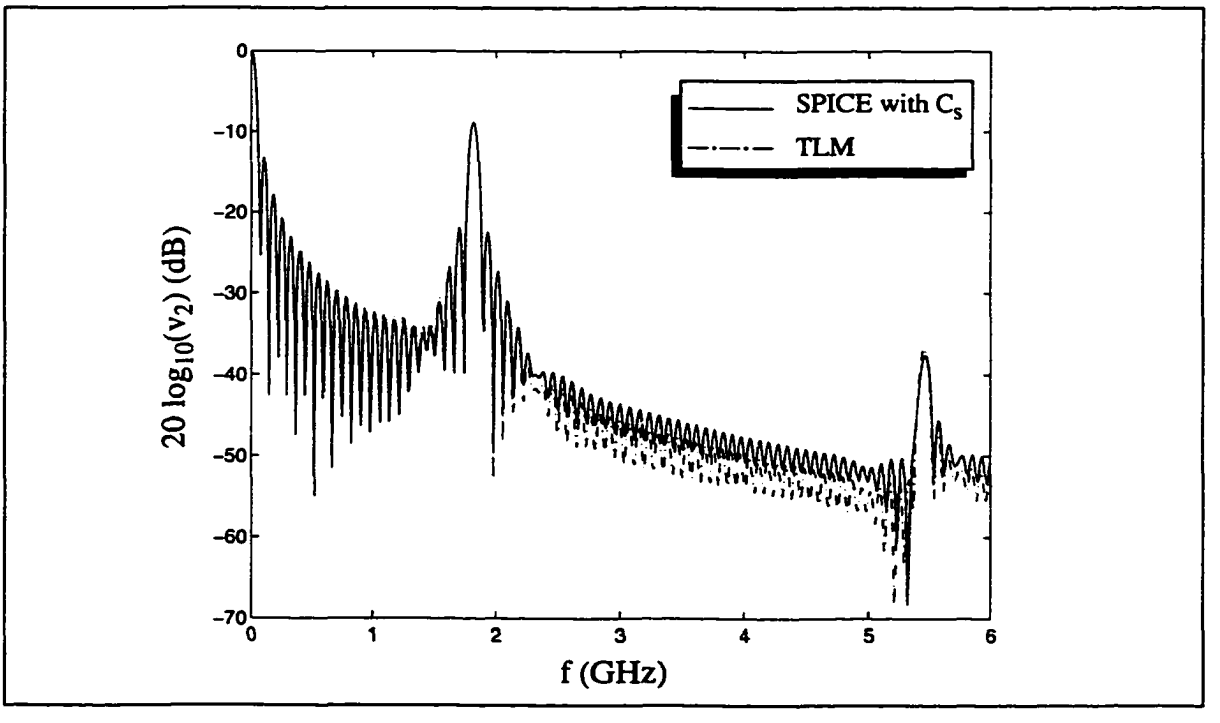

Figure 5.20 Fourier transform of the time-domain responses shown in Figure 5.19

In the previous simulations, the nonlinear behavior governing the Gunn diode has been directly incorporated into the current-voltage equation, which has then been solved by means of numerical techniques. As mentioned earlier, another possible approach consists in the approximation of the nonlinear conductance with its value at the previous time step (5.17). The time-domain response has been calculated with this method and

compared with the SPICE simulation, as well as with the response obtained with the other TLM approach. As expected, the results obtained with this procedure (Figure 5.21) are slightly less accurate than those shown in Figure 5.19, because of the backward approximation.

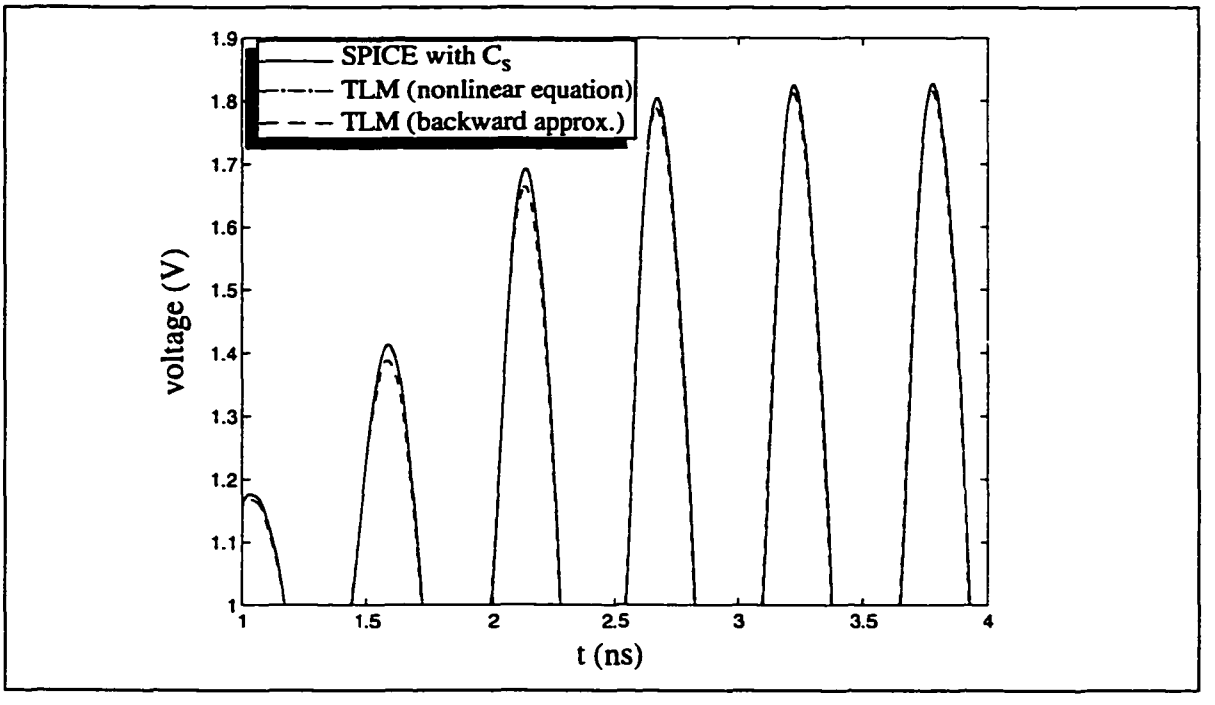

Figure 5.21 Detail of the comparison between the TLM simulation with the backward approximation of the nonlinear conductance, the TLM simulation with numerical resolution of the nonlinear equation, and the SPICE response.

5.4.2 Validation of the p-n junction diode model

In order to verify the accuracy of the p-n junction diode model, a simple circuit constituted by the transmission line of Figure 5.7, terminated at one extremity by a diode and excited at the other extremity by a matched 200MHz source has been utilized.

The dynamic characteristics of the diode are described by the formulae in (3.2, 3.4), where the zero-bias junction capacitance is $C_j(0) = 0.1$pF, and the transit time $\tau_d =$ 0.1ns. The saturation current is $I_s=10^{-14}$A.

As for the Gunn diode example, an analytical solution of the problem is not available in this case and a comparison with SPICE has been performed. Since the lumped devices are located at the center of the TLM cells (having size Δl=1mm), the effective

distance between the source and the diode is l'=19mm. The comparison between the TLM and SPICE simulations is shown in Figure 5.22. Note that the SPICE circuit used for the comparison does not contain any additional capacitance to take into account the device stub effect.

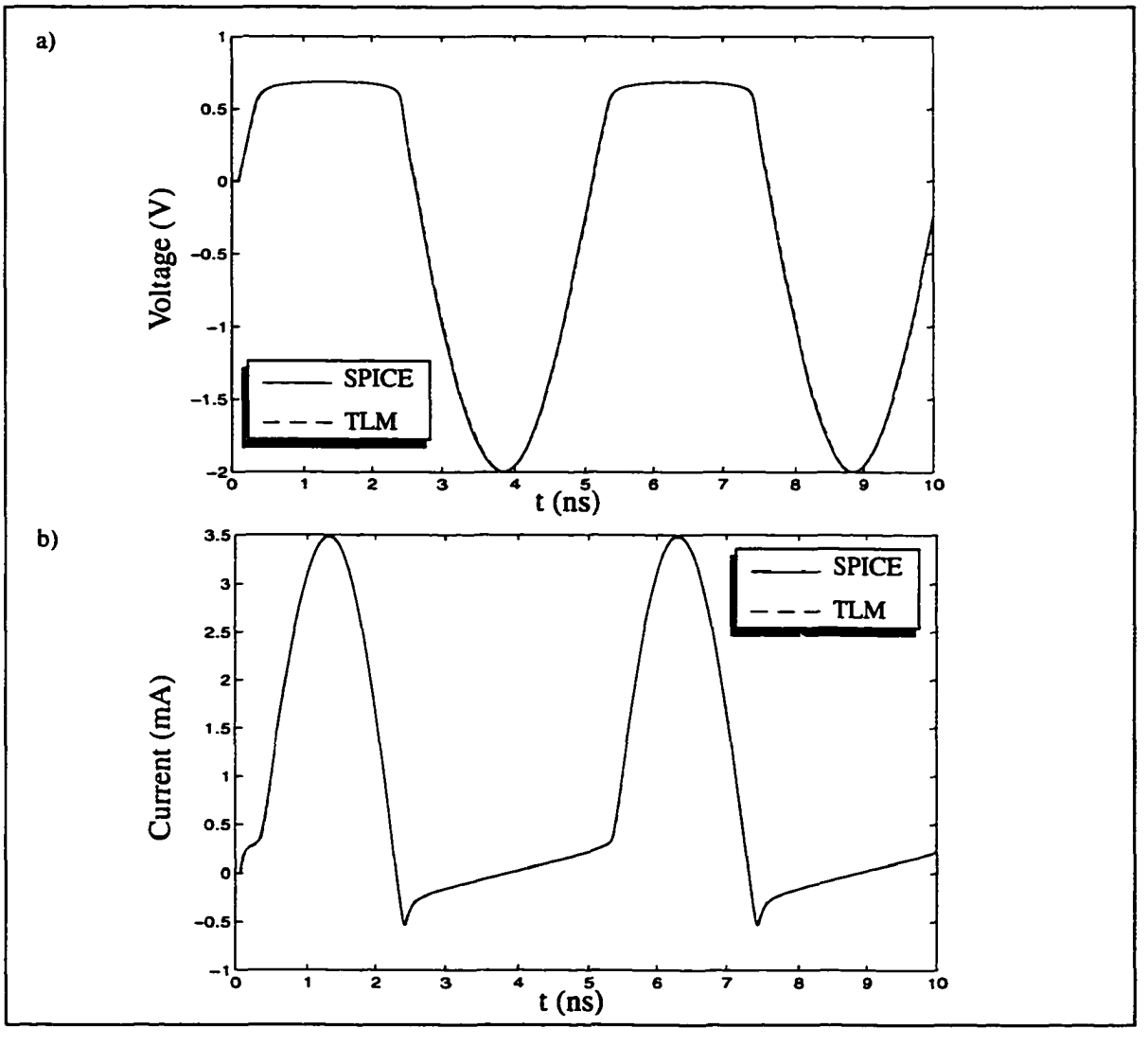

Figure 5.22 Evaluation of the dynamic behavior of a p-n junction diode. a) Voltage across the diode, b) current flowing into the device.

Once again, the comparison shows that the method agrees well with the results determined with the SPICE simulator. To better visualize the little discrepancies between the TLM and SPICE simulations, the difference between the two time domain current signals have been plotted in Figure 5.23. For comparison, the difference between the TLM

results and the SPICE simulation with the inclusion of the device stub capacitance has also been determined. It appears that for this particular example the capacitive effect introduced by the device stubs is not the main reason for the discrepancy between the results. The difference between the two simulations can rather be explained considering that SPICE uses an adaptive time step in the integration scheme.

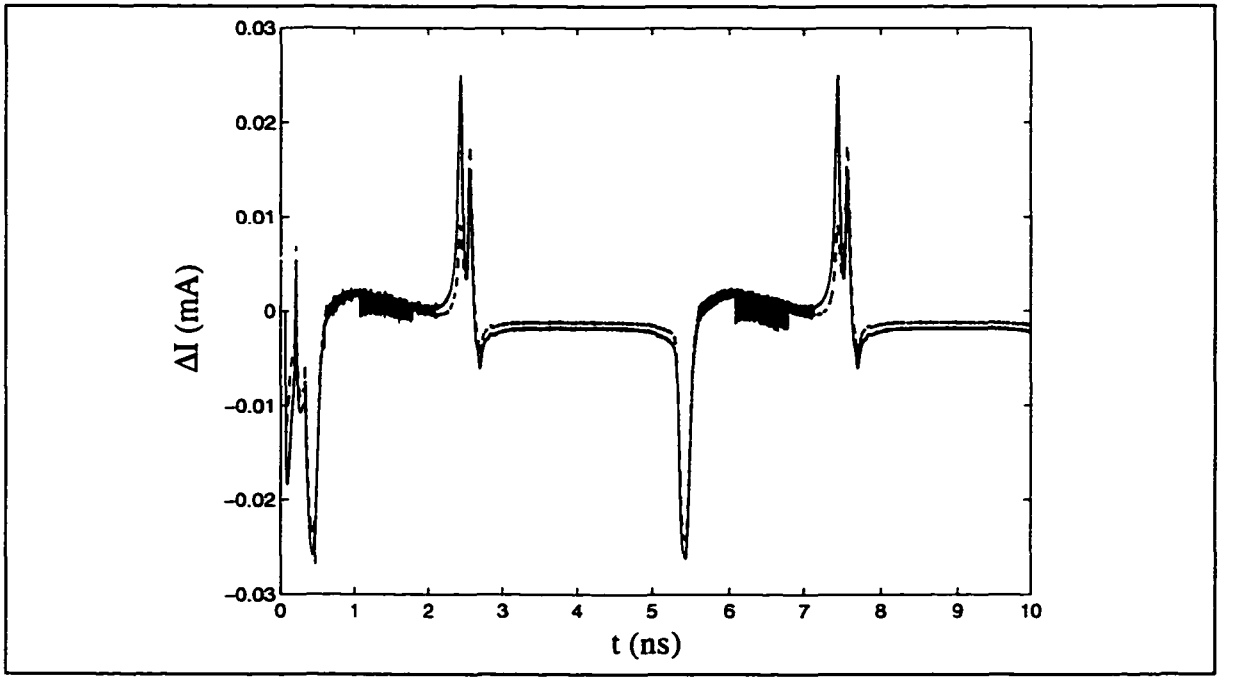

Figure 5.23 Evaluation of the capacitive effect introduced by the device stubs for the p-n junction diode example. Solid line: deviation $i(t)|_{TLM}$-$i(t)|_{SPICE\ with\ Cs=0}$. *Dashed line: deviation* $i(t)|_{TLM}$-$i(t)|_{SPICE\ with\ Cs}$

It is appropriate to underline that one advantage of the proposed method consists in limiting the number of nonlinear equations to be solved at each iteration. Since the device is not split-up in the series connection of M equivalent elements in the direction of the feeding voltages, only a single equation must be solved at each time step.

5.5 Modeling of two-port nonlinear devices in the TLM network: the bipolar junction n-p-n transistor

This procedure can be extended to include nonlinear two-port devices into the TLM network. The main aspects of the technique have already been described in Section

4.5, where the general relation to obtain the new incident voltages has been determined (4.4). As in the case of one-port circuits, this relation must then be formulated for the specific device being embedded in the TLM network. In the following, the *large-signal* equivalent circuit of a bipolar transistor has been modeled. The bipolar transistor is described by a network of ideal p-n junction diodes, current-controlled current sources and nonlinear capacitances, as shown in Section 3.3. The biasing circuit of the transistor, constituted by a DC voltage source of amplitude V_{cc} and an internal resistance R_c, is also included into the lumped element model. The connection between the lumped circuit and the TLM mesh is provided by two sets of series-connected stubs, arranged as in Figure 5.1 (the reader is also referred to Figure 4.8 for the full representation of the connection). The circuit is assumed to occupy two adjacent clusters of TLM nodes along the z-direction; it is also assumed that the number of cells (M) occupied in the y-direction is the same for both the base-emitter and the collector-emitter regions.

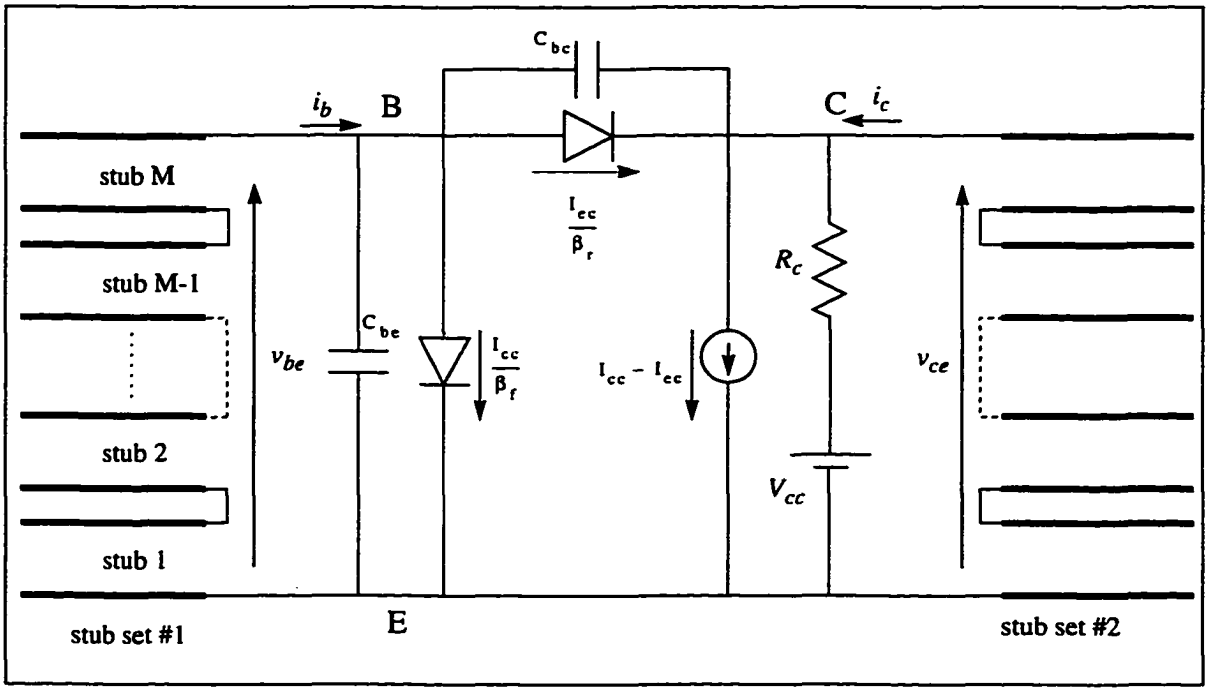

Figure 5.24 Connection of the bipolar transistor equivalent circuit to a the TLM mesh by means of two sets of device stubs. The biasing circuit is also included in the lumped model.

The time-domain equations to be solved are:

$$
\begin{aligned}
i_b &= \frac{i_{cc}}{\beta_f} + \frac{i_{ec}}{\beta_r} + C_{be}(v_{be})\ \frac{dv_{be}}{dt} + C_{bc}(v_{bc})\ \frac{dv_{bc}}{dt} \\
i_c &= i_{cc} - i_{ec} - \frac{i_{ec}}{\beta_r} + \frac{v_{ce} - v_{cc}}{R_c} - C_{bc}(v_{bc})\ \frac{dv_{bc}}{dt}
\end{aligned}
\tag{5.28}
$$

where:

$$
\begin{aligned}
i_{ec} &= I_s\left[e^{qv_{bc}(t)/(kT)} - 1\right] \\
i_{cc} &= I_s\left[e^{qv_{be}(t)/(kT)} - 1\right] \\
v_{bc} &= v_{be} - v_{ce}
\end{aligned}
\tag{5.29}
$$

β_f and β_r are, respectively, the forward and reverse current gain of a common-emitter BJT, and C_{be} and C_{bc} are the sum of the nonlinear junction and diffusion capacitances for the base-emitter and the base-collector junctions (3.7-3.8).

As in the previous examples, the total currents and voltages are expressed as a function of the incident and reflected voltages traveling in the two sets of stubs; in order to obtain the unknown incident voltages, a set of coupled nonlinear equations must be solved numerically at each iteration. The numerical treatment of nonlinear coupled equations is generally very difficult and few algorithms are available in the literature for this kind of problems; the Powell hybrid method has been used for the resolution of the system [75]. In this specific case, if a central difference scheme is applied to the numerical simulation, spurious oscillations due to roundoff errors are generated. It is evident that in the case of ideal transistors, the capacitive effects are neglected and an instantaneous relationship between the currents and voltages exists. The discrete version of eqs. (5.28) can be then written as:

$$
{}_kI_b = \frac{I_s}{\beta_f}\left[e^{q_k V_{be}/(kT)} - 1\right] + \frac{Is}{\beta_r}\left[e^{q_k V_{bc}/(kT)} - 1\right]
$$

$$
\begin{aligned}
{}_kI_c = I_s\left[e^{q_k V_{be}/(kT)} - 1\right] - \frac{Is}{\beta_r}(\beta_r + 1)\left[e^{q_k V_{bc}/(kT)} - 1\right] \\
+ \frac{{}_kV_{ce} - {}_kV_{cc}}{R_c}
\end{aligned}
\tag{5.30}
$$

The nonlinear capacitances can be then taken into consideration by approximating

them with their value at the previous time-step (backward approximation); in this way a more robust approach is obtained. The final discretized equations used to model the non-ideal bipolar transistor are thus given by:

$$
\begin{aligned}
{}_kI_b &= \frac{I_s}{\beta_f}\left[e^{q_k V_{be}/(kT)} - 1\right] + \frac{Is}{\beta_r}\left[e^{q_k V_{bc}/(kT)} - 1\right] \\
&+ C_{be}({}_{k-1}V_{be})\frac{{}^kV_{be} - {}_{k-1}V_{be}}{\Delta t} + C_{bc}({}_{k-1}V_{bc})\frac{{}^kV_{bc} - {}_{k-1}V_{bc}}{\Delta t} \\
{}_kI_c &= I_s\left[e^{q_k V_{be}/(kT)} - 1\right] - \frac{Is}{\beta_r}(\beta_r + 1)\left[e^{q_k V_{bc}/(kT)} - 1\right] \\
&+ \frac{{}^kV_{ce} - {}^kV_{cc}}{R_c} - C_{bc}({}_{k-1}V_{bc})\frac{{}^kV_{bc} - {}_{k-1}V_{bc}}{\Delta t}
\end{aligned}
\tag{5.31}
$$

It is important to mention that a forward approximation for the capacitances can also be used; again, in this case no roundoff errors are introduced in the simulation. Yet, during the validation process, the backward scheme has proven to offer better agreement with SPICE simulations.

5.5.1 Validation results

In order to validate the modeling of the BJT, the common-emitter amplifier described in Figure 5.25 has been analyzed. First, the simulation has been performed for an ideal transistor (eq. (5.31)) having inverse saturation current $I_s = 10^{-16}$A, and forward and reverse current gain respectively $\beta_f = 100$ and $\beta_r = 1$.The driving RF voltage consists of a sinusoidal 200MHz waveform, offset by 875mV, with an amplitude of 75mV; the application of this voltage is delayed by 100 time-steps, during which a ramp signal provides a smooth transition to the offset point. The source internal resistance is R_{int}=1kΩ. The biasing circuit is composed of a 5V DC voltage source (V_{cc}) and a resistor of value R_c=377Ω.

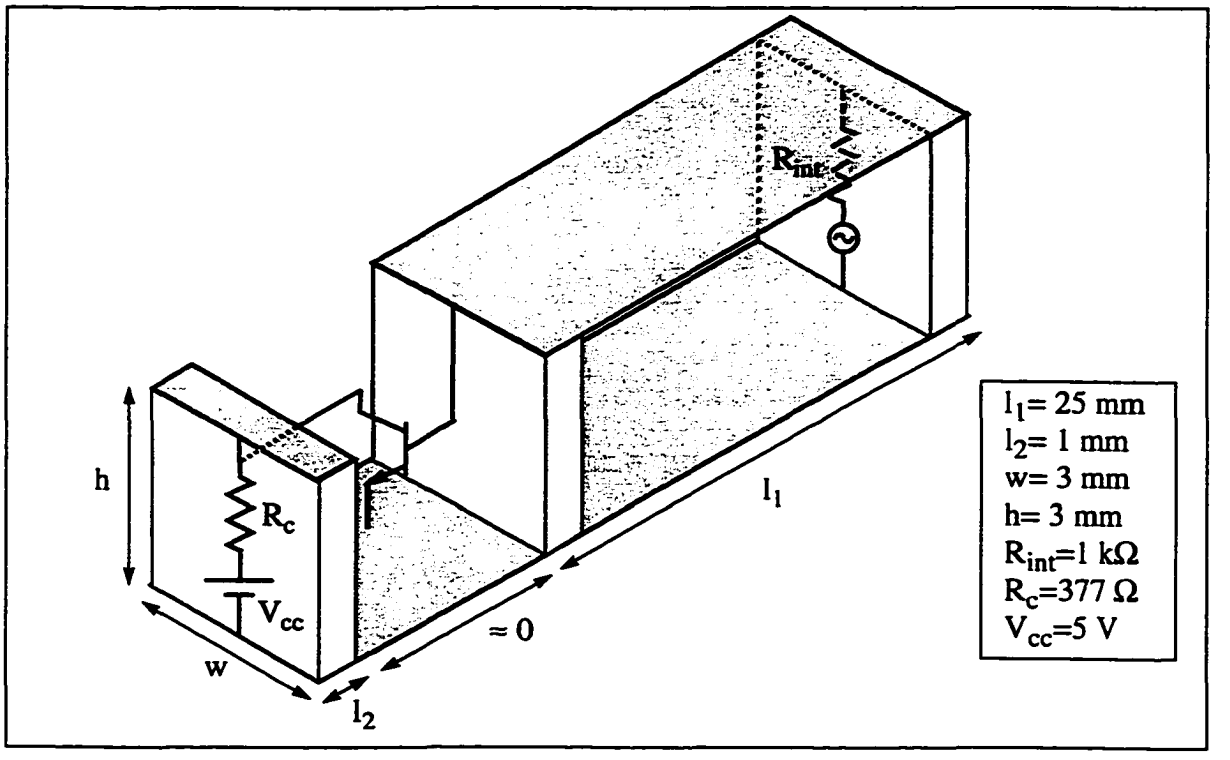

Figure 5.25 Three-dimensional representation of a common-emitter amplifier in a TLM network: the base-emitter and collector-emitter regions have been distributed over two adjacent cross sections of the transmission line. The transistor biasing circuit has also been included in the model.

The validity of the method has been proven by comparing the transient response of voltage across the collector-emitter (C-E) section, $v_{ce}(t)$, determined with the TLM simulation and with the SPICE analysis. Since the two-port device occupies two cells in the direction of propagation of the signal, it is more difficult to derive an equivalent SPICE model. The problem consists in the appropriate determination of the distance between the RF voltage source and the transistor. Since the voltage in the C-E section is of interest, a reasonable approach consists in accurately modeling the distance between the source and the collector region, so that the appropriate time-delay is simulated in the SPICE representation. The comparison, shown in Figure 5.26, shows a very good agreement between the two methods. Once again, it can be shown that the small difference appearing in the transient region is due to the capacitive effect of the device stubs.

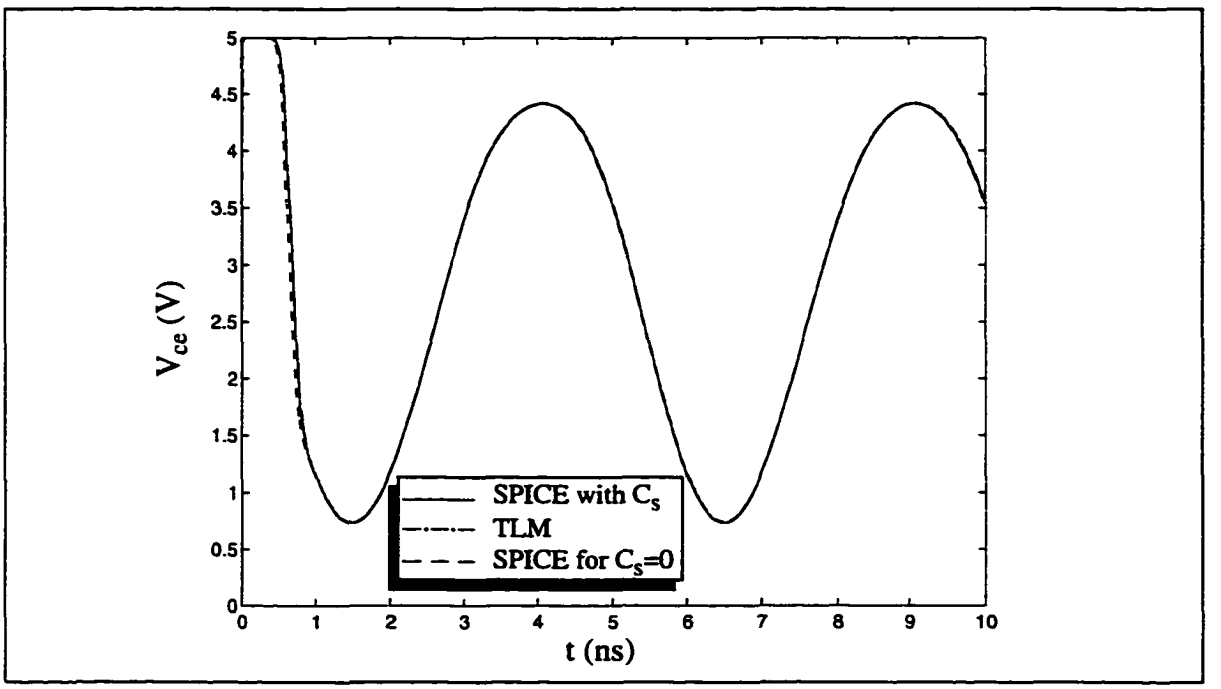

Figure 5.26 Transient response for the common-emitter amplifier of Figure 5.25. The transistor has been modeled as an ideal npn junction. The solid line corresponds to the SPICE model with the inclusion of parasitic capacitances C_s connected to the sources and the transistor base-emitter section.

The comparison has then been extended to verify the accuracy of the dynamic behavior of the transistor, described by eq. (5.31); in this case the zero-bias junction capacitances have been chosen to be $C_{JE}(0) = C_{JC}(0) = 0.1$ pF, and a linear doping profile has been used (m=.33). The transit times characterizing the diffusion capacitances are: $\tau_f = \tau_r = 0.1$ ns. The new time-domain waveforms are displayed in the following figure:

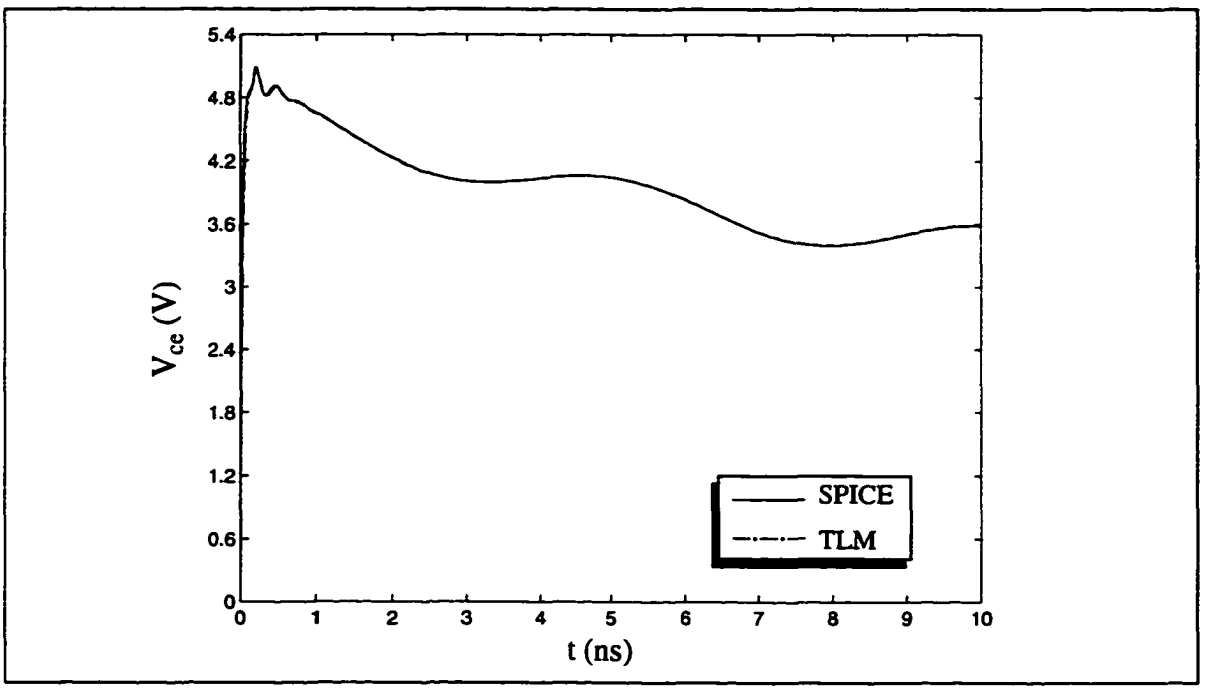

Figure 5.27 Dynamic behavior of the common-emitter amplifier with the inclusion of the nonlinear junction and diffusion capacitances. Comparison between the TLM and SPICE simulations.

Also in this case the agreement is good; it is conceivable that the accuracy could be further improved with a more sophisticated and robust algorithm for the resolution of the nonlinear system of equations, so that a central difference approximation of the capacitances could be implemented.

5.6 Connection of lumped devices to stub-loaded TLM symmetrical condensed nodes

As mentioned in the previous Chapter, the procedure to connect lumped devices to the symmetrical condensed node can be extended without difficulty to the case of stub-loaded cells. In particular, when the device is interfaced to a dielectric region with constant permittivity, the equations derived in this Chapter to describe the various components remain valid. The only substantial difference consists in the modification of the scattering matrix to accommodate the extra device stubs, as delineated in eq. (4.10), and on the evaluation of the stub admittance according to eq. (4.11).

In order to test the validity of the modified algorithm, the same structure used to verify the model of the p-n junction diode has been considered (Section 5.4.2); unlike in that example, a portion of the transmission line of length 11 mm (on the side of the diode), has been filled with dielectric (ε_r=4.0).

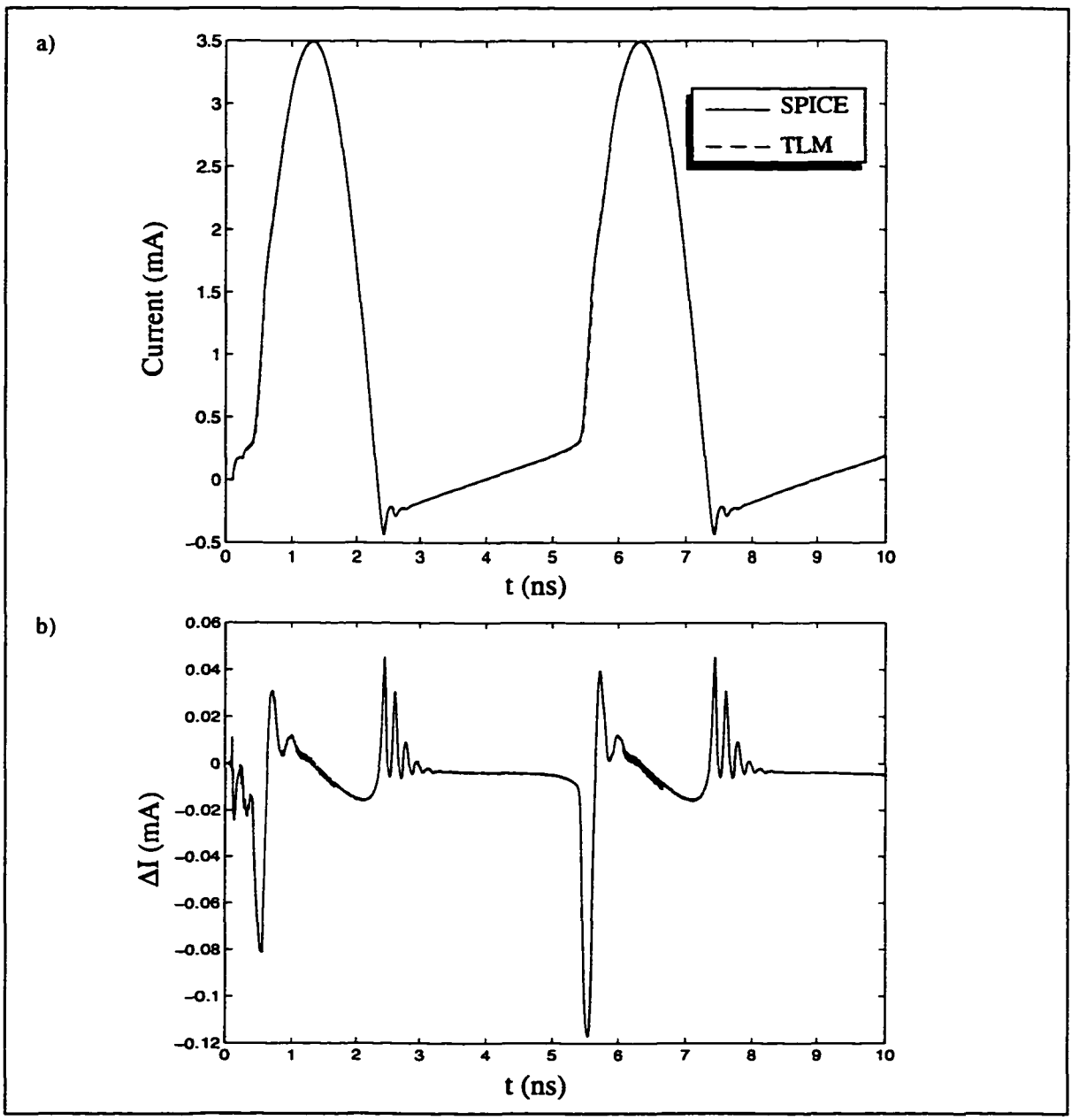

Figure 5.28 Evaluation of the dynamic behavior of a p-n junction diode. a) current flowing into the diode, and b) Deviation $i(t)|_{TLM}$-$i(t)|_{SPICE}$.

The comparison between the current deviation in Figure 5.23 and the one obtained in this example (Figure 5.22.b) reveals a larger error in the second case. The discrepancy is due to the larger parasitic capacitance added by the device stubs in the dielectric-loaded medium, and to the dispersion error introduced in the modeling of such a region. Introducing the additional stub capacitances in the SPICE model the maximum current deviation is reduced from 0.1172 mA to 0.0517 mA.

5.7 A three-dimensional example

In order to test the method for a general situation, the analysis of a fully 3D problem in the presence of graded meshes, heterogenous media and lumped devices has been carried out. The capacitively coupled bandpass filter of Figure 5.29 has been examined, and the modeling results have been compared with the measurements available in the literature [21].

The structure consists of a microstrip resonator series-connected to the input and output ports by means of two chip capacitors. The characteristic impedance of the line is Z_0=50 Ω. The capacitors, of value 0.16 pF, are connected to the central part of the microstrip cross-sections, as shown in Figure 5.29.

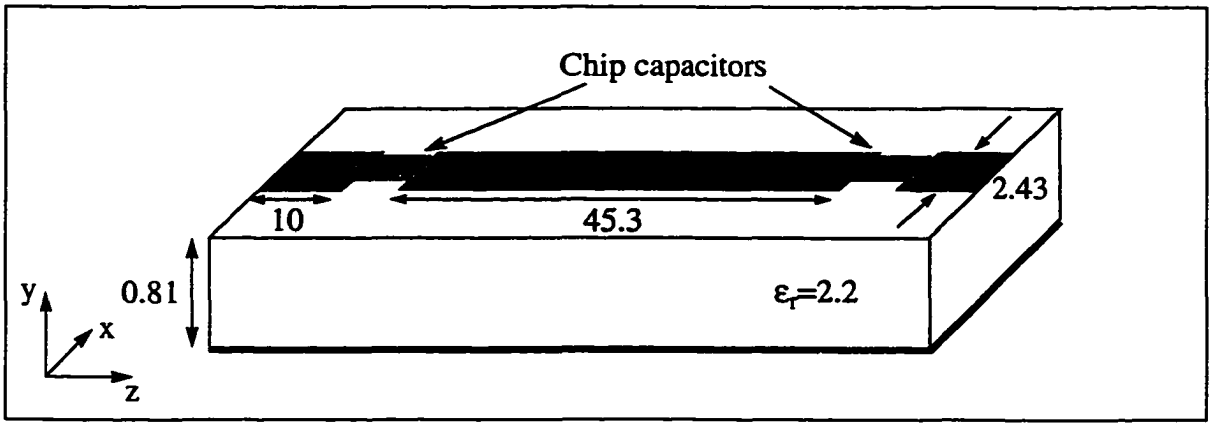

Figure 5.29 Geometry of the capacitively coupled bandpass filter (dimensions in mm)

In order to accurately model the field behavior in the vicinity of the strip edges, a graded discretization has been used in the three-directions (Figure 5.30). The computational domain has been terminated by single reflection coefficient absorbing boundaries; the symmetry of the structure along the y-direction has also been exploited to reduce the

computational effort. The total mesh size is: 29x32x234. Because of their superior dispersion characteristics, hybrid nodes [10] have been employed to model the structure, while modified stub-loaded nodes have been used to accommodate the lumped capacitors (Section 4.4). The capacitors, which have been distributed over the four central cells of the strip cross-section, have been modeled with the procedure outlined in Section 5.3.

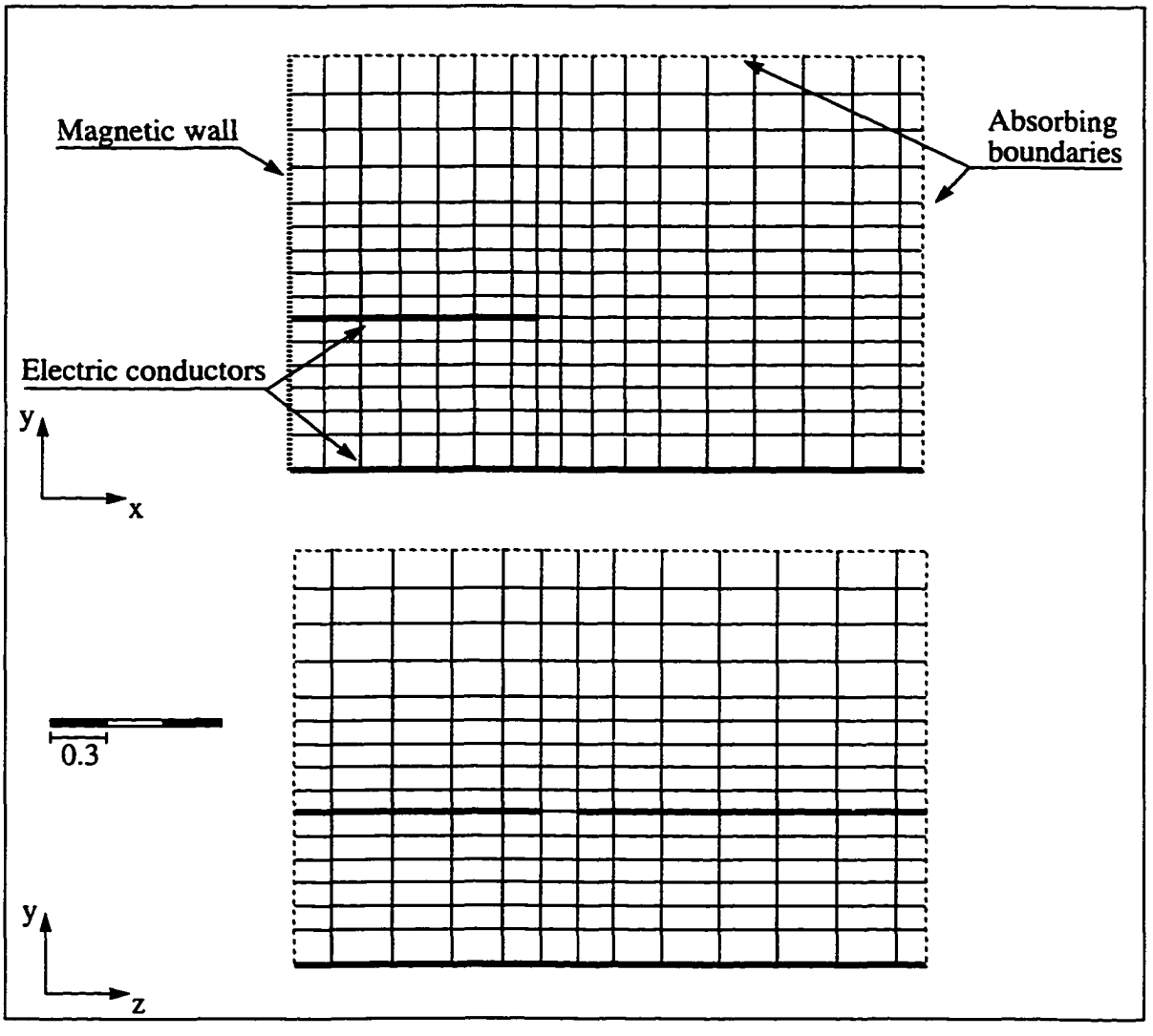

Figure 5.30 Detail of the graded mesh used for the modeling of the microstrip circuit. (Dimensions in mm)

The simulation requires approximately 19 MBytes of RAM and 20 hours of computational time on a HP-735 workstation. The major cause for the long computational time is that the stub-loaded symmetrical condensed nodes containing the lumped elements

limit the maximum time step usable in the simulation. In order to reduce the memory and computation requirements, the absorbing boundary conditions can probably be placed closer to the circuit. In order to increase the maximum time-step allowed, it is necessary to extend the algorithm presented in this thesis to the case of hybrid nodes. The time domain waveforms at the input and output ports have been determined with the TLM simulation (Figure 5.31); the presence of a resonant effect is clearly visible.

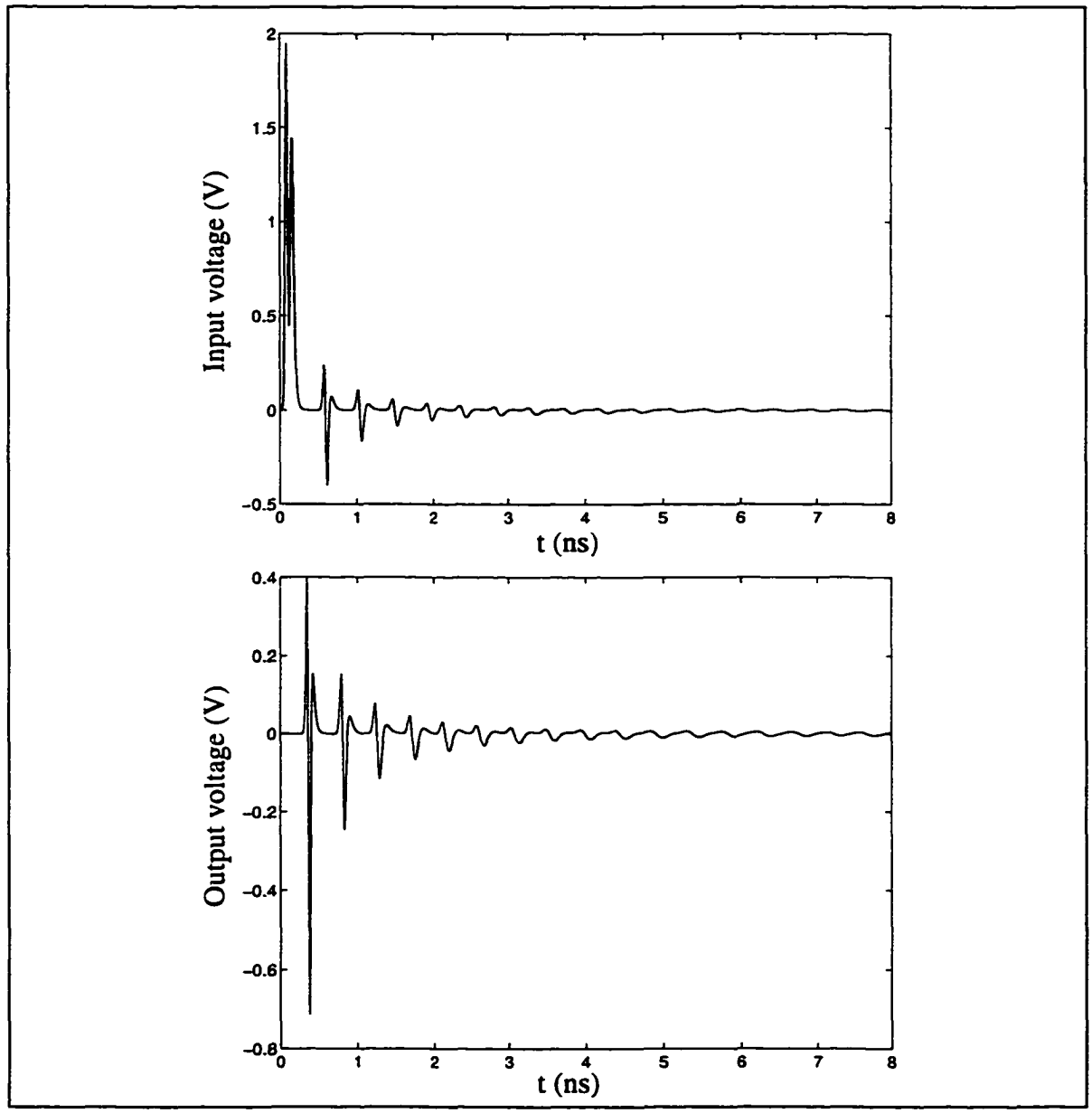

Figure 5.31 Time domain waveforms at the input and output ports of the bandpass filter.

The S-parameters of the structure have also been computed, and compared with measurements available in the literature [21]. The good agreement obtained between the two results confirms the validity of the method.

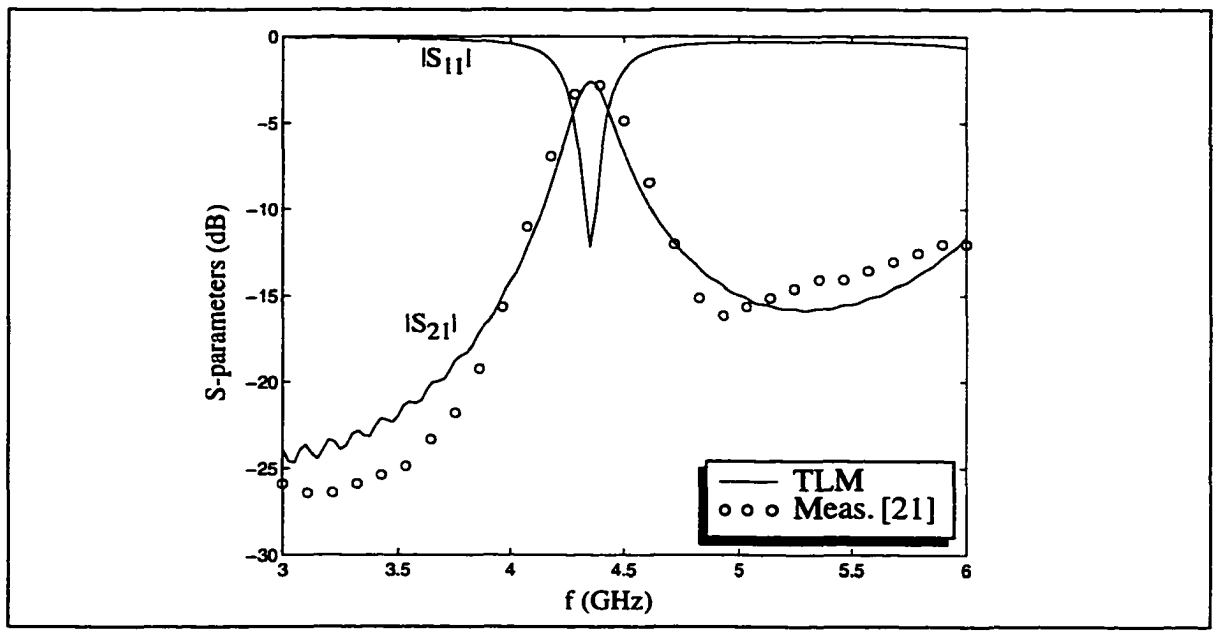

Figure 5.32 Comparison between the computed and measured [21] S-parameters for the structure in Figure 5.29

5.8 Conclusions

In this Chapter, the procedure for the connection of lumped circuits to the three-dimensional TLM network has been specialized for several types of devices. First, simple linear circuits have been considered, and successively nonlinear passive and passive elements have also been embedded in the distributed TLM mesh.

A number of canonical problems have been examined to verify the correctness of the method. The simulation results provided by the TLM procedure have always proven to be in good agreement with the theoretical behavior, when available, or with SPICE simulations in the case of nonlinear problems, thus confirming that the connection between the devices and the TLM have been correctly implemented. A three-dimensional example including a graded mesh and heterogenous material properties has finally been examined, showing a very good agreement between the numerical analysis performed with the proposed method and independent measurements published in [21].

A numerical analysis of the capacitive effect introduced by the device stubs has also been performed: the knowledge of the value of such additional capacitance is useful to predict when its presence is negligible in a simulation.

Chapter 6

Conclusions and Future Work

6.1 Introduction

The numerical modeling of electromagnetic fields is an area of research in continuous evolution. In the last few years, numerous contributions have been made to improve the characteristics of time-domain numerical methods, in order to increase their efficiency and the range of their applications. Nowadays, several electromagnetic field solvers based on time-domain numerical methods have been developed and commercialized and, although none of them has yet surpassed the popularity of frequency-domain simulators, their use is becoming widespread.

Nonetheless, in order to analyze complex electromagnetic structures, the use of a single numerical method is often insufficient, because either the method cannot handle the specific problem or the computational effort is overwhelming. A promising philosophy consists in coupling two (or more) resolution methodologies to obtain accurate results with reasonable computational expenditures. The underlying purpose of such hybrid techniques is to exploit the advantages of each method in performing its most suitable task, thus enhancing the overall accuracy and flexibility.

The direct application of a time-domain method, such as TLM or FDTD, to the solution of complex electromagnetic problems containing also nonlinear devices is not practical with the actual computing resources, since the discretization required to model the nonlinear device is usually much smaller than that necessary to describe the field behavior in the rest of the structure. An appealing solution then consists in using a simpler description of the nonlinear element, such as an equivalent circuit, in conjunction with a full wave analysis of the distributed part of the structure, thus reducing the computational effort to acceptable levels.

In the present thesis, the possibility of modeling nonlinear devices with the three-dimensional TLM method has been explored; a new procedure has been successfully developed and implemented, linking the equivalent circuit representation of the nonlinear device to the transmission line model of the electromagnetic fields in the TLM network. No restrictions are applied on the size of the device, which can thus occupy more than a TLM cell. In order to model devices embedded in heterogenous media, a modification of the TLM node and relative scattering matrix has also been proposed.

In view of linking the TLM field solver with a lumped element circuit CAD tool, the modified TLM scattering algorithm has remained independent of the specific device connected to the mesh. Although an automatic procedure to connect the TLM method and a lumped circuit solver has not been implemented yet, the general methodology shown in this thesis appears to be a promising approach to solve a large variety of electromagnetic problems containing nonlinear elements. A brief discussion of the connection between the TLM algorithm and SPICE, based on the theory proposed in this thesis, is presented in the next Section.

6.2 The connection with SPICE

The device stub approach described in this thesis constitutes a suitable basis for interfacing the TLM algorithm with a lumped circuit CAD tool. In fact, the decoupling obtained by appropriately choosing the device stub admittance value (4.5, 4.11) allows to separately solve the field and lumped circuit behavior at each iteration. The next step consists in increasing the class of lumped circuits that can be interfaced with the TLM network.

An attractive and efficient solution consists in linking the TLM field simulator with SPICE. Such a connection would open up a number of possibilities for the simulation of devices which currently cannot be solved with the sole TLM method, because of the presence of nonlinear elements. In this way, the tremendous investment of time that has already been spent for the development of SPICE would be immediately transferred for the analysis of hybrid problems.

The advantages offered by this link can be summarized as follows:

- A large variety of nonlinear components, including their nonideal behavior, is already available in SPICE

- The integration scheme developed for SPICE is more flexible than the fixed time step integration procedure used in this thesis. SPICE uses an adaptive time step and stores more information to perform the integration.
- It is straightforward to substitute the nonlinear device or to modify its characteristics. With the device stub approach, the TLM algorithm does not depend on the circuit connected to the mesh; the modification is then carried out by simply modifying the SPICE input file describing the device.
- It is possible to create new 'ad hoc' lumped element circuits with SPICE, to model HBTs, HEMPTs, etc., and immediately link them with the field simulator.

The essence of the procedure to link the TLM solver to SPICE has already been outlined in this thesis. The TLM network is a discretized equivalent circuit model for the resolution of Maxwell's equations, and this allows the direct application of circuit theory when the inclusion of nonlinear devices is involved.

As explained in Chapter 4, the key process to establish the connection between the TLM cells and the lumped circuit consists in determining the new incident voltages traveling from the device towards the nodes as a function of the reflected voltages, of the old voltage and current values and of the device characteristics (note that the complete time stream of the old electrical quantities may be stored to improve the accuracy in the integration scheme). Since this process clearly requires the resolution of a mixed transmission line-lumped element circuit in the time-domain, the SPICE simulator can then be used to obtain the new incident voltages at each time step.

For the case of one-port devices, the general SPICE circuit to be solved at each TLM iteration has the topology shown in Figure 6.1 (the extension to two-port elements is straightforward). The excitation is provided by a Thevenin equivalent representation of the TLM voltage. The transmission line represents the TLM device stub and therefore has the stub characteristic admittance; some care must be taken in the determination of the equivalent length of the line: the velocity of propagation of the pulses in the TLM mesh is twice the real velocity of light in the modeled medium; to achieve synchronism the SPICE line (modeling a real medium) must be therefore half the length of the TLM stub, that is $\Delta l/4$. The transmission line is terminated by the lumped circuit representing the device that we want to model.

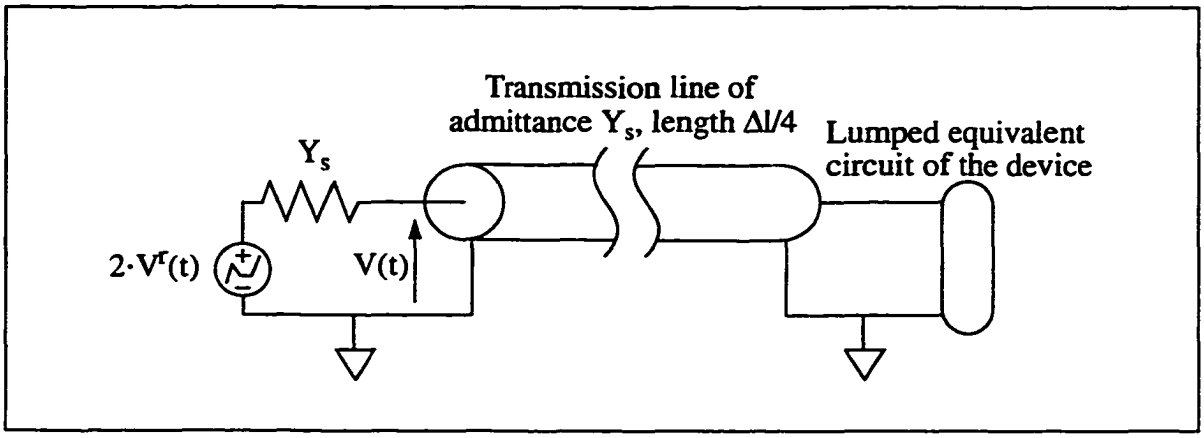

Figure 6.1 SPICE layout for the determination of the new incident voltage to be inserted in the TLM simulation. The time evolution of the source $2 \cdot V^r(t)$ is updated at each iteration after the TLM scattering process.

At each iteration, the voltage source value is updated according to the impulses generated during the TLM scattering process; the voltage source is assumed to be constant during each TLM time step.

As mentioned in Section 4.6, a similar approach has been adopted to connect the FDTD algorithm to SPICE [27]; in that case the circuit solved by SPICE consisted of the nonlinear device and a shunt capacitance, and was used to update the electric field evolution in the FDTD cell in the presence of the lumped circuit.

The proposed technique to link the TLM algorithm and SPICE can be summarized by the steps illustrated in Figure 6.2:

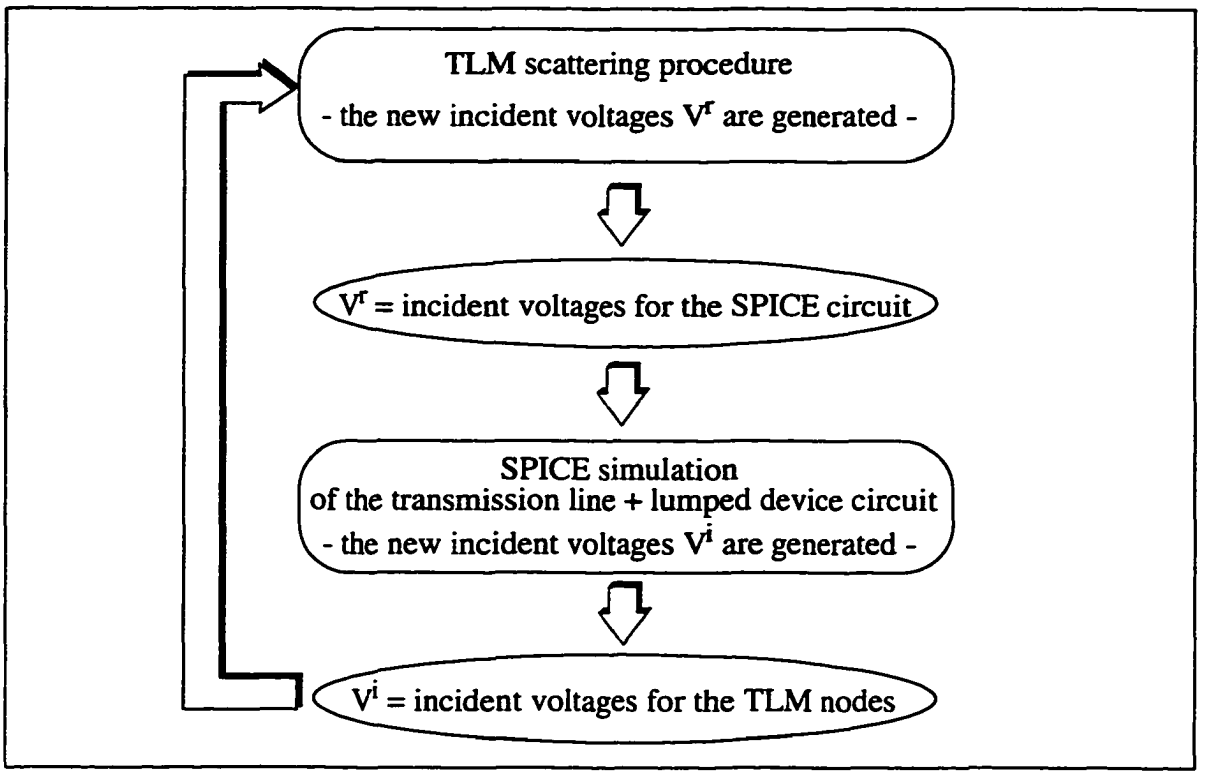

Figure 6.2 Schematic representation of the link between the TLM algorithm and the SPICE simulator. The process occurs during a TLM time-step

In SPICE, the circuit is analyzed in terms of total current and voltage, and it is not possible to directly determine the behavior of the incident and reflected voltages traveling in the line. In particular, SPICE can calculate the total voltage V(t) across the transmission line, at any instant in a given time range. A possible solution to determine the new incident voltage at the time step $k\Delta t$ consists in setting to zero the voltage source at $t=k\Delta t$, and prolonging the SPICE simulation for an extra time step, until $(k+1)\Delta t$, so that the new incident voltage, $V^i(t)$, is simply given by the value of the total voltage in this time frame. The incident voltage is then fed back into the TLM algorithm. The disadvantage of this approach is that the SPICE simulation must be run for an extra time-step at each iteration. A more efficient approach consists in sampling the total voltage at the device plane at $(k+1/2)\Delta t$, and obtain the new incident voltage as difference between V(t) and $V^r(t)$. In this way both the TLM and SPICE simulations are maintained synchronous at each iteration.

In order to illustrate the procedure, a simple SPICE simulation has been carried out.

The transmission line has been terminated by an open circuit, and excited with a voltage source $2 \cdot V^r(t)=2$ V during the first time-step ($0 < t < 1.66$ ps), and $2 \cdot V^r(t)=1$ V for the second time-step ($1.66 < t < 3.33$ ps). With a SPICE simulation, it is possible to determine the value of V^i that must be injected in the TLM simulation for at each iteration. When a unitary impulse is excited at the source plane (point A in Figure 6.3), the sum of this impulse and of the new incident voltage appears at the device plane after a half time step (point B in the same graph). Therefore, subtracting the value of the known reflected voltage from the total voltage yields to the new incident voltage to be used in the TLM simulation.

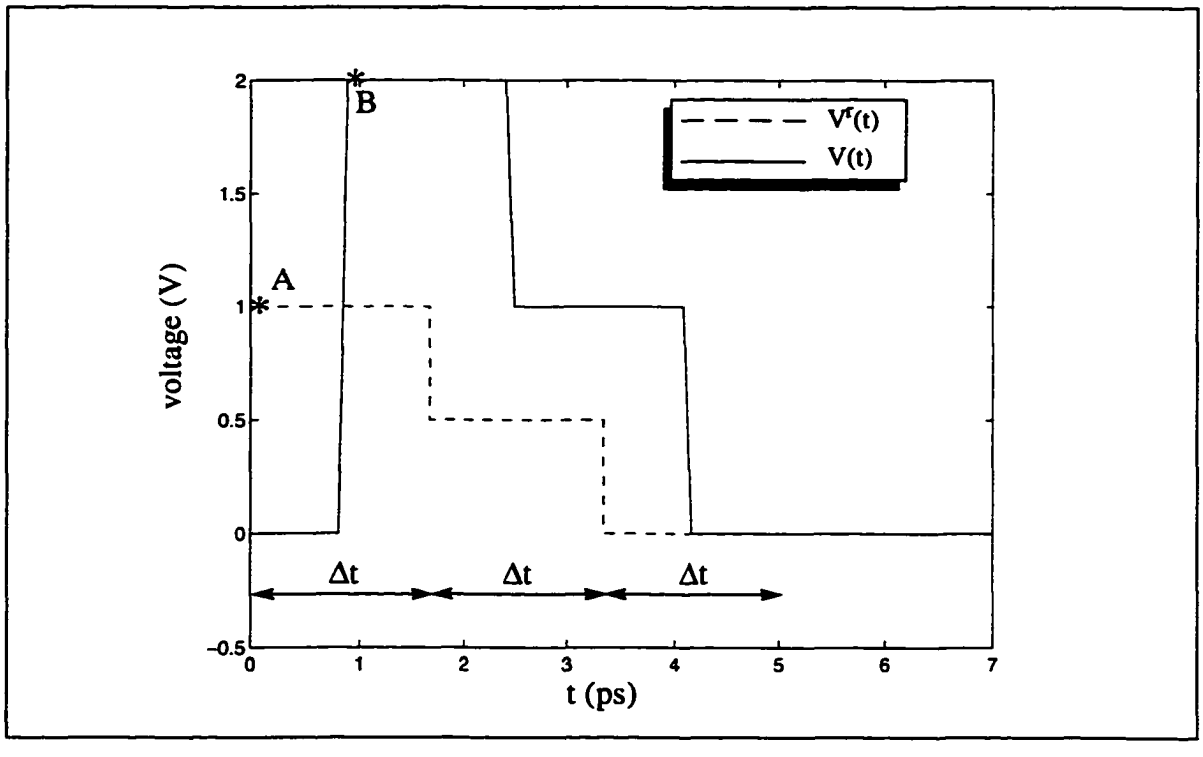

Figure 6.3 Example of calculation of the new incident voltage V^i for the TLM time step k=1, using a SPICE simulation. The voltage source $2 \cdot V^r$ is set to 2 volts when t=0. After half a time-step, the total voltage across the device corresponds to V^i+V^r

Although the value of the new incident voltage can, in principle, be sampled at any instant in the range $(k+1/2)\Delta t < t < (k+3/2)\Delta t$, it is recommended to evaluate the voltage at the center of this time interval, that is at $(k+1)\Delta t$. In fact, the previous figure reveals the presence of a trapezoidal shape in the V(t) curve, when t approaches the upper limit of

the interval. This is due to the maximum time discretization allowed in SPICE to compute the transient behavior (for this example, the maximum was set to $\Delta t/20$). The smaller the maximum discretization allowed, the better is the approximation to an ideal rectangular shape, at the expense of longer simulation times.

6.3 Future work

This thesis presented a novel and general approach for the modeling of complex electromagnetic problems involving nonlinear devices, represented by suitable lumped equivalent circuits. The technique consists in linking the TLM cells and the lumped circuit by means of device stubs with suitable characteristic admittance. With the proposed approach, the basic TLM algorithm is maintained independent of the specific device that is connected to the mesh. The method appears to be easily extensible to link a lumped circuit CAD simulator to the TLM field solver.

The first objective of future investigations will be to verify the feasibility of the approach described in the previous Section to connect the TLM simulator and SPICE; for this purpose, the assistance of a software engineer will be needed. Successively, the TLM-SPICE link will be extended to model two- and multi-port devices, removing also the restriction for the device to occupy one TLM cell.

In this thesis, complex problems involving nonlinear devices, graded meshes and heterogeneous media have been handled with a mixed approach: because of their superior dispersion characteristics, hybrid nodes have been used to describe the distributed part of the structure, while the modified stub-loaded SCN nodes have been used to model the lumped devices. In the future, the procedure presented in this thesis should be also extended to model nonlinear devices in 3D TLM hybrid nodes. In order to exploit the better integration scheme offered by SPICE, the possibility of using a flexible time step in the TLM simulation should also be considered.

Thermal phenomena occurring in the device may also be taken into account. For some devices, the thermal effect is already described in SPICE, therefore this kind of information would be readily available when the connection between SPICE and TLM is completed.

The possibility of using other CAD tools instead of SPICE should also be explored.

Finally, further investigations on the stability of the method presented in this thesis

should be carried out. In principle, since the procedure is based on an equivalent circuit model of both the electromagnetic distributed part and the lumped nonlinear device, the only nonphysical instabilities arising during the simulation should be generated by the numerical resolution of the nonlinear equations. This is certainly true when the device occupies a single TLM cell in the direction of the feeding voltage. Although no instabilities have been encountered in the several simulations performed so far, even when run for very long simulation times, it should be pointed out that when the device extends over several cells in the direction of the voltage, some concerns about the causality of the procedure may arise. It is expected that a possible critical situation may arise in the analysis of high-Q resonant structures containing an active element occupying several cells in the direction of propagation of the electromagnetic wave.

6.4 Overall conclusions

With the help of the theory developed in this thesis, the TLM modeling of high frequency circuits containing nonlinear devices has become possible. The introduction of device stubs to link the TLM cells and the lumped equivalent circuit describing the nonlinear element avoids the need to change the TLM scattering matrix if a new device is simulated. With this approach, the connection between the TLM simulator and a lumped circuit CAD solver such as SPICE becomes feasible. The framework of this connection has been outlined in this Chapter.

The link between TLM and SPICE will certainly provide a new tool to efficiently and accurately analyze complete electromagnetic subsystems, containing nonlinear active and passive devices. In this way it will become feasible to accurately solve complex electromagnetic structures, such as MMIC, high-speed digital interconnects, and packaging problems, while retaining all the advantages of a full-wave time domain method.

Bibliography

[1] M. N. O. Sadiku, *"Numerical Techniques in Electromagnetics"*, CRC Press, Boca Raton, 1992

[2] R. Sorrentino ed., *"Numerical Methods for Passive Microwave and Millimeter Wave Structures"*, IEEE Press, New York (NY), 1989

[3] T. Itoh ed., Numerical Techniques for Microwave and Millimeter-Wave Passive Structures, John Wiley & Sons, New York (NY), 1989

[4] R. C. Booton, Jr. *"Computational Methods for Electromagnetics and Microwaves"*, John Wiley & Sons, 1992

[5] R. B. Wu and T. Itoh, "Hybridizing FD-TD Analysis with Unconditionally Stable FEM for Objects of Curved Boundary", *1995 IEEE MTT-S International Microwave Symposium Digest*, Orlando (FL), 1995, pp. 833-836

[6] P. P. M. So, *"Modeling of Complex Electromagnetic Structures with TLM - Theory and Practice"*, Ph.D. Dissertation, University of Victoria, 1996

[7] L. W. Nagel, *"SPICE-2: A Computer Program to Simulate Semiconductor Circuits"* ERL-M520, Electronics Research Laboratory, Univ. of California, Berkeley, 1975

[8] R. W. Jackson, "A Circuit Topology for Microwave Modeling of Plastic Surface Mount Packages", *IEEE Transactions on Microwave Theory and Techniques*, vol. 44, July 1996, pp. 1140-1146.

[9] M. A. Alsunaidi, S. M. Sohel Imtiaz, S. M. El-Ghazali, "Electromagnetic Wave Effects on Microwave Transistors Using a Full-Wave Time-domain Model", *IEEE Transactions on Microwave Theory and Techniques*, vol. 44, no. 6, pp. 799-808, June 199€

[10] C. Christopoulos, *"The Transmission Line Modeling Method: TLM"*, IEEE Press, Piscataway, NJ, 1995

[11] K. S. Yee, "Numerical Solution of Boundary Value Problems Involving Maxwell's Equations in Isotropic Media", *IEEE Transactions on Antennas and Propagation*, vol. 14, no. 5, May 1966, pp. 302-307

[12] C. Eswarappa, W. J. R. Hoefer, "Absorbing Boundaries for Time-Domain TLM and FDTD Analysis of Electromagnetic Structures", *Electromagnetics*, vol. 16, no. 5, Sept.-Oct. 1996, pp. 489-519

[13] J. Xu, A. P. Zhao, A. V. Räisänen, "A Stable Algorithm for Modeling Lumped Circuit Source Across Multiple FDTD Cells", *IEEE Microwave and Guided Wave Letters*, vol. 7, no. 9, September 1997, pp. 308-310

[14] P. B. Johns, M. O'Brien, "Use of the Transmission Line Modelling (T.L.M.) Method to Solve Nonlinear Lumped Networks", *Radio Electronic Engineer*, vol. 50, Jan./Feb. 1980, pp. 59-70

[15] P. Russer, W. J. R. Hoefer, P. P. M. So, "Modeling of Nonlinear Active Regions in TLM", *IEEE Microwave and Guided Letters*, vol. 1, no. 1, Jan. 1991, pp. 10-13

[16] B. Isele, P. Russer, "Modeling of Nonlinear Dispersive Active Elements in TLM", *1992 IEEE MTT-S International Microwave Symposium Digest*, Albuquerque (NM), 1992, pp. 1217-1220

[17] M. Al-Assadi, T. M. Benson, C. Christopoulos, "Interfacing field problems modelled by TLM to lumped circuits", *Electronic Letters*, vol. 30, no. 4, Feb. 1994, pp. 290-291

[18] J. L. Herring, W. J. R. Hoefer, "Improved Excitation of 3D SCN TLM Based on Voltage Sources", *1996 IEEE MTT-S International Microwave Symposium*, S. Francisco (CA), June 1996, pp. 1031-1034

[19] R. H. Voelker, R. J. Lomax, "A Finite-Difference Transmission Line Matrix Method Incorporating a Nonlinear Device Model", *IEEE Transactions on Microwave Theory and Techniques* vol. 38, no. 3, March 1990, pp. 302-312

[20] J. S. Nielsen, W. J. R. Hoefer, "Modeling of Nonlinear Elements in a Three-Dimensional Condensed Node TLM Mesh", *Int. Journal of Microwave and Millimeter Wave Computer-Aided Engineering*, vol. 3, no. 1, 1193, pp. 61-66

[21] L. Albasha, C. M. Snowden, "New Integrated Simulation Techniques for the Electromagnetic Analysis of Microwave Circuits Using the TLM Method", *Int. Jour-*

nal of Numerical Modeling, vol. 9, no. 5, Sept.-Oct. 1996, pp. 375-393

[22] W. Sui, D. A. Christensen, C. H. Durney, "Extending the Two-Dimensional FDTD method to Hybrid Electromagnetic Systems with Active and Passive Lumped Elements", *IEEE Transactions on Microwave Theory and Techniques*, vol. 40, no. 4, Apr. 1992, pp. 724-730

[23] B. Toland, B. Houshmand, T. Itoh, "Modeling of Nonlinear Active Regions with the FDTD Method", *IEEE Microwave and Guided Letters*, vol. 3, no. 9, Sept. 1993, pp. 333-335

[24] B. Toland, J. Lin, B. Houshmand, T. Itoh, "FDTD Analysis of an Active Antenna", *IEEE Microwave and Guided Letters*, vol. 3, no. 11, Nov. 1993, pp. 423-425

[25] P. Ciampolini, P. Mezzanotte, L. Roselli, D. Sereni, R. Sorrentino, P. Torti, "Simulation of HF Circuits with FDTD Technique Including Non-Ideal Lumped Elements", *1995 IEEE MTT-S International Microwave Symposium*, Orlando (FL), 1995, pp. 361-364

[26] P. Ciampolini, P. Mezzanotte, L. Roselli, R. Sorrentino, "Accurate and Efficient Circuit Simulation with Lumped-Element FDTD Technique", *IEEE Transactions on Microwave Theory and Techniques*, vol. 44, no. 12, Dec. 1996, pp. 2207-2215

[27] V. A. Thomas, M. E. Jones, M. Piket-May, A. Taflove, E. Harrigan, "The Use of SPICE Lumped Circuits as Sub-grid Models for FDTD Analysis", *IEEE Microwave and Guided Letters*, vol. 4, no. 5, May 1994, pp. 141-143

[28] M. Piket-May, A. Taflove, J. Baron, "FDTD Modeling of Digital Signal Propagation on 3-D Circuits with Passive and Active Loads", *IEEE Transactions Microwave Theory and Techniques*, vol. 42, no. 8, August 1994, pp. 1514-1523

[29] P. B. Johns and R. L. Beurle, "Numerical Solution of 2 Dimensional Scattering Problems using a Transmission Line Matrix", *Proceedings of the IEE*, vol. 118, no. 9, Sept. 1971, pp. 1203-1208

[30] P. B. Johns, "A Symmetrical Condensed Node for the TLM Method", *IEEE Transactions on Microwave Theory and Techniques*, vol. 35, no. 4, April 1987, pp. 370-377

[31] R. E. Collin, "Foundations for Microwave Engineering", (2nd ed.), Mc Graw-Hill,

New York, 1992

[32] W. J. R. Hoefer, "The Transmission Line Matrix Method - Theory and Applications", *IEEE Trans. Microwave Theory and Tech.*, vol. 33, no. 10, Oct. 1985, pp. 882-893

[33] S. Ramo, J. R. Whinnery, T. Van Duzer, *"Fields and Waves in Communication Electronics"*, Second Edition, John Wiley & Sons, New York (NY), 1984

[34] W. J. R. Hoefer and P. P. M. So, *"The Electromagnetic Wave Simulator"*, John Wiley & Sons, Chichester, 1991

[35] *Proceedings of the First International Workshop on Transmission Line Matrix (TLM) Modeling - Theory and Applications*, Victoria (BC), Canada, August 1993

[36] S. Akhtarzad, P. B. Johns, "The Solution of Maxwell's Equations in Three Space Dimensions and Time by the TLM Method of Numerical Analysis", *Proc. IEE*, vol. 122, no. 12, Dec. 1975, pp. 1344-1348

[37] P. Saguet and E. Pic, "Utilisation d'un nouveau type de noeud dans la methode TLM en 3 Dimensions", *Electronic Letters*, vol. 18, no. 11, May 1982, pp. 478-490

[38] P. Naylor, R. A. Desai, "New Three-Dimensional Symmetrical Condensed Node for the Solution of EM Wave Problems by TLM", *Electronic Letters*, vol. 26, 1990, pp. 492-494

[39] F. J. German, G. K. Gothard, L. S. Riggs, "Modeling of Materials with Electric and Magnetic Losses with the Symmetrical Condensed TLM Method", *Electronic Letters*, vol. 26, 1990, pp. 1307-1308

[40] D. A. Al-Mukhtar, J. E. Stich, "Transmission-Line Matrix Method with Irregularly Graded Space", *Proc. IEE*, vol. 128, no. 6, Dec. 1981, pp. 299-305

[41] R. A. Scaramuzza and A. J. Lowery, "Hybrid Symmetrical Condensed Node for the TLM Method", *Electronic Letters*, vol. 26, 1990, pp. 1947-1949

[42] V. Trenkic, C. Christopoulos, T. M. Benson, "Theory of the Symmetrical Super-Condensed Node for the TLM Method", *IEEE Transactions on Microwave Theory and Techniques*, June 1995, vol. 43, no. 6, pp. 1342-1348

[43] V. Trenkic, C. Christopoulos, T. M. Benson, "Development of a General Symmet-

rical Condensed Node for the TLM method", *IEEE Transactions on Microwave Theory and Techniques*, December 1996, vol. 44, no. 12, pp. 2129-2135

[44] J. S. Nielsen, "*TLM Analysis of Microwave and Millimetre Wave Structures with Embedded Nonlinear Devices*", Ph. D. Dissertation, University of Ottawa, 1992

[45] M. Krumpholz and P. Russer, "On the Dispersion in TLM and FDTD", *IEEE Transactions on Microwave Theory and Techniques*, vol. 42, no. 7, July 1994, pp. 1275-1279

[46] L. de Menezes and W. J. R. Hoefer, "Accuracy of TLM Solutions of Maxwell's Equations", *IEEE Transactions on Microwave Theory and Techniques*, vol. 44, no. 12, December 1996, pp. 2512-2518

[47] S. Lindenmeier, B. Isele, R. Weigel, P. Russer, "A Fast Spatial Domain Method for the Suppression of Excitation-Inducted Spurious Modes in SCN-TLM", *1996 IEEE MTT-S Int. Microwave Symposium*, San Francisco (CA), 1996, pp. 351-354

[48] A. V. Oppenheim, R. W. Schafer, *"Digital Signal Processing"*, Prentice-Hall, Englewood Cliffs (NJ), 1975

[49] P. Saguet, E. Pic, "An Improvement for the TLM Method", *Electronic Letters*, vol. 16, no. 7, March 1980, pp. 247-248

[50] M. Righi, M. Mongiardo, R. Sorrentino, W. J. R. Hoefer, "Efficient TLM Diakoptics for Separable Structures", *IEEE Transactions on Microwave Theory and Techniques*, vol. 43, no. 4, April 1995, pp. 854-859

[51] M. Righi, J. L. Herring, W. J. R. Hoefer, "Efficient Hybrid TLM/Mode-Matching Analysis of Packaged Components", *IEEE Transactions on Microwave Theory and Techniques*, vol. 45, no. 10, October 1997, pp. 1715-1724

[52] J. P. Berenger, "A Perfectly Matched Layer for the Absorption of Electromagnetic Waves", *Journal of Comput. Physics*, vol. 114, no. 2, October 1994, pp. 110-117

[53] C. Eswarappa, W. J. R. Hoefer, "A Hybrid 3-D TLM-FDTD Model of Microwave Fields", *IEEE MTT-S International microwave Symposium Digest*, San Francisco (CA), 1996, pp. 1063-1066

[54] N. Penã and M. M. Ney, "Absorbing-boundary Conditions Using Perfectly Matched-Layer (PML) Technique for Three-Dimensional TLM Simulations",

IEEE Transactions on Microwave Theory and Techniques, vol. 45, no. 10, October 1997, pp. 1749-1755

[55] G. Ghione, A. Benvenuti, "Discretization Schemes for High-Frequency Semiconductor Device Models", *IEEE Transactions on Antennas and Propagation*, vol. 45, no. 3, March 1997, pp. 443-456

[56] S. M. Sze, *"Physics of Semiconductor Devices"*, second edition, John Wiley & Sons, New York, 1981

[57] T. K. Ishii, *"Practical Microwave Electron Devices"*, Academic Press Inc., San Diego, 1990

[58] J. Singh, *"Semiconductor Devices: An Introduction"*, McGraw-Hill Inc., New York, 1994

[59] P. Antognetti, G. Massobrio, *"Semiconductor Device Modeling with SPICE"*, Mc Graw-Hill, New York, 1987

[60] A. J. Wlodarczyk and D. P. Johns, "New Wire Interface for Graded 3-D TLM", *Electronic Letters*, vol. 28, no. 8, 1992, pp. 728-729

[61] A. P. Duffy, J. L. Herring, T. M. Bendon, C. Christopoulos, "Improved Wire Modeling in TLM", *IEEE Transactions on Microwave Theory and Techniques*, vol. 42, no. 10, October 1994, pp. 1978-1983

[62] D. P. Johns, A. Mallik, A. J. Wlodarczyk, "TLM Enhancements for EMC Studies", *Proceedings of the 1992 IEEE Regional Symposium on EMC*, Tel Aviv, 3.3.3, 1992, pp. 1-6

[63] P. B. Johns, G. F. Slater, "Transient Analysis of Waveguides with Curved Boundaries", *Electronic Letters*, vol. 9, no. 21, October 1873, pp.486-487

[64] U. Muller, W. J. R. Hoefer, "The Implementation of Smoothly moving Boundaries in 2D and 3D TLM Simulations", *1992 IEEE MTT-S International Microwave Symposium Digest*, Albuquerque (NM), 1992, pp. 791-792

[65] F. J. German, "Infinitesimally Adjustable Boundaries in Symmetrical Condensed node TLM Simulations", *Proceedings of the 9th Annual Review of Progress in Applied Computational Electromagnetics (ACES)*, Monterey (CA), 1993, pp. 482-490

[66] J. L. Herring and C. Christopoulos, "Solving Electromagnetic Field Problems Using a Multiple Grid Transmission-Line Modeling Method", *IEEE Transactions on Antennas and Propagation*, vol. 42, no. 12, December 1994, pp. 1654-1658

[67] J. L. Herring and W. J. R. Hoefer, "Compensation of Coarseness Error in TLM Modeling of Microwave Structures with the Symmetrical Condensed Node" *1995 IEEE MTT-S International Symposium Digest*, Orlando, May 1995, pp. 23-26

[68] L. Cascio, G. Tardioli, T. Rozzi, and W. J. R. Hoefer, "A Quasi-Static Modification of TLM at Knife Edge and 90° Wedge Singularities", *IEEE Transactions on Microwave Theory and Techniques*, vol. 44. no. 12, Dec. 1996, pp. 2519-2524

[69] M. Righi, W. J. R. Hoefer, B. Bader, R. Doerner, P. Russer, "Lumped Element Equivalent Circuit Parameter Extraction of Coplanar MMIC Components via TLM Simulation", *Proceedings of the 1995 MIOP Conference*, Sindelfingen, pp. 253-257

[70] L. de Menezes and W. J. R. Hoefer, "Modeling Constitutive Medium Relationships in SCN TLM", *IEEE Transactions on Microwave Theory and Techniques*, vol. 44, no. 6, June 1996, pp. 854-861

[71] W. H. Press et al., "*Numerical Recipes in Fortran 77: the Art of Scientific Computing*", Cambridge University Press, 1988

[72] http://www.microsim.com/index.html

[73] P. W. Tuinenga *"SPICE - A guide to Circuit Simulation & Analysis Using PSpice®"*, Prentice Hall, Englewood Cliffs, New Jersey, 1988

[74] W. Banzhaf, *"Computer-Aided Circuit Analysis Using SPICE"*, Englewood Cliffs, New Jersey, 1989

[75] http://math.nist.gov/cgi-bin/gams-serve/list-module-components/MINPACK/HYBRJ1/8375.html